

Aus dem Institut für Virologie
der Universität zu Köln
Direktor: Universitätsprofessor Dr. med Florian Klein

Facilitating Humanized Mouse Models to Study Novel HIV-1 Prevention Compounds

Inaugural-Dissertation zur Erlangung der Doktorwürde
der Medizinischen Fakultät
der Universität zu Köln

vorgelegt von
Franziska Marisa Kleipaß
aus Dormagen

promoviert am 06. November 2024

Gedruckt mit Genehmigung der Medizinische Fakultät der Universität zu Köln

2024

Dekan: Universitätsprofessor Dr. med. G. R. Fink

1. Gutachter: Universitätsprofessor Dr. med. F. Klein
2. Gutachter: Universitätsprofessor Dr. med. Dr. nat. med. J. Rybniker

Erklärung

Ich erkläre hiermit, dass ich die vorliegende Dissertationsschrift ohne unzulässige Hilfe Dritter und ohne Benutzung anderer als der angegebenen Hilfsmittel angefertigt habe; die aus fremden Quellen direkt oder indirekt übernommenen Gedanken sind als solche kenntlich gemacht.

Bei der Auswahl und Auswertung des Materials sowie bei der Herstellung des Manuskriptes habe ich keine Unterstützungsleistungen erhalten.

Weitere Personen waren an der geistigen Herstellung der vorliegenden Arbeit nicht beteiligt. Insbesondere habe ich nicht die Hilfe einer Promotionsberaterin/eines Promotionsberaters in Anspruch genommen. Dritte haben von mir weder unmittelbar noch mittelbar geldwerte Leistungen für Arbeiten erhalten, die im Zusammenhang mit dem Inhalt der vorgelegten Dissertationsschrift stehen.

Die Dissertationsschrift wurde von mir bisher weder im Inland noch im Ausland in gleicher oder ähnlicher Form einer anderen Prüfungsbehörde vorgelegt.

In der vorliegenden Dissertationsschrift präsentierte Daten wurden bereits publiziert:

Vanshylla K, Held K, Eser TM, Gruell H, **Kleipass F**, Stumpf R, Jain K, Weiland D, Münch J, Grüttner B, Geldmacher C, Klein F. CD34T+ Humanized Mouse Model to Study Mucosal HIV-1 Transmission and Prevention. *Vaccines (Basel)*. 2021 Feb 27;9(3):198. doi: 10.3390/vaccines9030198. PMID: 33673566; PMCID: PMC7997265.

Kalusche S, Vanshylla K, **Kleipass F**, Gruell H, Müller B, Zeng Z, Koch K, Stein S, Marcotte H, Klein F, Dietrich U. Lactobacilli Expressing Broadly Neutralizing Nanobodies against HIV-1 as Potential Vectors for HIV-1 Prophylaxis? *Vaccines (Basel)*. 2020 Dec 13;8(4):758. doi: 10.3390/vaccines8040758. PMID: 33322227; PMCID: PMC7768517.

Die dieser Arbeit zugrunde liegenden Experimente sind von mir selbstständig nach entsprechender Anleitung durch Frau Dr. Kanika Vanshylla sowie mit Unterstützung durch Frau Dr. Kanika Vanshylla durchgeführt worden. In der praktischen Umsetzung der Injektionen und Blutentnahmen bei den Versuchstieren wurde ich des Weiteren unterstützt durch die medizinisch-technische Assistentin Frau Ricarda Stumpf und die biologisch-technische Assistentin Frau Nicole Riet.

Erklärung zur guten wissenschaftlichen Praxis:

Ich erkläre hiermit, dass ich die Ordnung zur Sicherung guter wissenschaftlicher Praxis und zum Umgang mit wissenschaftlichem Fehlverhalten (Amtliche Mitteilung der Universität zu Köln AM 132/2020) der Universität zu Köln gelesen habe und verpflichte mich hiermit, die dort genannten Vorgaben bei allen wissenschaftlichen Tätigkeiten zu beachten und umzusetzen.

Köln, den 02.05.2024,

Unterschrift:

Detailed description of my contribution to the data and analysis presented in this thesis

Parts of this thesis are based on an article that is already published in the peer-reviewed journal *Vaccines*:

Vanshylla K, Held K, Eser TM, Gruell H, Kleipass F, Stumpf R, Jain K, Weiland D, Münch J, Grüttner B, Geldmacher C, Klein F. CD34T+ Humanized Mouse Model to Study Mucosal HIV-1 Transmission and Prevention. *Vaccines (Basel)*. 2021 Feb 27;9(3):198. doi: 10.3390/vaccines9030198. PMID: 33673566; PMCID: PMC7997265.

I contributed to this study by planning and carrying out mouse experiments together with Kanika Vanshylla.

Parts of this thesis are based on an article that is already published in the peer-reviewed journal *Vaccines*:

Kalusche S, Vanshylla K, Kleipass F, Gruell H, Müller B, Zeng Z, Koch K, Stein S, Marcotte H, Klein F, Dietrich U. Lactobacilli Expressing Broadly Neutralizing Nanobodies against HIV-1 as Potential Vectors for HIV-1 Prophylaxis? *Vaccines (Basel)*. 2020 Dec 13;8(4):758. doi: 10.3390/vaccines8040758. PMID: 33322227; PMCID: PMC7768517.

I contributed to this study by performing the in vitro neutralization assay against HIV-1 BAL, designing and carrying out the included mucosal HIV-1 exposure mouse experiment and visualising the results together with Kanika Vanshylla.

Acknowledgements

The work would never have been possible without the support of a variety of people for whom I am deeply grateful. I extend my sincere appreciation to Professor Florian Klein, my supervisor, who provided me with the opportunity to conduct my research in his laboratory. His unwavering support, encouragement, and enthusiasm for profound biomedical research have inspired me and greatly shaped my own passion.

Furthermore, I am indebted to the German Centre for Infection Research (DZIF) and the German Academic Scholarship Foundation (Studienstiftung) for their scholarships, providing financial and idealistic support that allowed me to fully concentrate on my laboratory work.

Words cannot express my gratitude to Dr Kanika Vanshylla, my mentor, and by now, certainly a friend. I could not imagine a better teacher. Kanika is one of the most dedicated, disciplined, and responsible-minded individuals I have ever met. It has been a pleasure and a privilege to learn from and with her. The insights into research I gained through working with Kanika have shaped my scientific understanding and most certainly allowed me to grow as a researcher, doctor, and human. I fondly remember the endless 96-well plates, pipet tips, Excel sheets, and coffee cups.

I also extend my deep thanks to all current and former members of the Klein Lab. It fills me with honour and joy to have been part of such a leading-edge, inspiring, and supportive team. In particular, I want to express my gratitude to Maike Schlotz and Ricarda Stumpf, who not only lent a helping hand but also provided much emotional support and honest friendship.

Starting my project in late 2019 in the virology department, I certainly did not expect many parts along the way. Yet, even in the middle of an unprecedented global virus pandemic, I could not have been in a more uplifting environment. Looking back, I feel deeply humbled and delighted to have contributed a tiny bit to the Klein Lab's research in that time.

I would never have been capable of finishing this work without the great emotional support from my friends and family, especially my best friend Judith, with her honest interest and thoughtful critique throughout the entire process, and my sister Johanna, who knows me like only siblings do and whom I could always rely on. I am deeply grateful for my parents, who have always supported me and imparted the importance of education and the enthusiasm to never stop questioning.

Last but definitely not least, I am profoundly grateful to my husband Florin. He opens my mind and broadens my horizons every day. His patience, belief in my abilities, and encouragement have been my anchor every step of the way. I extend my deepest appreciation for his sacrifices, understanding, and enduring love. Home is you.

Für meine Großeltern.

TABLE OF CONTENTS

LIST OF ABBREVIATIONS AND ACRONYMS	9
1. SUMMARY	13
2. ZUSAMMENFASSUNG	15
3. INTRODUCTION	17
3.1. The Human immunodeficiency Virus 1 (HIV-1)	17
3.2. Mucosal HIV-1 transmission and prevention strategies	18
3.2.1. The modes of transmission in majority of new HIV-1 infections	18
3.2.2. Pivotal steps in mucosal HIV-1 transmission and established preventive measures	18
3.2.3. Cell-virus interaction and viral cell entry	20
3.3. Compounds with neutralizing activity against HIV-1 in the prevention of mucosal transmission	21
3.3.1. The adaptive immune system interacts with pathogens at the site of infection by formation of neutralizing antibodies	21
3.3.2. Broadly neutralizing antibodies against HIV-1 occur in a small subset of infected individuals throughout the course of infection	22
3.3.3. Neutralization breadth of bnAbs can be quantified <i>in vitro</i>	22
3.3.4. bnAbs can mediate protection from HIV-1 infection <i>in vivo</i>	23
3.4. Nanobodies in HIV-1 prevention	23
3.4.1. Nanobodies are the smallest naturally occurring functional Ab fragments	23
3.4.2. Considerations on favourable features of nanobodies against HIV-1	24
3.5. Animal Models for Prevention Studies	27
3.5.1. General criteria of suitable animal models	27
3.5.2. NHP models	27
3.5.3. Humanized mouse models	30
3.5.3.2.1. Peripheral blood derived mononuclear cells (PBMCs)	33
3.6. Aims of this thesis	37
4. MATERIALS AND METHODS	38

4.1. Materials	38
4.1.1. Mice	38
4.1.2. Viruses	39
4.1.3. Cells	39
4.1.4. Equipment	42
4.1.5. Consumables	43
4.1.6. Kits	45
4.1.7. Reagents and Chemicals	45
4.1.8. Media, buffers and solutions	47
4.1.9. Antibodies, nanobodies, interleukins and plasmids	50
4.1.10. Software	51
4.2. Methods	51
4.2.1. Determination of cell concentrations	51
4.2.2. Virus production	52
4.2.3. Preparation of the luciferase assay buffer	52
4.2.4. Determination of infectivity of the produced viral stocks	53
4.2.5. Neutralization assay	54
4.2.6. Production of bnAbs	55
4.2.7. Humanization	57
4.2.8. Mononuclear cell injection	59
4.2.9. Injection of interleukin 7 (IL-7)	60
4.2.10. Mucosal HIV-1 challenge	60
4.2.11. Isolation of cells from the murine spleen and gut-associated lymphoid tissue	61
4.2.12. Immunofluorescence imaging and In-Situ Hybridisation for HIV-1-RNA on murine tissue samples	62
4.2.13. Viral load determination	62
4.2.14. Statistical analysis and result interpretation	66
5. RESULTS	66
5.1. A novel mouse model with improved T cell reconstitution is highly susceptible to mucosal HIV-1 infection	66
5.1.1. The hCD34T+ model displays a significant increase in human T cell reconstitution in the peripheral blood	66
5.1.2. Human T leukocyte reconstitution is significantly higher in CD34T+ in comparison to CD34+ mice	69
5.1.3. The prior humanization with donor-matched HSCs is essential for an enhanced human leukocyte reconstitution post UCBC administration	73

5.1.4.	The CD34T+ model displays a significant increase in the human T cell presence in the gut mucosal tissue	77
5.1.5.	The CD34T+ mouse model is highly susceptible to mucosal HIV-1 infection	81
5.1.6.	Highly potent bnAbs can prevent mucosal HIV-1 infection in CD34T+ mice	82
5.2.	HIV-1 specific nanobody A6 can prevent mucosal HIV-1 infection <i>in vitro</i> and <i>in vivo</i>	85
5.2.1.	V _H H A6 neutralizes HIV-1 _{BAL} in TZM-bl assay	85
5.2.2.	HIV-1 _{BAL} has a high infection rate in intrarectal exposure to CD34T+ mice	86
5.2.3.	HIV-1 _{BAL} infection in humanized mice in a combined mucosal administration with V _H H A6 is inhibited	87
6.	DISCUSSION	90
6.1.	Discussion of the novel CD34T+ Mouse Model	90
6.2.	Conclusions of this work for the potential of V _H H A6	94
6.3.	Perspectives for V _H H A6 in clinical use	95
7.	REFERENCES	98
8.	APPENDIX	115
8.1.	List of tables	115
8.2.	List of figures	115
9.	PUBLICATIONS	117

List of Abbreviations and Acronyms

AAV	adeno-associated virus
Ab	antibody
ADA	anti-drug antibody
AGM	African green monkey
AIDS	acquired immunodeficiency syndrome
ART	combination antiretroviral therapy
BC	B cell
BCR	B cell receptor
BLT	Bone marrow liver thymus
bnAb	broadly neutralizing antibody
CCR5	C-C motif chemokine receptor type 5
CD	cluster of differentiation
CD4	cluster of differentiation 4
CDR	complementary determining region
C _H	constant domain of the heavy chain
C _L	constant domain of the light chain
CoA	coenzyme A
CRF	circulating recombinant form
CRISPR	Clustered Regularly Interspaced Short Palindromic Repeats
CXCR4	C-X-C motif chemokine receptor type 4
CXCR6	C-X-C motif chemokine receptor type 6
DC	dendritic cell
DNA	deoxyribonucleic acid
DNA-PK	DNA-dependent protein kinase
dsDNA	double-stranded DNA
EBV	Ebstein Barr virus
ELISA	Enzyme-linked Immunosorbent Assay
Env	envelope protein
EtOH	ethanol
FACS	fluorescence-activated cell sorting
FBS	foetal bovine serum
F _c	crystallisable fragment
FGT	female genital tract
FTC	emtricitabine
GALT	Gut associated lymphoid tissue
G-CSF	granulocyte colony stimulating factor
GvHD	graft-versus-host disease
GV-SOLAS	Society of Laboratory Animal Science

HC	heavy chain
HCAb	heavy chain only antibody
HCS	haematopoietic stem cell
HIV	Human immunodeficiency virus
HIV-1	Human immunodeficiency virus 1
HLA	human leukocyte antigen
HMCC	Humanized Mouse Core Cologne
HSC	hematopoietic stem cells
HSIV	human-simian immunodeficiency virus
huMouse	humanized mouse
HvGR	host-verus-graft reaction
i.h.	intrahepatic
i.p.	intraperitoneal
i.r.	intrarectal
i.s.	intrasplenic
i.v.	intravenous
IC ₅₀	50% inhibitory concentration
IEL	intraepithelial layer
IF	immunofluorescence
Ig	immunoglobulin
IgG	immunoglobulin G
Il-2	interleukin 2
Il2rg	interleukin 2 receptor common gamma chain encoding gene
Il2ry	interleukin 2 receptor common gamma chain
Il-7	interleukin 7
IMC	infectious molecular clone
IVC	individually ventilated cages
LANUV	Landesamt für Natur, Umwelt und Verbraucherschutz NRW
LC	Light chain
LP	lamina propria
LTR	long terminal repeat
MACS	magnetic-activated cell sorting
MHC	major histocompatibility complex
min	minute(s)
MM	Master mix
MSM	men having sex with men
nAb	neutralizing antibody
NEG	Negative control in the viral load measurement
NHP	non-human primate
NK	natural killer cells

NOD	non-obese diabetic
NRG	NOD.Cg-Rag1 ^{tm1Mom} Il2rg ^{tm1Wjl} /SzJ
NSG	NOD.Cg-Prkdc ^{scid} Il2rg ^{tm1Wjl} /SzJ
PBL	peripheral blood leukocytes
PBMC	peripheral blood mononuclear cells
PCR	polymerase chain reaction
PCR	polymerase chain reaction
PEI	Polyethylenimine
PEP	post-exposure prophylaxis
PrEP	pre-exposure prophylaxis
PTM	pigtailed macaque
qPCR	quantitative PCR
r.t.	room temperature
R5-tropic	exhibiting a tropism for CCR5
Rag	recombination activation gene
RCT	randomized controlled trial
RLU	relative light units
RNA	ribonucleic acid
RT	reverse transcriptase
s.c.	subcutaneous
SCID	severe combined immunodeficiency
SHIV	simian-human immunodeficiency virus
SIRP	signal-regulatory protein
SIV	simian immunodeficiency virus
SIV _{agm}	african-green-monkey-specific SIV
SIV _{cpz}	chimpanzee-specific SIV
SIV _{mac}	macaque-specific SIV
SIV _{sm}	sooty-mangabey-specific SIV
SM	sooty mangabey
SOP	standard operating procedure
SSA	sub-Saharan Africa
STD	Viral standard sample for qPCR
SV40	simian vacuolating virus 40
TALEN	Transcription activator-like effector nuclease
TC	T lymphocyte, T cell
TCID	tissue culture infective dose
TFV	tenofovir disproxil fumarate
TKO	triple knock-out
TOM	T-cell only mouse
TVT	Tierärztliche Vereinigung für Tierschutz e.V.

UCBC	umbilical cord blood mononuclear cells
UNAIDS	Joint United Nations Programme on HIV and AIDS
V _H	variable domain of the heavy chain
V _H H	variable domain of heavy-chain only antibody
V _L	variable domain of the light chain
VRC01	a bnAb targeting the HIV-1 env CD4-binding site
X4-tropic	exhibiting a tropism for CXCR4

1. Summary

The ongoing human immunodeficiency virus 1 (HIV-1) pandemic still remains without an effective vaccine so far. The predominant route of infection is via sexual intercourse rendering the mucosa the primary site of infection. Novel strategies in targeted prevention of HIV-1 transmission include the application of small molecules such as nanobodies. Nanobodies formed by *Camelidae spp.* are the smallest naturally occurring functional antibody fragments. Their long CDR3 loops resemble those of some broadly neutralizing HIV-1 antibodies. Their small size, acid-stability and the possibility of bacterial expression seem favourable features.

First *in vivo* testing is critical to select promising agents for further investigations. Animal models play a central and currently irreplaceable role in pre-clinical testing. Humanized mice are the most frequently used platform in HIV-1 research. They consist of an immunodeficient mouse strain harbouring a human immunograft. The extend of humanization varies significantly between graft types and mouse strains. As human graft, haematopoietic stem cells, mature leukocytes, lymphoid tissues and all combinations of the latter have been described. To address the mucosal route of HIV-1 transmission, a sufficient degree of human immune reconstitution at the site of infection is required. So far, only foetal tissue-reliant methods have allowed for consistent mucosal HIV-1 susceptibility. Due to ethical, legal and technical obstacles associated with utilization of foetal tissue, there is a research endeavour to obtain mucosally HIV-1 susceptible tissue-independent models.

This work addresses this unmet need by presenting and characterizing the novel CD34T+ mouse model. In a second step the model is readily employed to test the preventive potential of an HIV-1 specific nanobody in an *in vivo* setting.

The CD34T+ model is a modification of a well-established human hematopoietic stem cell based model with cells derived from cord blood. As murine genetic background NOD.Cg-Rag1^{tm1Mom} Il2rg^{tm1Wjl}/SzJ (NRG) mice were employed. We enhanced human reconstitution by additional injection of donor-matched mononuclear cells accompanied by human interleukin 7 (IL-7) administration. The human reconstitution was investigated by measuring human leukocyte populations in the peripheral blood and in distinct organ tissues via flow cytometry. In comparison to the original model, CD34T+ mice exhibited ubiquitously higher human T cell reconstitution and a consistent, significantly higher susceptibility to intrarectally applied HIV-1.

We conducted one of the first *in vivo* nanobody experiments in HIV-1 prevention employing the broadly neutralizing nanobody V_HH A6. CD34T+ mice were challenged intrarectally with either V_HH A6 or a non-HIV-1-specific nanobody alongside an infectious molecular HIV-1

clone. Blood viral loads were followed up for 6 weeks by RNA purification and quantitative reverse-transcription PCR. V_HH A6 exhibited a significant protective potential.

The novel CD34T⁺ mouse model is a valuable addition to current platforms used in pre-clinical HIV-1 prevention research due to its independence from foetal tissue and reliable mucosal HIV-1 susceptibility. As with all models it is essential to critically evaluate the suitability for the corresponding scientific question.

Nanobodies as passive immunity against HIV-1 have a promising potential. Our work contributed to the promotion towards clinical testing. This data can be regarded as a proof-of-principle experiment. Ensuing questions that require further investigation include the neutralization breadth against different HIV-1 strains, the nanobody's potential in the female genital tract and the functionality of bacteria expressed nanobodies *in vivo*.

2. Zusammenfassung

Das humane Immundefizienz-Virus 1 (HIV-1) ist Ursache einer andauernden weltweiten Pandemie. Eine effektive Impfung ist bislang nicht verfügbar. Der größte Anteil an Neuinfektionen ist auf sexuelle Übertragung zurückzuführen, womit die Mukosa den primären Infektionsort darstellt. Neuartige Strategien in der zielgerichteten HIV-1-Prävention beinhalten den Einsatz kleiner Moleküle wie Nanobodies. Nanobodies, die von Camelidae spp. gebildet werden, sind die kleinsten natürlicherweise vorkommenden wirksamen Antikörperfragmente. Im Gegensatz zu Immunglobulinen wie den humanen IgG-Subtypen, die ein Heterotetramer aus zwei leichten und zwei schweren Ketten sind, entsprechen Nanobodies ausschließlich der variablen Domäne einer schweren Kette. Sie ähneln einigen breit neutralisierend HIV-1-Antikörpern in den überdurchschnittlich langen CDR-3-Loops. Gleichzeitig weisen sie einige Eigenschaften auf, die für die klinische Anwendung vorteilhaft erscheinen: Ihre geringe Größe, Säurefestigkeit und die Möglichkeit einer bakteriellen Expression.

Die initiale *in-vivo*-Testung ist ein essentieller Schritt in Translation von *in-vitro*-Ergebnissen in mögliche klinische Anwendungen. Tiermodelle spielen in der translationalen HIV-Forschung weiterhin eine zentrale Rolle und sind in der präklinischen Testung neuer Substanzen aktuell unentbehrlich. Am häufigsten werden hier humanisierte Mausmodelle eingesetzt. Diese bestehen aus einer immundefizienten Mauslinie, die mit einem menschlichen Immunograft rekonstituiert wird. Der Grad der Humanisierung variiert signifikant zwischen verschiedenen transplantierten Geweben und Zellen sowie zwischen unterschiedlichen Mauslinien. Als humanes Transplantat werden hämatopoetische Stammzellen, reife Leukozyten, Lymphgewebe und alle daraus resultierenden Kombinationen verwendet. Um eine mukosale HIV-1-Übertragbarkeit im Mausversuch zu adressieren, ist eine hinreichende mukosale Immunrekonstitution mit HIV-1-empfindliche Zellen erforderlich. Bislang zeigen nur Mausmodelle, die auf der Verwendung von humanem fetalen Gewebe basieren, eine konsistente mukosale HIV-1-Infizierbarkeit. Die Verwendung von fetalem Gewebe unterliegt strengen gesetzlichen Regulationen und ist des Weiteren mit ethischen und technischen Hürden verbunden. Hieraus ergibt sich das Bestreben nach humanisierten Mausmodellen, die nicht auf fetalem Gewebe basieren und dennoch für die mukosale HIV-1-Infektion empfänglich sind.

Wir widmeten uns in dieser Arbeit daher der Entwicklung eines entsprechenden Modells. Hier wird das neue CD34T⁺-Mausmodell vorgestellt und charakterisiert. In einem zweiten Schritt wird das Modell direkt verwendet, um das präventive Potential eines HIV-1-spezifischen Nanobody in vivo zu untersuchen.

Das CD34T+-Modell ist eine Modifikation eines bereits etablierten Modells (CD34), das humane hämatopoetische Stammzellen aus Nabelschnurblut zur Rekonstitution verwendet. Als muriner genetischer Hintergrund wurden NOD.Cg-Rag1^{tm1Mom} Il2rg^{tm1Wjl}/SzJ (NRG) Mäuse verwendet. Den neugeborenen Mäusen wurden im Alter von maximal 5 Tagen nach Präkonditionierung mittels myeloablativer Radiation CD34+ humane Zellen injiziert. Nach 12 Wochen wurde die erfolgreiche Humanisierung mittels Durchflusszytometrie aus dem peripheren Blut überprüft. Wir stimulierten die humane Rekonstitution durch die zusätzliche Injektion von Spender-gematchten mononukleären Zellen begleitet von der Applikation von humanem Interleukin 7. Es konnte gezeigt werden, dass die humane T-Zell-Rekonstitution sowohl im peripheren Blut als auch in unterschiedlichen Organgewebe ubiquitär gesteigert war. Die verschiedenen Leukozytenpopulationen wurden mittels Durchflusszytometrie gemessen, die Präsenz der Zellen im Gewebe exemplarisch mittels Immunfluoreszenzfärbung bestätigt. Die erhöhte Rekonstitution mit T-Zellen korrelierte mit einer signifikant erhöhten HIV-1-Übertragbarkeit durch intrarektale Exposition. Die Übertragung konnte durch eine Kombination breit neutralisierender Antikörper verhindert werden, was die Eignung als Plattform für die Erforschung präventiver Wirkstoffe bestätigte.

In dieser Arbeit führten wir eins der ersten *in-vivo*-Experimente mit einem HIV-1-spezifischen Nanobody durch. Wir verwendeten den *in-vitro* breit HIV-1 neutralisierenden Nanobody V_HH A6. CD34T+ Mäuse wurden intrarektal mit V_HH A6 und einem infektiösen HIV-1-Klon behandelt. Als Kontrolle diente ein nicht-HIV-1-spezifischer Nanobody parallel zu derselben Virusexposition. Wir verfolgten die HIV-1-Viruslast im Blut der Mäuse über 6 Wochen mittels RNA-Aufreinigung aus peripherem Blut und anschließender quantitativer reverser PCR. V_HH A6 zeigte ein signifikantes präventives Potential.

Das neue CD34T+ Mausmodell ist eine wertvolle Ergänzung zu bisherigen Plattformen in der präklinischen HIV-1-Präventionsforschung aufgrund seiner verlässlichen mukosalen HIV-1-Empfänglichkeit und seiner Unabhängigkeit von fetalem Gewebe. Wie bei allen Modellen ist die kritische Evaluation der Limitationen erforderlich und die Eignung für die jeweilige wissenschaftliche Fragestellung zu prüfen.

Nanobodies als passive Immunisierung gegen HIV-1 zeigen ein vielversprechendes Potential. Unsere Arbeit trägt zur Translation in die klinische Testung bei. Die erhobenen Daten können im Sinne eines Proof-of-Principle-Experimentes gewertet werden. Es schließen sich weitere Fragestellungen an, so insbesondere bezüglich der Neutralisationsbreite gegen verschiedene HIV-1-Varianten *in vivo*, der Wirksamkeit im weiblichen Genitaltrakt sowie der Funktionalität von bakteriell exprimierten Nanobodies.

3. Introduction

3.1. The Human immunodeficiency Virus 1 (HIV-1)

The human immunodeficiency virus 1 (HIV-1)² is a human pathogenic member of the genus *Lentivirus* in the family of *Retroviridae*. Common features of lentiviruses are the establishment of chronic infection and comparably long incubation periods until clinical disease manifestation³. HIV-1 virions contain the viral genome as single stranded RNA and viral proteins necessary for cell invasion and integration of the viral genome into the host's cellular DNA including a reverse transcriptase (RT) enzyme⁴. The virions are enveloped in lipid membrane material taken up from the releasing host cell and carry a single viral protein, the envelope protein (Env) which is exhibited in comparably low density⁵, while being one of the most heavily glycosylated of viral glycoproteins^{6,7}. Env mediates cell attachment by interaction with its primary cellular receptor cluster of differentiation 4 (CD4) and a secondary receptor, either C-X-C motif chemokine receptor type 4 (CXCR4) or C-C motif chemokine receptor type 5 (CCR5). Corresponding HIV-1 strains are designated as X4-, R5- or dual-tropic respectively³. Their target cells are CD4+ T cells (TC) and to some extent other CD4+ cell populations like macrophages^{1,8}.

An unprecedented genetic diversity is observed in HIV-1, both between different as well as within one infected individual, mainly attributed to the RT's high mutation rate and frequent recombination within dual-infected host cells⁴.

HIV-1 descends from simian immunodeficiency viruses (SIVs), of which it is closest related to chimpanzee-specific SIV (SIV_{cpz})⁹. First published as a new symptom complex in 1981^{10,11} the clinical manifestation of an HIV-1 infection received its contemporary name as acquired immunodeficiency syndrome (AIDS) in 1982¹². A year later the causing agent was first isolated¹³. HIV-1 infection can lead to a progressive decline in the infected population of CD4+ T cells, ultimately impairing the adaptive immune response and allowing for opportunistic infections and tumours³.

HIV-1 gave rise to an ongoing pandemic that remains without an effective vaccine so far¹⁴. In 2022 there were around 39 million people worldwide living with HIV, of which the vast majority can be attributed to HIV-1¹⁵, including 1.3 million new infections and 630,000 deaths due to AIDS in 2022 according to UNAIDS¹⁶. 4 phylogenetic groups of HIV-1 are distinguished (M, N, O and P) each of which is believed to have arisen from a separate transmission from primates to humans¹⁷. Group M is responsible for the ongoing HIV-1 pandemic and further subdivided

into as yet the nine subtypes A-K⁴ of which subtype C is predominant accounting for around 45% of all HIV-1 infections worldwide¹⁸.

The HIV-1 pandemic exhibits a drastically uneven global distribution with the African continent and sub-Saharan Africa (SSA) in specific representing the majority of new cases world-wide¹⁶. In this key population, especially the risk for young women is to be emphasized. Whilst only representing around 10% of the population, women aged 15-24 years form 80% of the occurring HIV infections¹⁹. Besides various socioeconomic and educational factors, also biological aspects render women especially vulnerable since many approved pharmacological prevention tools appear to be less efficient in transmission through the female genital tract (FGT) in comparison to rectal or penile exposure²⁰. AIDS and AIDS-related conditions are the primary cause of death in young women in SSA²¹.

3.2. Mucosal HIV-1 transmission and prevention strategies

3.2.1. The modes of transmission in majority of new HIV-1 infections

HIV-1 can be transmitted by contact to free virus containing body fluids or exposure to infected cells through different routes. The three predominant ways of HIV-1 transmission are namely mother-to-child transmission (vertical transmission), intravascular exposure and mucosal transmission during sexual intercourse²², the latter occasioning approximately 70% of new infections. It is thus the epidemiologically largest target for preventive measures²².

3.2.2. Pivotal steps in mucosal HIV-1 transmission and established preventive measures

Mucosal transmission can be subdivided into different steps and prevention methods can be assigned to their site of action:

- (1) Presence of HIV-1 in the secretion of the infected individual
- (2) Contact of HIV-1 containing secrete with the partner's mucosal epithelium
- (3) Attachment to a target cell and induction of cell entry
- (4) Establishment of productive infection in the cell and dissemination in the body

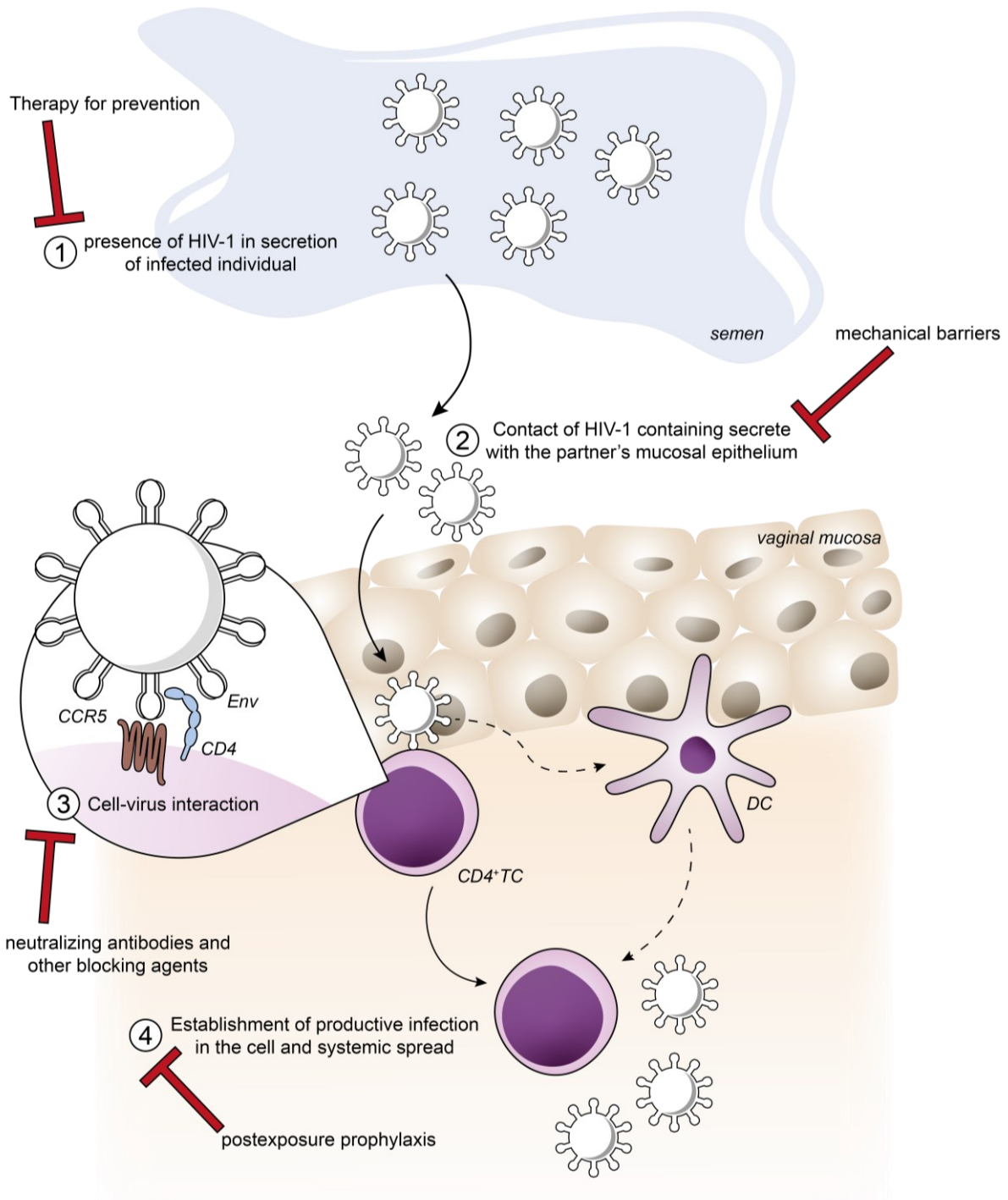


Figure 3.1 course of vaginal HIV-1 infection through infected semen depicting targets for prevention

Noteworthy a distinct microenvironment contributes to altered risks¹ (not depicted in figure). Description from top to bottom: Infectious virus particles from semen come into contact with the vaginal mucosa. When reaching cells carrying the required surface receptors CD4 and CCR5 (or less frequently CXCR-4 is engaged as coreceptor), cell-virus interaction including conformational changes of the Env trimer take place and ultimately mediate cell entry. The virus establishes productive infection in the cell which travels through the lymph vessels and spreads infection eventually leading to disseminated infection.

CD4⁺TC CD4 positive T cell, DC dendritic cell, dotted arrows indicate the hitherto controversial involvement of DCs in the mucosal HIV infection

The concentration of viral RNA in the blood (viral load) is a suitable surrogate parameter for its concentration in other body fluids such as semen or vaginal secretion. The higher the viral load, the more likely the transmission of virus due to mere stochastics²². This reveals the potential of efficient therapy in preventing transmission.

Combination antiretroviral therapy (ART) consists of drugs targeting various critical steps of the viral replication cycle. ART has not only revolutionized HIV-1 treatment. It drastically reduces viral loads, even below detection limits⁵. Observational studies unambiguously present that therapy of the positive partner can reduce risks by magnitudes^{23,24} and the proclaimed concept of “Undetectable = untransmissible” (U = U) proved true in multiple large clinical studies in heterosexual intercourse as well as in men having sex with men (MSM)⁵. However, access and adherence moderate efficacy⁵.

Inhibitors of the reverse transcriptase have also been established as either pre- or post-exposure-prophylaxis (PrEP and PEP) and proved their potential in a range of clinical trials²⁵. Oral PrEP with either tenofovir disoproxil fumarate (TFV) or emtricitabine (FTC) is regarded as safe^{25,26}. The overall risk reduction of HIV-1 infection throughout 11 different placebo-controlled clinical trials was around 51%²⁵. The effectiveness of PrEP was demonstrated to be highly moderated by medication adherence; in studies with an adherence rate below 40%, there was no significant effect of PrEP detectable²⁵.

A mechanical rather than biochemical method of HIV-1 transmission prevention consists of the use of condoms or other barrier methods. By their nature the effectiveness of barrier methods HIV prevention is difficult to assess since data on correctness and frequency of use can only be anamnestically gathered. However, an effectiveness of around 80% in preventing heterosexual transmission is estimated²⁷.

3.2.3. Cell-virus interaction and viral cell entry

The entry of HIV-1 virions into target cells requires interaction between the heterotrimeric Env and its main receptor CD4 on cell surfaces initiating a conformational change of Env allowing for interacting with the secondary receptor CCR5 or CXCR4²⁸. Noteworthy the vast majority of transmitted initial viruses (so-called founder viruses) are R5-tropic rendering CCR5 the predominant co-receptor in mucosal HIV-1 transmission²². This stable cell attachment enables the virion to fuse with the cellular membrane and release its content into the cell²⁸. Cell attachment can be inhibited by molecules that interfere at critical binding sites on either the cellular receptors or Env epitopes.

3.3. Compounds with neutralizing activity against HIV-1 in the prevention of mucosal transmission

3.3.1. The adaptive immune system interacts with pathogens at the site of infection by formation of neutralizing antibodies

Neutralization of viruses can be defined as the ability to bind to critical structures on viral surfaces that block steps within the cell attachment or invasion consequentially inhibiting cell infection²⁹.

The human body is capable of forming highly specific antibodies (Abs) against a broad variety of pathogens, a process that usually takes place during an infection or artificially induced by vaccine immunogens. In brief, activation of B cells (BC) is either mediated directly through their B cell receptor (BCR) or T cell dependent and causes somatic hypermutation towards a BCR with high affinity against the corresponding bacterial, viral, fungal or other antigen. The BCR is a transmembrane protein whose soluble part represents the immunoglobulin (Ig) or Ab. There are 5 different Ig classes determined and class switch is known to be guided by a certain microenvironment of cytokine signalling.

IgG, the most abundant Ig class³⁰ is a heterotetramer of two identical light (LC) and two identical heavy (HC) chains arranged in a Y-like shape³¹. The LC is subdivided into two subunits, one highly conserved throughout the Ab repertoire referred to as the constant domain (C_L) and the other highly variable between different Abs, designated the variable domain (V_L). In analogy, the HC also exhibits a variable domain (V_H) and its constant part consists of 3 consecutively numbered domains (C_{H1} , C_{H2} , C_{H3}). The conjunction of two variable domains (V_L and V_H) forms the antigen binding face and is present twice in the IgG. In both V_H and V_L , the antigen specificity is mediated by 3 variable loops, the so-called complementary determining regions (CDRs)³². The paired C_{H2} and C_{H3} of the two HCs together form the crystallisable fragment (F_c) which mediates a variety of functions including immune cell recruitment through F_c receptor signalling, complement activation and protection from degradation³³. The IgG tetramer is interconnected by disulphide bonds formed between the HC and LC at the C_{H1} domain of the HC and between the two HCs in the so-called hinge region between C_{H1} and C_{H2} ³⁰.

Functionally, Igs bind to epitopes on pathogens and can tag them to attract cellular immunity or the complement system. Furthermore some Abs are intrinsically capable of virus neutralization and termed neutralizing antibodies (nAbs)²⁹.

3.3.2. Broadly neutralizing antibodies against HIV-1 occur in a small subset of infected individuals throughout the course of infection

Env is the only viral protein exhibited on HIV-1 virion surfaces and therefore the only target for Abs mediating neutralization³⁴. HIV-1 incorporates a variety of mechanisms to evade nAb responses. The low density of Env trimers per virion renders it comparably little immunogenic³⁵. The enormous genomic diversity is also reflected in Env constraining Abs to target highly conserved regions for broad neutralization. High conformational flexibility and extensive glycosylation³⁶ hide these vulnerable epitopes and prevent Ab binding to these faces³⁵.

When studying the natural response to HIV-1 in infected individuals a common scheme can be found: The initial Ab response is insufficient and does not neutralize all circulating viruses³⁵. After a few months, Abs with the ability of neutralizing some viruses are elicited, viral diversification in the meantime easily overcomes this immune response³⁵. Throughout the course of infection, the neutralization breadth of Abs increases and in a fraction of infected individuals, Abs with neutralizing activity against a broad range of HIV-1 strains, so-called broadly neutralizing Abs (bnAbs) can be detected. Around 1% of HIV-1 positive individuals harbour bnAbs with exceptionally high potency and large neutralization breadth against HIV-1^{37,38}. These so-called elite neutralizers are often not capable of clearing the virus off the system and also only seldomly maintain ability to suppress viral replication continually³⁹. Nevertheless their bnAbs are of interest in the preventive setting, since protection is less challenging than maintaining viral suppression in view of a highly accommodable virus^{22,34}.

Those bnAbs have some unique features that are rarely observed in human Abs which emphasizes the difficulties in eliciting those⁴⁰. BnAbs commonly exhibit a high extent of somatic hypermutation; on average over 30 mutations per antibody V_H sequence are found whereas below 20 mutations are observed for conventional IgG^{41,42}. A long CDR3 is another characteristic shared throughout bnAbs, which has been shown to be advantageous in reaching conserved epitopes by forming a penetrating loop⁴³.

3.3.3. Neutralization breadth of bnAbs can be quantified *in vitro*

In view of the diversity of circulating HIV-1 strains, it is a major task to spot those nAbs with favourable neutralization profiles and render nAb neutralization breadth objectively comparable. Different reference panels of HIV-1 Env strains have been compiled and remain under constant evaluation⁴⁴. HIV-1 Envs differ in their sensitivity to nAbs mainly due to the stochastic likelihood of different conformational states wherein Envs with frequent open

conformation are more easily accessible for nAbs⁴⁴. Correspondingly, HIV-1 strains are categorised into the 4 tiers 1A, 1B, 2 and 3, 1A being the most and 3 the least sensitive tier⁴⁴. With regard to the tier distribution throughout circulating strains, a broad neutralization of tier 2 strains appears to be aspired in order to mediate protection⁴⁴.

3.3.4. bnAbs can mediate protection from HIV-1 infection *in vivo*

Many different bnAbs have been identified so far and progressed from *in vitro* characterisation to animal studies and clinical trials for both treatment and prevention. Whilst single bnAbs have repeatedly been shown to be insufficient in suppressing viral replication^{45,46}, combinations of different bnAbs have the potential to effectively control infection in animal models^{47,47}. A recent combination bnAb small-scale randomized controlled trial (RCT) in infected humans has also found the potential for sustained control without emergence of escape variants throughout the yet short time of observation of 24 months⁴⁸.

The preventive potential of bnAbs is also currently assessed both pre-clinically and clinically. Despite promising data from animal experiments⁴⁹, results from two RCTs employing VRC01 underlined the higher requirements in a clinical setting⁵⁰. Whilst hinting at protection against VRC01 sensitive HIV-1 strains, overall risk of acquisition was not reduced⁵⁰. Noteworthy, rational combination of bnAbs has not yet been studied sufficiently in preventive settings⁵¹ and further insight is an important starting point of current and future clinical studies.

3.4. Nanobodies in HIV-1 prevention

3.4.1. Nanobodies are the smallest naturally occurring functional Ab fragments

The formation of Abs is a crucial component of the adaptive immune response throughout vertebrates. The heterotetrameric overall structure of conventional Abs is highly conserved and comparable across species.

First described in 1993⁵², *Camelidae* (including camels, llamas and dromedaries) exhibit a remarkable and to current knowledge peerless exception throughout mammals. In their bloods, three IgG subclasses occur, two of which (IgG2 and IgG3 respectively) do not possess a C_H1 domain and consecutively no adjacent L chain, thereby being naturally occurring heavy chain only Abs (HCAb)^{32,52,53} (see also Figure 3.2). The F_{ab} fragment of these HCAb is thereby only formed from the H chain and the corresponding domain is termed V_HH. HCAb exist alongside the conventional tetrameric IgG1 and it has been demonstrated that responses to pathogens

mount both Ab types in parallel³². The proportion of HCAb of all circulating IgG varies between camelid species and may be as high as 80% in camels⁵⁴.

The V_{HH} of HCAb is of particular clinical interest, since it can independently bind to its antigen which is not the case for conventional V_H domains that rely on the interaction with V_L ³². The recombinant V_{HH} is therefore regarded as the smallest naturally occurring functional Ab fragment in mammals with a size of around 15 kDa⁵⁵ which lead to the name nanobody³².

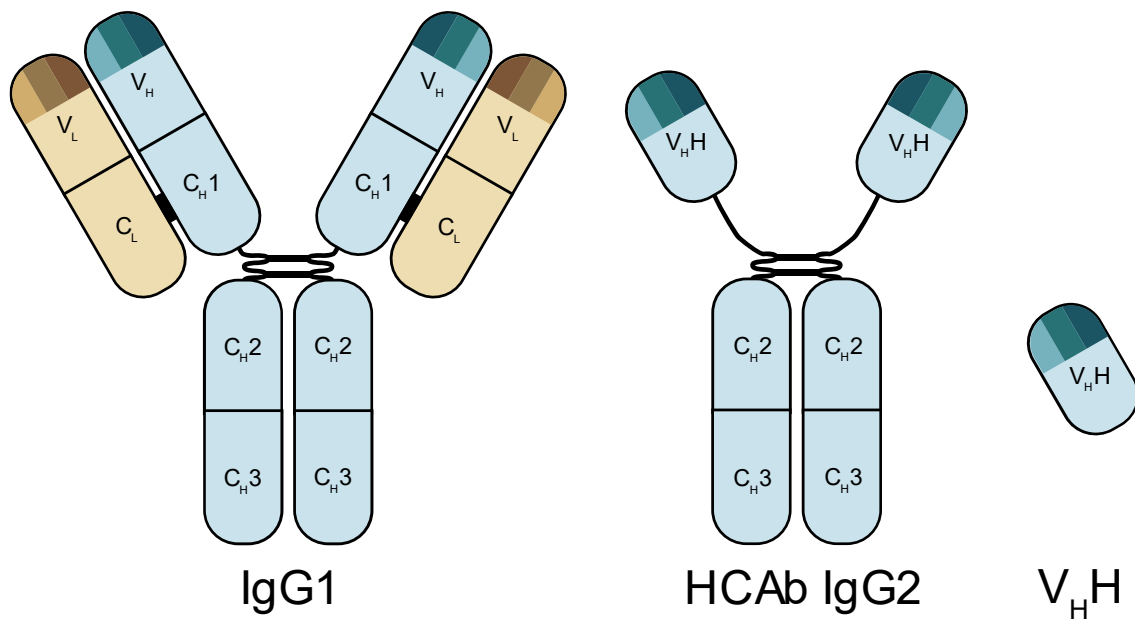


Figure 3.2 schematic illustration of V_{HH} in comparison to HCAb and IgG1

Depicted are from left to right the heterotetrameric structure of an quintessential Ig, a heavy-chain-only Ab as naturally occurring in the family of *Camelidae* and its smallest antigen-binding fragment, the V_{HH} . Heavy chain depicted in light blue, light chain in beige. Each variable domain (V_H , V_L and V_{HH}) contains 3 CDRs, signified by the 3 colour shades on top of the domain.

Illustration is not true to scale.

3.4.2. Considerations on favourable features of nanobodies against HIV-1

Whilst the artificial construction of conventional IgG derived V_H only fragments leads to impaired functioning, natural selection has apparently overcome these restrictions in V_{HH} ³². V_{HH} are highly soluble in contrast to human V_H only fragments⁵⁶. They also possess an increased heat-resistance and can be easily produced in large scale by bacterial cells due to their single chain structure⁵⁶.

As outlined a major obstacle in the generation of neutralizing Abs against HIV-1 is the protection of highly conserved and vulnerable epitopes on the HIV-1 virion mainly by extensive glycosylation³⁶. Structural and sequential analysis of bnAbs have revealed some common

features that are rare in human Abs. One of these is a protruding CDR3 loop of the V_H allowing for recognition of antigens despite heavy glycosylation⁴³. Longer CDR3 loops with an average length of around 15 aa versus 13 aa in human IgG are an indigenous feature of V_HH with additional mechanisms such as additional disulphide bonds for stabilisation readily in place⁵⁷. The increased CDR length is believed to compensate for the absence of a V_L domain³².

Nanobodies against HIV-1 have been generated and isolated by several researcher groups^{58,59}. An established work-flow to generate HIV-1 specific V_HH is sketched in Figure 3.3.

Nanobodies have readily proven their broad neutralization potential against a variety of HIV-1 reference strains⁵⁸. The nanobody with the broadest neutralizing activity in the described study is termed A6⁵⁸ and has a CDR3 length of 18aa⁵⁸ which is consistent with the increased CDR3 length being advantageous^{43,60}. V_HH A6 exhibited neutralising potential against 16 out of 21 tested HIV-1 pseudoviruses in previous analysis⁵⁸. Its IC₅₀ values against the most sensitive strains were as low as 0.012 µg/mL by that keeping totally up with highly potent bnAbs³⁴. Neutralization was present against all tested Tier 1 strains, some Tier 2 and 3 strains showing highest activity against Clade B and C whilst none was observed against Clade A and recombinant circulating strains CRF07/BC. Interestingly, other nanobodies isolated alongside with V_HH A6 were found to have somewhat complementary sensitivities which affords the opportunity for a combination of V_HHs to broaden the neutralization spectrum⁵⁸. *In vivo* potency of nanobodies against HIV-1 had not been assessed prior to this work.

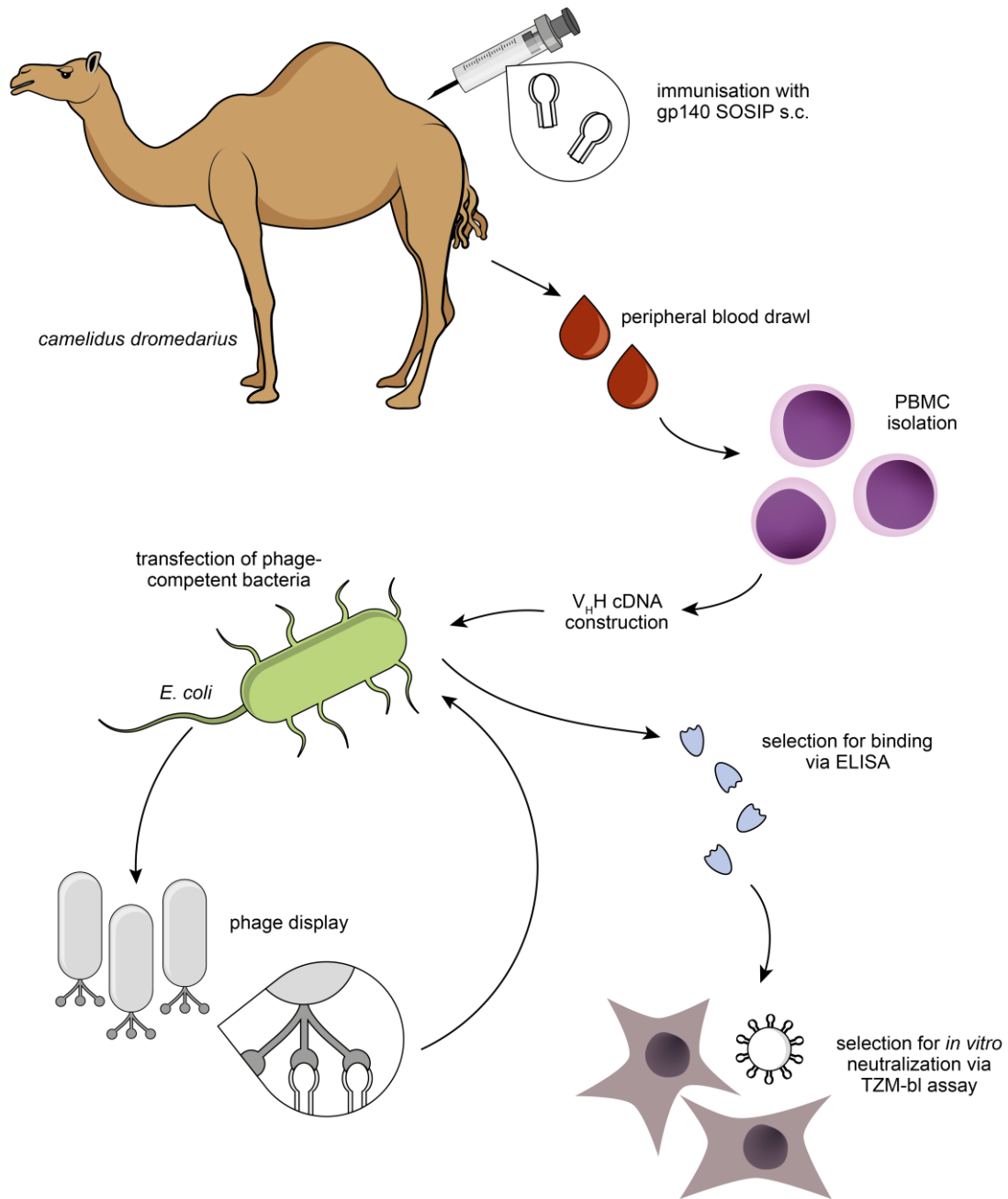


Figure 3.3 Simplified workflow of the generation of neutralizing nanobodies

Nanobodies can be isolated from immunised animals and characterised as depicted. Dromedaries are immunised with a suitable immunogen, in case of HIV-1 most frequently a stabilised soluble Env trimer construct (gp140 SOSIP) by subcutaneous injection. Different timelines are followed but repeated administrations followed by a delayed booster are favourable. After immunisation, peripheral blood is obtained and PBMCs are isolated. CDNA is synthesized and V_H cDNA is selectively amplified by nested PCR and ligated into a phagemid to introduce it into phage-competent bacteria eventually superinfected with a phage. Phage display is used for screening and primary selection of gp140 SOSIP specific V_H. The circular arrow arrangement indicates several rounds of selection. Obtained V_H are further selected by ELISA and eventually neutralization assays against pseudo- and infectious viruses. Figure based on [14, 80, 125].

3.5. Animal Models for Prevention Studies

3.5.1. General criteria of suitable animal models

As for all models, animals utilized to model HIV infection do not mimic the entirety of the situation in humans. Suitable animal models require the susceptibility to HIV-1 or a considerably similar lentivirus. On a cellular level, HIV-1 susceptibility implicates both presence of the proteins involved in the viral replication cycle and absence of fatal restriction factors⁶¹. The endeavours to create and improve HIV-1 animal models are as old as the knowledge of the virus itself⁶².

It appears to stand to reason to employ non-human primates (NHPs) since HIV-1 is a direct descendant from the chimpanzee specific SIV (SIV_{cpz}) which is endemic in some chimpanzee populations^{61,63} and NHPs are the closest relatives of humans incorporating reasonable host similarities⁶⁴.

On the other hand, small rodents including mice and rats have a long history of being utilized as animal models for human diseases and have notable advantages regarding their availability.

In the following, the available animal models will be described in further detail including their advantages and disadvantages.

3.5.2. NHP models

HIV-1 is a descendant of SIV¹⁷ which includes a range of species-specific viruses⁶¹. Occasionally cross-species transmission occurred and lead to either non-productive isolated cases or gave rise to productive spread within a new species and consecutively the formation of a new species-adapted strain¹⁷ as it was eventually the case with HIV-1^{17,65}.

3.5.2.1. HIV-1 in NHPs

Despite HIV-1 being derived from SIV_{cpz}, chimpanzees are seldomly susceptible to it^{17,61}. Resistance to HIV-1 in chimpanzees and other Old World Monkeys (*Catarrhini*) is caused by multiple restriction factors along the viral replication cycle. Slight but essential alteration of molecular structures explain the low rate of productive cross-species transmission of SIVs. Most New World Monkey (*Platyrrhini*) species support HIV-1 infection to a certain extent⁶⁶ but do not develop any clinical symptoms. Besides, they are phylogenetically more distinct from humans limiting their relevance as a suitable animal model⁶⁴.

3.5.2.2. SIV in NHPs

SIVs are endemic in more than 40 different African primate species and have long been believed to be apathogenic for their natural hosts⁶¹. Whilst this turned out to be untrue for HIV-1 precursor SIV_{cpz} in chimpanzees, it is confirmed for SIV strains in sooty mangabeys (SM) and African green monkeys (AGM)⁶⁷.

Despite exhibiting an initial CD4+ cell decline the further course of apathogenic SIV infection in SM and AGM is characterised by CD4+ cell recovery⁶⁸. Chronic immune impairment and subsequently progression to AIDS are absent⁶⁵. A factor contributing to the pathogenicity of SIV_{cpz} and HIV-1 might be the alteration of co-receptor usage⁶⁷ that occurred in the divergence of SIV_{cpz} from other strains. All of the most closely related SIV strains, including SIV_{agm} in AGMs and SIV_{sm} in SMs use CXCR6 as a co-receptor, whilst SIV_{cpz} and HIV-1 do not possess this feature and consequentially infect different cell populations⁶⁷.

Investigations into the phylogeny of primate lentiviruses has led to a differentiated knowledge of the origins of HIV-1¹⁷. Furthermore, outlining how avirulence in natural SIV hosts is mediated allows insight into critical steps of viral pathogenesis revealing potential HIV-1 treatment targets. However, altered co-receptors for viral entry render them rather unsuitable for prevention experiments.

SIV_{cpz} infection in chimpanzees is associated with increased mortality, decreased fertility and a CD4+ cell depletion in post-mortem analyses¹⁷. Many pieces of evidence hint at SIV_{cpz} being a rather young SIV strain¹⁷. However practical and ethical factors contribute to chimpanzees not being considered as a research platform. They exhibit many behavioural features of humans, including complex social interactions and emotions. Obtaining a sufficient number of individuals required for significant results is barely feasible in terms of cost, equipment and facilities⁶⁹. In addition, their endangered status deters from carrying out chimpanzee experiments, being therefore prohibited in an increasing amount of countries including entire Europe^{70,71}.

The first known pathogenic SIV strain was SIV_{mac} in captive Asian macaques in 1985 and was traced back to prion disease monkey experiments in which they were unwittingly exposed to SIV_{sm}. Artificially enforced animal-to-animal passage bore the opportunity for the virus to adapt^{61,72,73}. SIV_{mac} infected macaques develop an AIDS-like disease including predisposition for opportunistic infections accompanied by progressive loss of CD4+TCs⁷². Despite these similarities to HIV-1, some considerable differences are also present. The latent chronic infection phase is shorter in macaques and they tend to reach the AIDS stadium within 1-2

years after infection⁶¹. Notably the genetic similarity is only around 53% leaving a lot of drugs targeting HIV-1 structures ineffective against SIV_{mac}⁶¹. SIV_{mac} rarely gains ability to interact with CXCR4 as co-receptor like HIV-1 commonly does, but interacts with co-receptors that HIV does not^{61,67,74}.

Macaques are the predominantly used NHP platform in HIV-1 research and especially in pre-clinical vaccine testing⁷⁵. Even though less expensive and more available than chimpanzees, also the utilization of macaques grapples with limited availability and achieving sufficiently high numbers of animals per experiment⁷⁵.

3.5.2.3. SHIV and HSIV

Derived from the findings about restriction factors against productive HIV-1 infection in NHPs were aims to engineer a recombinant virus with the most possible resemblance to HIV-1 whilst still being infective for NHPs. In brief, either HIV-1 genes can be introduced into SIV (creating so-called SHIV) or, coming from the other side, SIV genes can be introduced into an HIV-1 clone (termed HSIV correspondingly).

The most frequently exchanged gene in SHIV is *env*⁶¹ leaving a corresponding model suitable for Env-targeting vaccination and prevention measures. It turned out that the first generated SHIVs despite being highly pathogenic to the macaques also seemed rather easy to be neutralized by vaccine-elicited Abs⁶¹ which is proposed to be related to these SHIV strains evolving to an X4 tropism much rather than remaining R5 tropic. Additionally they were highly sensitive to Abs elicited in the infected individuals which is not the case for acute HIV-1 infections in humans⁷⁶. More recent attempts emphasizing the creation of R5-tropic SHIV strains with Env proteins from founder HIV-1 variants⁷⁷ seem to resemble HIV-1 more closely.

A HSIV clone only altered in its *vif* gene was shown to lead to a longer lasting viraemia compared to its HIV-1 ancestor⁷⁸ in pigtailed macaques (PTMs)⁶¹. When investigating its potential adaption to the new host, changes in the *env* gene were found causing a higher affinity to the macaque CD4 viral receptor but however could not be shown to have any impairments on the infectivity in human cells *in vitro*⁷⁹. Notably, for this HSIV the same dual tropic *env* genes from HIV_{89.6} that evolved towards X4-tropism in first generation SHIV strains⁷⁸.

The generation of chimeric SHIV and HSIV variants is a still refining approach to reduce differences to HIV-1 in humans on a molecular level.

In summary, NHPs in combination with pathogenic SIV or more recently SHIV and HSIV have a major advantage regarding the intact immune system allowing for studies of the immune

response including the induction of an active immunity by vaccination. However, transferability of NHP studies should be treated with reasonable care. In the past, essential differences between HIV-1 in humans and the artificial infection of NHPs with SIV or chimaeras have been revealed retrospectively as mentioned for the illusive successes in vaccinating macaques against SHIV.

Noteworthy, the utilization of NHPs has some major practical constraints due to high costs of maintaining a primate facility, the limited availability of animals and their rather long life-span and generation times implicating long experiment durations. Their inter-individual variation leads to large fluctuations in susceptibility to the virus as well as altered immune responses and requires appropriately large numbers of experiment animals that are often not achieved.

Especially for first-*in-vivo* and large scale testing of a variety of direct antiviral substances, smaller, cheaper and more uniform animals appear preferential.

3.5.3. Humanized mouse models

Initial attempts in infecting small rodents with HIV-1 were unsuccessful⁸⁰. Various reasons were determined including restriction factors and lack of the required virus receptors⁶¹. Transgenic modification of mice and rats^{81,82} enabled hCD4 and hCCR5 expression allowing HIV-1 cell-entry but yet without productive replication⁸³.

The observation of mice with a genetic condition leading to an inherited severe immunodeficiency (SCID) being engraftable with human immune cells became the starting point for the generation of so-called humanized mice (huMice). HuMice became a generic name for a vast variety of mouse models based on the concept of an immunodeficient host engrafted with a human immune system to a certain extent. The research on huMice is looking back on many major ameliorations since the descriptions of very first prototypes in 1988⁸⁴. However there is currently a broad range of available huMouse models for HIV-1 research, each bearing its limitations and advantages and none incorporating the entirety of the human immune system. The following is aimed to serve as an overview of the most relevant available models, their drawbacks and potential questions to assess with.

All humanized mouse models are based on two founding pillars:

- a. the immunodeficient genetic background of the mouse strain allowing for a human engraftment
- b. the human graft and its introduction route

Especially in the recent developments further modifications have been made or suggested which contain two major aspects:

- c. enhancement of the humoral environment required for human immune differentiation and functionality
- d. reconstitution of a human microbiome

Technically, all existing versions of these features can be combined amongst themselves. However some combinations developed to be used most frequently. In order to allow an overview, the features will primarily be regarded distinctly and consequentially the most relevant models will be described.

3.5.3.1. Immunodeficient genetic background

Since the first successful human engraftment in a mouse strain called SCID mice⁸⁵ a variety of genetic backgrounds was determined to extend host immunodeficiency and improve human engraftment.

The SCID mutation affects the *Prkdc* gene, encoding the catalytic subunit of the DNA-dependent protein kinase (DNA-PK), which is crucial for repair of double-strand (ds) DNA breaks as occurring during T and B cell receptor rearrangement or through radiation induced DNA damage⁸⁶. The SCID mutation averts lymphocyte maturation but also renders the mice highly radiation-sensitive. Furthermore it is regarded as “leaky” allowing for low levels of functional T and B cells nevertheless⁸⁶. Human engraftment is only transient since the unimpaired innate immunity still counteract the foreign tissue⁸⁶.

The non-obese diabetic (NOD) genetic background has multiple mutations of both innate and adaptive immunity favourable for human engraftment. In addition to the eponymous insulinitis by autoreactive TCs, NOD mice also exhibit reduced natural killer (NK) cell and complement activation⁸⁷. This additionally lessens a potential disturbing factor in HIV-1 research since murine complement effectively counteracts HIV-1 virions⁸⁸. A polymorphism in the signal-regulatory protein α (SIRP α) reduces phagocytosis of human cells^{89,90}.

Backcrossed NOD-SCID mice exhibit a non-diabetic phenotype⁸⁷ with significantly lower graft rejection compared to SCID mice. However, the NOD-SCID strain has a significantly shortened life span due to the development of thymoma⁸⁷.

In contrast to *Prkdc*, the recombination activation genes 1 and 2 (*Rag1* and *Rag2*)⁹¹ are exclusively expressed during lymphocyte maturation and do not interfere with ds damage

repair mechanisms thus retaining normal radiation tolerance⁹². Rag mutations are non-leaky and absence of either gene fully bans BC and TC maturation⁹¹. NOD-*Rag1*^{-/-} or NOD-*Rag2*^{-/-} mice are also not thymoma-prone.

As observed in X-linked SCID, the interleukin (Il) 2 receptor common gamma chain (*Il2rg*) was determined as another versatile target structure of the immune system. Despite its name, *Il2rg* serves as subunit to Il receptors 2, 4, 7, 9, 15 and 21⁹³. The homozygotic knockout of the *Il2rg* gene (*Il2rg*^{tm1Wjl})⁹⁴ therefore interrupts a broad range of important signalling pathways, which inhibits NK cell formation⁹³ and impairs dendritic cell (DC) signalling⁹⁵.

Currently, either the *scid* mutation *Prkdc*^{scid} or the *Rag1* null mutation *Rag1*^{tm1Mom} and the *Il2rg* null mutation *Il2rg*^{tm1Wjl} on a NOD background are basis to the two most frequently employed strains for HIV-1 research in huMice⁹². Their formation denotations⁹⁶ are

- NOD.Cg-*Prkdc*^{scid}*Il2rg*^{tm1Wjl}/SzJ
(common name **NSG** mice, Jackson Laboratories Strain #:005557^{85,94})
- NOD.Cg-*Rag1*^{tm1Mom}*Il2rg*^{tm1Wjl}/SzJ
(common name **NRG** mice, Jackson Laboratories Strain #:007799^{91,94})

Despite the prevention of thymomas in NSG mice through the introduction of the *Il2rg*^{null} mutation⁹⁵ reduced survival rates are observed in both NRG and NSG mice compared to NOD-*Rag1*^{null} or NOD-SCID mice respectively when transplanted with human haematopoietic stem cells (hHSCs)⁹². The engraftment of human cells however is significantly increased in both strains⁹². Noteworthy, all strains possessing the *Il2rg*^{null} mutation suffer from incomplete architecture of the secondary lymphoid tissues⁸⁹, which also affects the development of engrafted human cells as outlined below. NRG mice are advantageous over NSG mice in irradiation studies due to their preserved radio-tolerance⁹².

Research in the field of genetic backgrounds for huMice appears to be by far not completed. Several approaches are pursued in order to improve human reconstitution and reduce graft-versus-host-disease (GvHD)^{70,97}. Efforts are also made to further diminish the remaining murine immune system, which mediates host-versus-graft reactions (HvGR) and might warp experimental results in huMice e.g. when mounting an own response against an investigated pathogen⁹⁸. In order to reduce GvHD, antigenic recognition of xenogenic tissue needs to be circumvented. Therefore “murine” recognition markers are either abolished or substituted with the human correlate. For example a knockout in the gene encoding CD47 leads to reduced GvHD rates⁹⁹ in the so-called triple knock-out mice (B6 TKO, formally B6.129S-*Rag2*^{tm1Fwa}*CD47*^{tm1Fpl}*Il2rg*^{tm1Wjl}/J with a C57BL/6 background (Jackson Laboratories stock

#:000664)). B6 TKO mice allow for high levels of human cell reconstitution in blood, bone marrow and secondary lymphoid tissues¹⁰⁰. They have a functional complement system¹⁰⁰ which, as aforementioned, bears the risk to overestimate protection against HIV-1 due to direct HIV-1 counteraction⁸⁸.

Introduction of a deficiency in the major histocompatibility complex (MHC) I or II encoding crucial proteins for self and foreign distinction on cell surfaces into NSG mice delays GvHD when engrafted with human peripheral blood mononuclear cells (hPBMCs)⁹⁸ which is however not the case when employing hHSCs instead⁹⁸.

Despite the significant facilitation of generating transgenic mice through techniques such as TALENs and CRISPR, the identification of appropriate target genes however remains challenging and subject to current research⁷⁰.

3.5.3.2. Human graft

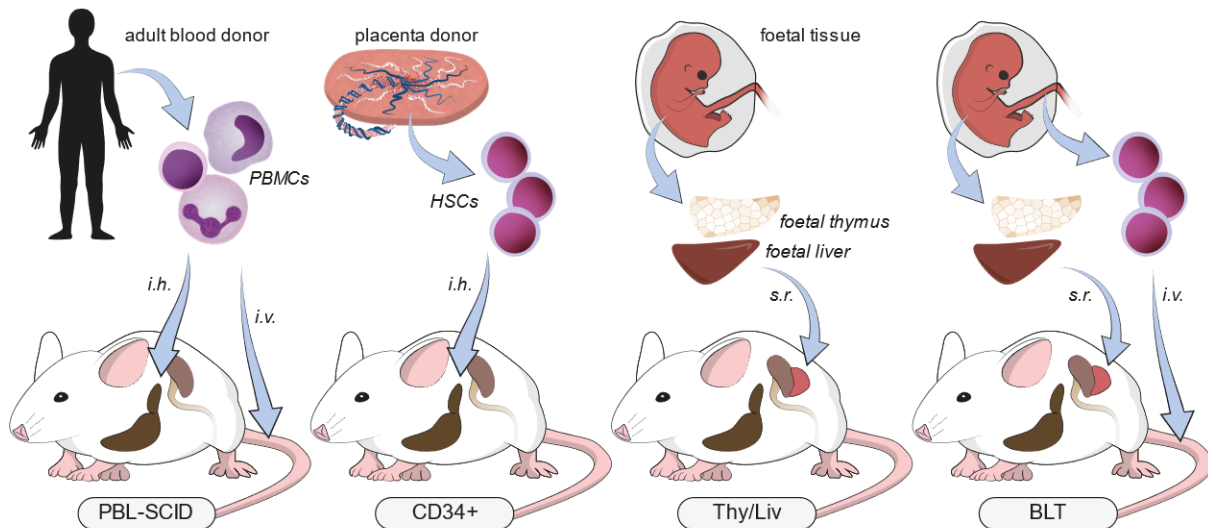


Figure 3.4 Schematic overview of the four most common engraftment methods in humanized mice

From left to right: hPBMCs from peripheral blood of adult blood donors can be introduced intrahepatic (*i.h.*) or intravenous (*i.v.*), the first description of this method resulted in the peripheral blood leukocyte (PBL) SCID model. HSCs can be isolated from umbilical cord and placenta blood obtained from donors, these are injected *i.h.*, usually to new-born pups (not depicted), resulting in hCD34+ mice (CD34+ model). Foetal thymic and liver tissue can be transplanted together, usually beneath the renal capsule, giving rise to a new conjoint organoid. When used exclusively, the resulting model is referred to as Thy/Liv mice. It can be combined with the administration of donor matched HSCs, that are injected *i.v.* resulting in the bone marrow liver thymus (BLT) model.

3.5.3.2.1. Peripheral blood derived mononuclear cells (PBMCs)

The simplest approach for human immune cell engraftment in mice utilizes hPBMCs from adult blood donors. PBMCs can be administered through different routes. Established regimes include intravenous (*i.v.*), intraperitoneal (*i.p.*), intrahepatic (*i.h.*) or intrasplenic (*i.s.*) injections⁷⁰. Mice engrafted with hPBMCs are also commonly referred to as hu-PBL-mice (human peripheral blood leukocytes mice)⁷⁰. After engraftment, human cells are measurable in various murine organs. The engraftment rate, determined by presence of hCD45+ cells in the peripheral blood or organ tissue is practically 100%¹⁰¹. It is possible to modify the immune reconstitution by pre-selecting the PBMCs and e.g. exclusively transferring certain cell populations. With a non-depleted PBMC graft, the reconstitution in hu-PBL mice consists of mature lymphocytes, predominantly CD3+ TCs with some extend of BCs whilst other leukocytes are not stably detectable¹⁰¹. Since the human graft consists of mature cells which are recognizing the murine tissue as foreign, the PBMC engraftment is usually followed by a rapid human immune cell activation and consecutively the development of TC mediated GvHD within a few weeks, which prohibits the employment in long-term experiments^{97,102}. The expanding human TCs become activated due to recognition of foreign in the mice by that mounting a xenoreactive response⁷⁰. Hu-PBL-mice therefore are not a model for the physiological human immune homeostasis.

HIV-1 infection is usually introduced by *i.v.*, *i.s.* or *i.p.* administration of virus or directly by transferring HIV-1 infected PBMCs from patient blood. Hu-PBL-mice appear predominantly unsusceptible to mucosal HIV-1 infection. Successful infection through these routes was highly variable which drastically limits the employment of this model for prevention studies¹⁰³

Thus, hu-PBL-mice exhibit certain important limitations making them unsuitable for mucosal prevention experiments with their main application field in addressing allograft rejections or immune pathologies like autoimmunity¹⁰¹.

The application of immature human immune cells in contrast aims to establish their differentiation in the host, leading to improved host tolerance and a more complete human immune system with the potential capacity to mount physiological immune responses of both innate and adaptive pathways.

3.5.3.2.2. Human haematopoietic stem cells

HSCs exhibit the capacity to renew themselves and give rise to all lymphoid and myeloid cell populations³³. HSCs, defined by the expression of hCD34, can be obtained from various sources: In adult humans, CD34+ cells are located in the bone marrow and can be mobilized into the periphery by G-CSF application¹⁰¹. Furthermore, hHSCs are located in the blood-

building foetal liver and in umbilical cord blood. It was shown that engraftment of foetal and cord hHSCs is more efficient than employment of adult hHSCs⁸⁹.

A differentiation of multiple human immune cell lineages can be achieved by employment of HSCs derived from umbilical cord blood¹⁰⁴. The best results in terms of human reconstitution have been achieved by a procedure containing a preconditioning of the already immunodeficient mice (most commonly NSG and NRG as described above) by sublethal irradiation⁹⁷. Consecutively the hHSCs can be administered by variable routes. Feasibility depends on whether adult mice or new-born pups are transplanted. In adults, *i.v.* or intraosseous injection into the femoral bone (*i.o.*) are most common whereas in pups, intracardiac (*i.c.*), intrahepatic (*i.h.*) or *i.v.* administration routes are predominant¹⁰⁵. Intrinsic homing signals of the HSCs lead to a migration into the bone marrow, where consecutively the human haematopoiesis is located. Naïve TCs travel to the murine thymus where they mature into functional CD4+ or CD8+ TCs. The multilineage maturation results in the formation of TCs, NK cells, monocytes, DCs and BCs that are detectable throughout all tissues. However, whilst precursors of all myeloid cells including erythrocyte progenitors and megakaryocytes are well engrafted in the bone marrow, their peripheral blood circulation is poor¹⁰². That has exemplarily been shown to be caused by the absence of the required human cytokines to mediate mobilisation, homing and activation and can be overcome by the admission of the same¹⁰². Noteworthy, employing new-born mice ameliorates the TC reconstitution since immunodeficient mice like NRG or NSG mice in the absence of lymphocytes otherwise only form a poorly developed thymus¹⁰⁵.

CD34+ mice can be infected with HIV-1 by *i.p.* and *i.v.* application with high infection rates. Mucosal susceptibility is however low and highly variable¹⁰⁶ despite some reports about consistent and high transmission rates¹⁰⁷.

3.5.3.2.3. Foetal tissue

The usage of foetal thymus and liver tissue leads to the generation of human thymus/liver mice (hu-Thy/Liv mice). The established procedure consists of the implantation of human foetal thymus and liver tissue caudally of the kidney capsule of the mouse. The implant forms a new conjoint organ that gets vascularized and has been shown to allow for differentiation of the foetal liver derived HSC into naïve TCs, both cytotoxic (CD8+) and T helper (CD4+) cells¹⁰⁸. In hu-Thy/Liv mice, human TCs are systemically present, while other human cell lines are barely detectable^{108,109}. In this setting, human TC maturation takes place under the mediation of autologous human thymus stromal cells resulting in MHC restriction. Despite the robust and

sustainable TC development, immune function and peripheral reconstitution is rather low. HIV-1 infection was initially only attainable by direct injection of virus into the conjoint organ¹¹⁰. By increasing the amount of human tissue implanted per host, a systemic susceptibility can be introduced and disseminated HIV-1 infection is achievable through *i.p.* inoculation¹¹⁰. However, mucosal infection still remains ineffective. Another advance was made by using the NSG instead of the NOD/SCID background, that also lead to better systemic TC reconstitution. The NSG background Thy/Liv model was designated as T-cell only mice or TOM¹⁰⁹.

Besides the biological aspects of foetal tissue employment, ethical and legal restrictions have to be acknowledged. The use of foetal tissue for research objectives is e.g. prohibited in Germany¹¹¹.

3.5.3.2.4. *Combination of foetal tissue and CD34+ cells*

The combination of foetal tissue and stem cell transfer consists of the implantation of foetal thymus and liver tissue accompanied by the *i.v.* injection of donor-matched HSCs¹¹². In the first description of this method, mice received the thymus and liver transplant at 6 to 8 weeks of age. Previously, parts of the liver tissue were used to isolate CD34+ cells that were consecutively kept frozen until used. After 3 weeks, the mice were preconditioned by sublethal irradiation and received the prepared CD34+ cells intravenously¹¹².

BLT mice have human MHC restricted TCs capable of mounting an immune response to human viruses such as EBV¹¹². Their cell engraftment throughout all leukocyte populations is higher compared to HSC-only mice¹⁰⁷. Importantly, BLT mice show the overall highest human cell reconstitution in the gut mucosa and exhibit a distinct lymph node architecture⁷⁰.

One major shortcoming of BLT mice on the NSG background is their development of fatal GvHD¹¹³. Histopathological features of GvHD are virtually present in all successfully engrafted individuals. When investigating the molecular characteristics of the BLT mice' GvHD, it can be argued that their major strength – the human TC functionality is their draw-back at the same time, since the inflammation is predominantly CD4+ TC mediated¹¹³. Differentiation and maturation in a human thymic tissue allows formation of a competent immune response against pathogens whilst at the same time mimicking reactions similar to chronic GvHD and eventual loss of host tolerance¹¹³. CD34+ mice in contrast experience human TC maturation in a murine thymus which leads to a detectable population of mature TCs tolerating both autologous human and murine cells whilst showing reactivity to allogenic human cells¹¹⁴. This observation is consistent with the lower rate of GvHD in CD34+ mice compared to BLT mice¹¹⁴.

Importantly the B6-TKO genetic background engrafted with the BLT method resulting in B6-TKO BLT mice leads to a comparable phenotype of human cell reconstitution in blood and tissue but seldomly experience GvHD¹⁰⁰.

3.6. Aims of this thesis

The HIV-1 pandemic is still ongoing and the declared UNAIDS goals in reducing new infections by 75% from 2010 to 2020 drastically failed.

The predominant route of transmission is by far during sexual intercourse. Therefore the most effective preventive measures should target the risk of mucosal infection. To accelerate and improve research in this field, suitable animal models remain currently without alternative. Small animal models allow the testing of more different approaches in shorter time intervals in comparison to NHP models. However, most of the current humanized mouse models have major restrictions due to their limited human immune reconstitution. So far, only the BLT mouse serves as a solid model for mucosal HIV-1 transmission with consistent reports of mucosal infectability throughout different research groups. Since its generation is challenging and relies on the usage of foetal tissue implicating moral and ethical restrictions in various countries, a mouse model independent of foetal tissue and complex surgical procedures for mucosal HIV-1 transmission is required. The US National Institutes of Health have repeatedly pointed out the great relevance for improved and non-foetal tissue relying mouse models for a variety of purposes including HIV-1 research and announced their funding support (NOT-AI-19-040 and NOT-OD-19-042).

This work aims to enlarge the repertoire of reliable and feasible mouse models for the exploration and testing of novel compounds in the prevention of mucosal HIV-1 transmission. We present and characterize the novel CD34T+ mouse model as a foetal tissue independent humanized mouse model with enhanced mucosal human CD4+ cell reconstitution and consistent mucosal HIV-1 susceptibility.

Nanobodies have many structurally, pharmacologically and practically favourable features making them promising new precise compounds counteracting HIV-1 at the site of infection. Despite an elaborate *in vitro* characterisation of different anti-HIV-1 nanobodies, *in vivo* data is still very limited. We aimed to conduct one of the first *in vivo* studies with the nanobody V_HH A6 as potential protection against mucosal HIV-1 transmission. This work focusses on the transferability of the *in vitro* neutralization activity into a mucosal exposure setting as a proof-of-concept study. The novel and previously characterized CD34T+ model was chosen as *in vivo* testing platform.

4. Materials and Methods

4.1. Materials

4.1.1. Mice

For all mouse experiments of this project, we employed mice with a NOD.Cg-Rag1^{tm1Mom} Il2rg^{tm1Wjl}/SzJ (NRG) background⁹². This strain is based on a NOD background with two additional mutations, a knockout of *Rag1* and a complete null allele of the *IL2rg*.

The mice were purchased from The Jackson Laboratory (JAX stock #007799) and maintained through breeding in the Decentralized Animal Facility Cologne as part of the Humanized Mouse Core Cologne (HMCC). They were always kept under specific-pathogen-free conditions in a system of individually ventilated cages (IVC) at a 12h day-night circadian rhythm. Food was provided ad libitum employing ssniff®¹¹⁵ complete feed products (Ssniff Spezialdiäten GmbH, Soest, Germany, “Rat/Mouse – Maintenance” for maintenance or “Mouse Breeding” for breeding).

4.1.1.1. Handling of the mice

All treatments were performed according to hygienic standards and cages were only opened under sterile conditions. All mouse experiments were authorized under the protocol AZ.84-02.04.2015.A353 by the State Agency for Nature, Environmental Protection and Consumer Protection North Rhine-Westphalia (LANUV).

4.1.1.1.1. Anaesthesia

If necessary to ensure work safety or to minimize suffering of the animals, the mice were anesthetized by placing them into an induction chamber (UNO Induction Box and Gas Exhaust Unit, For Medical Instruments, Seeheim-Ober-Beerbach, Germany), that was connected to a ventilation with regulatable mixture of oxygen and isoflurane (UniVet Porta, Groppler Medizintechnik, Deggendorf, Germany) as well as an outlet leading the gas through an anaesthetic gas filter (Contrafluran™ Narcosegasfilter, ZeoSys Medical, Luckenwalde, Germany) and a scavenger system (Lab Active Scvanger (L.A.S.), Groppler Medizintechnik, Deggendorf, Germany). Isoflurane proportion was set to 2-3%. In the induction chamber, mice were under intensive visual observation of respiratory frequency and muscle tone. After an accurate decline in respiratory frequency indicating a sufficient anesthetization, mice were

taken out and during the entire procedure and afterwards well observed for physiological regain of consciousness.

4.1.1.1.2. Submandibular vein bleeding

For all analysis methods requiring peripheral blood samples, mice were bled the necessary volume of blood from the submandibular vein according to the Recommendations for blood sampling in laboratory animals published by the GV-SOLAS and TVT¹¹⁶. For all procedures performed in the S3** safety area, mice were anesthetized (4.1.1.1.1). Mice were restrained by scuffing a large fold of the neck. Puncture site was located at the middle between ear and eye and punctured with a 5 mm animal lancet (Goldenrod, MEDpoint Inc., Mineola, NY, USA). Blood was collected by holding an EDTA microtube (Microtube 1.3 mL, K3-EDTA, Sarstedt, Nümbrecht, Germany) below puncture site. After blood collection, restraining was loosened and the wound was checked for haemostasis. If necessary, wooden cotton-tipped sticks (150 mm, AMPri, Winsen/Luhe, Germany) were used to stop bleeding by moderate pressure. Mice were consequentially replaced into the cages.

4.1.2. Viruses

HIV1 NL4-3_{YU2} (infectious molecular clone HIV-1_{YU2} in pNL4-3)¹¹⁷

HIV-1 NL4-3_{BAL} (infectious molecular clone HIV-1_{BAL} in pNL4-3)¹¹⁷

4.1.3. Cells

4.1.3.1. Human Umbilical Cord blood derived hematopoietic stem cells (hHSCs) and Human Umbilical Cord blood derived mononuclear cells (hUCBCs)

Placental and umbilical cord blood cells were isolated from placenta donors from the University Clinic Cologne or the Evangelisches Krankenhaus Weyertal who had afore given their informed written consent under the protocols 16-110 and 18-420 approved by the Institutional Review Board of the University of Cologne.

In brief, after Caesarean section, the placenta and umbilical cord were collected from the clinic. All further steps were performed under sterile conditions. The material was visually checked for damage to blood vessels or placenta tissue. The distal end of the cord was cut in an appropriate length to fit above a beaker with 2 mL of 0.1 M EDTA to prevent collected blood from clotting. For an effective perfusion of the blood vessels, the two umbilical arteries and one umbilical vein were identified. With respect of the original circulation, the umbilical vein could

be punctured with a cannula and perfused primarily with 50 mL of heparin followed by HBSS++++ solution and all cord blood collected in the beaker. The tissue turning pale indicated the successful perfusion.

All collected cord blood was slowly transferred into a tube prefilled with Histopaque®-1077 (Sigma-Aldrich®, Merck KGaA, Darmstadt, Germany) at a relation of 2:1 blood to Histopaque®-1077 and centrifuged at $400 \times g$ for 30 min at room temperature (r.t.) without acceleration or brake. The interphase containing mononuclear cells was collected with a serological pipet and transferred into a new tube prefilled with 1X PBS/E. The cell suspension was washed twice by centrifugation and resuspension in fresh 1X PBS/E containing a counting step in-between using a Neubauer improved counting chamber (4.2.1). Afterwards, the cell suspension was centrifuged, supernatant was discarded and the resulting pellet was resuspended in pre-cooled MACS-buffer. The CD34 MicroBead Kit UltraPure human (Miltenyi Biotec, Bergisch Gladbach, Germany) was applied according to the manufacturer's recommendations. It is based on the principle of magnetic cell separation (MACS) and contains magnetic beads binding to CD34 on cell surfaces. The suspension was administered onto an LS column (Miltenyi Biotec, Bergisch Gladbach, Germany) in a QuadroMACS™ Separator (Miltenyi Biotec, Bergisch Gladbach, Germany) as per manufacturer's recommendations and the labelled CD34+ fraction was eluted utilizing the provided plunger. The separated fractions (flow through containing UCBCs and the eluted fraction of CD34+ labelled cells, HSCs) were counted using a Neubauer improved chamber (4.2.1) and frozen in freezing medium consisting of 90% heat-inactivated foetal bovine serum (FBS) and 10% DMSO at -150°C at a concentration of 40×10^6 cells/mL for the UCBCs and 2×10^6 cells/mL for the HSCs.

4.1.3.2. Human peripheral blood mononuclear cells (hPBMCs)

HPBMCs were isolated from buffy coats provided by the blood bank from the Institute of Transfusion Medicine at the University Hospital of Cologne obtained as by-products of blood donations under informed consent by the donors following an established protocol¹¹⁸.

The buffy coats were collected in Heparin or EDTA blood collection tubes (Vacutainer™, Becton, Dickinson and Company, Franklin Lakes, NJ, USA). Primarily, samples were added to a falcon tube prefilled with HBSS at a ratio of 1:1. The dilution was well mixed using a serological pipet. The buffy coat HBSS mixture was slowly added on top of ACCUSPIN™ tubes (Sigma-Adrich, St. Louis, MO, USA) prefilled with 15 mL Histopaque®-1077 (Sigma-Aldrich®, Merck KGaA, Darmstadt, Germany) without mixing phases. The loaded tubes were centrifuged

at $900 \times g$ for 15 min without break or acceleration to separate cells. The interphase containing PBMCs was collected with a serological pipet and transferred into a new tube.

The PBMC enriched suspension was washed twice with 30 mL HBSS to reduce the platelet numbers, centrifugation was carried out at $400 \times g$ for 5 min at r.t. Cells were counted using a Neubauer improved chamber (4.2.1). Finally they were resuspended in the corresponding volume of freezing medium to obtain a concentration of 40×10^6 cells per mL. Cell suspensions were frozen in 1 mL aliquots at -80°C .

4.1.3.3. TZM-bl cells

The TZM-bl cells (also named JC53BL-13 cells) were obtained from the NIH AIDS Research & Reference Reagent Program, Division of AIDS, NIAID, Germantown, USA, Dr. John C. Kappes, Dr. Xiaoyun Wu and Tranzyme Inc.^{119–121}. This cell line is derived from HeLa cells and stably expresses the surface markers CD4, CCR5 and CXCR4, by that allowing infection by HIV-1 strains of all tropisms¹²⁰. Furthermore, a reporter gene for firefly luciferase and Escherischia coli β -galactosidase both under the control of the HIV-1 long terminal repeat (LTR) had been introduced so that an accurate quantification of infection in a culture is possible^{121,122}. TZM-bl cells grow adherently and were maintained in T-75 culture flasks (Sarstedt, Nümbrecht, Germany) under sterile conditions. The cell growth medium consisted of DMEM medium (Gibco™, Thermo Fisher Scientific, Waltham, MA, USA) supplemented with 10% heat-inactivated FBS and 50 $\mu\text{g}/\text{mL}$ gentamicin. The cells were split every few days using trypsin/EDTA to detach the cell layer, washed in medium and maintained at 37°C and 5% CO_2 .

4.1.3.4. HEK293T cells

HEK293T (293T) cells were obtained from the American Type Culture Collection (ATCC, CRL-11268™). The cell line is derived from the human embryonal kidney cell line 293 (HEK293) established in 1973 by van der Eb and Graham¹²³, containing a plasmid for Simian Vacuolating Virus 40 large T antigen (SV40T)¹²⁴. When utilizing plasmid DNA exhibiting the SV40 origin of replication, they exhibit a high production of the corresponding encoded product.

293T cells grow adherently as a monolayer. They were kept in 293T culture medium consisting of DMEM medium (Gibco™, Thermo Fisher Scientific, Waltham, MA, USA) supplemented with 10% FBS, 1% Pen/Strep, 1 mM sodium-pyruvate and 1 mM L-Glutamine and grown in T-75 flasks (Sarstedt, Nümbrecht, Germany) under sterile conditions. They were split every 2-3 days using trypsin/EDTA to detach the cell layer¹¹⁸.

After 18 to 24h, cells usually reached a density occupying 60% of the plate surface which was determined as the optimal density for transfection.

4.1.3.5. 293-6E cells

The 293-6E cell line was provided by the National Research Council Canada. Cells were kept at sterile conditions in FreeStyle293 Expression Medium DMEM (Gibco™, Thermo Fisher Scientific, Waltham, MA, USA) supplemented with 0.2% Pen/Strep incubating on a shaker at 120 rpm, 37°C and 6% CO₂ and split every day dependent on their density aiming for a final concentration of 0.5 x 10⁶ cells/mL. When utilizing for transfection with Ab plasmids, a cell concentration of approximately 0.8 x 10⁶ cells/mL was aimed for.

4.1.4. Equipment

Equipment	Name, Specifications and Company
Anaesthetic Gas Filter	Contrafluran™ Narkosegasfilter ZeoSys Medical GmbH, Luckenwalde, Germany
Autoclave	Type VX-150, SN 2820 Systec GmbH, Wettenberg, Germany,
Automated Nucleic Acid Extraction Machine	QIAcube classic QIAGEN GmbH, Hilden, Germany
Centrifuges	Eppendorf Centrifuge 5810 R Eppendorf Centrifuge 5424 R Eppendorf AG, Hamburg, Germany
Flow cytometer	BD FACSAria Fusion Flow cytometer Becton, Dickinson and Company, Franklin Lakes, NJ, USA
Fluorescence Microplate Reader	TriStar ² S LB 942 Berthold Technologies GmbH & Co. KG, Bad Wildbad, Germany
Heating Block	hlc Block Thermostat HBT130 HLC - Haep Labor Consult, Bovenden, Germany
Incubator	CO ₂ Incubator PHCbi PHC Europe B.V., Etten-Leur, The Netherlands
Isoflurane Evaporator	UniVet Porta Groppler Medizintechnik, Deggendorf, Germany
IVC Mouse Cages	IVC Blue Line SealSafe Tecniplast GmbH, Hohenpeißenberg, Germany
IVC Ventilation System	SmartFlow Air Handeling Unit (AHU) Tecniplast GmbH, Hohenpeißenberg, Germany
Laboratory Anesthesia Scavenger	Lab Active Scvanger (L.A.S.), UV 17014 Groppler Medizintechnik, Deggendorf, Germany
Light Microscope	Leica DM1000 Leica Mikrosysteme Vertrieb GmbH, Wetzlar, Germany
Magnetic Activated Cell Separator	QuadroMACS™ Separator and MultiStand Miltenyi Biotec B.V. & Co. KG, Bergisch Gladbach, Germany

Microvolume Spectrometer	NanoDrop™ One ThermoFisher Scientific™, Waltham, MA, USA
Mouse Dissection Equipment	Fine Surgical Instruments for Research™ Fine Science Tools GmbH, Heidelberg, Germany
- Surgical Scissors (Sharp-Blunt)	
- Tissue Forceps (1x2 Teeth)	
- Extra Fine Graefe Forceps	
Multichannel Pipets	BRAND™ Transferpette™ S 100µL, 300µL Brandt® GmbH & Co KG, Wertheim, Germany
Narcosis Induction Box	UNO Induction Box and Gas Exhaust Unit For Medical Instruments GmbH, Seeheim-Ober-Beerbach, Germany
Neubauer Improved Counting Chamber	Type ZK01-ZK06 A. Hartenstein GmbH, Würzburg, Germany
Peristaltic Pump	120S/D1 Peristaltic Pump Watson-Marlow GmbH, Rommerskirchen, Germany
Plate Cooler	Eppendorf™ PCR Cooler, 022510509 Eppendorf AG, Hamburg, Germany
qPCR Light Cycler	QuantStudio™ 5 Real-Time PCR System, 96-well 0.2 mL ThermoFisher Scientific, Waltham, MA, USA
Serological Pipettor	accu-jet® pro Brandt® GmbH & Co KG, Wertheim, Germany
Singlechannel Pipets	Glison PIPETMAN Classic P2, P20, P200, P1000 Glison®, Middelton, WI, USA
Sterile Workbench	Mars Class 2, LaboGene™, Allerød, Denmark ThermoScientific™ Maxisafe 2020 Class II Biological Safety, ThermoFisher Scientific, Waltham, MA, USA
Vortex Mixer	neoLab Vortex-Mixer Genie® 2 Migge GmbH, Heidelberg, Germany
Water bath	Waterbath WNB 7 Memmert GmbH + Co. KG, Schwabach, Germany
X-ray Irradiation System	MultiRad160, Serial-No.: 2329A60113 Faxitron Bioptics, LLC, Tucson, AZ, USA

4.1.5. Consumables

Consumable	Name and Company
18 G syringe needle	Sterican® Safety G 18 x 1 1/2" 1,2 x 40 mm B. Braun AG, Melsungen, Germany
96-well flat bottom black plate	96 Well Solid Microplate, flat bottom, black polystyrene Corning® Corning Inc., Corning, NY, USA
96-well flat bottom plate	96 Well Clear Polystyrene Microplate, flat bottom, Corning® Corning Inc., Corning, NY, USA

96-well conical bottom plate	Microplate, 96 well, conical, polystyrene, transparent, Sarstedt AG & Co. KG, Nümbrecht, Germany
adhesive plate seal	Applied Biosystems® MicroAmp® Clear Adhesive Film Thermo Fisher Scientific, Waltham, MA, USA
Alcohol-based surface disinfectant	Bacillo® AF Paul Hartmann AG, Heidenheim, Germany
Animal lancets 5 mm	Goldenrod MEDpoint Inc., Mineola, NY, USA
Bottle Top Filter	0.45 µm Bottle Top Filter w/ PES Membrane, Nalgene™ Rapid-Flow™ Thermo Fisher Scientific, Waltham, MA, USA
cell strainer	Pore size 40 µm (Cat.-No. 352340), Pore size 70 µm (Cat.-No. 352350), Falcon® Cell Strainer, Sterile Corning, Inc., Corning, NY, USA
centrifugation tubes for protein concentration	Amicon® Ultra-0.5 Centrifugal Filter Unit MWCO 10kDa, Amicon® Ultra-4 Centrifugal Filter Unit MWCO 30kDa Merck Millipore, Merck KGaA, Darmstadt, Germany
centrifuge tube for density isolation of leukocytes	ACCUSPIN™ Tubes Sterile Sigma-Adrich, St. Louis, MO, USA
Centrifuge Tubes	15 mL and 50 mL Falcon® Corning Inc., Corning, NY, USA
Cotton-tipped applicators	Disposable wooden stick cotton buds, 150 mm AMPri Handelsgesellschaft mbH, Winsen/Luhe, Germany
EDTA blood collection tube	BD Vacutainer™ K2-EDTA, 6 mL Becton, Dickinson and Company, Franklin Lakes, New Jersey, USA
EDTA microtube 1.3 mL	Microtube 1.3 mL, K3-EDTA Sarstedt AG & Co. KG, Nümbrecht, Germany
FACS tubes	5 mL Round Bottom Polystyrene Tubes w/ 35 µm cell strainer Falcon®, Corning Inc., Corning, NY, USA
Filter Tips	Biosphere® Filter-Tips P2, P20, P200, P1000 Sarstedt AG & Co. KG, Nümbrecht, Germany
Glass Columns	Econo-Columns 0.7 x 15 cm ² and 1.5 x 20 cm ² (Cat.-No.: 7370717, 7371522) Bio-Rad GmbH, Feldkirchen, Germany
Heparin blood collection tube	BD Vacutainer™ sodium heparin, 6 mL Becton, Dickinson and Company, Franklin Lakes, New Jersey, USA
Insulin syringe	Single use syringe U-100-Insulin (0,5 mL / 50 I.U.), B. Braun AG, Melsungen, Germany
LightCycler® Plates	LightCycler® 480 Multiwell Plates 96, Roche Molecular Systems, Inc. F. Hoffmann-La Roche Ltd, Basel, Switzerland
LightCycler® Sealing Foils	LightCycler® 480 Sealing Foils, Roche Molecular Systems Inc., F. Hoffmann-La Roche Ltd, Basel, Switzerland
MACS Columns	LS Columns, Miltenyi Biotec B.V. & Co. KG, Bergisch Gladbach, Germany
Nuclease Removal Solution	RNase AWAY®, Carl Roth GmbH + Co. KG, Karlsruhe, Germany

NuPAGE BisTrisGel	Invitrogen™ NuPAGE™ 10%, Bis-Tris, 1.0–1.5 mm, Mini Protein Gels, Thermo Fisher Scientific, Waltham, MA, USA
Safe-lock 1.5 mL Tubes	Safe-Lock Tubes, Eppendorf Quality™, Eppendorf AG, Hamburg, Germany
Serological pipet	Serological pipette, plugged, 2 mL, 5 mL, 10 mL, 25 mL, 50 mL Sarstedt AG & Co. KG, Nümbrecht, Germany
sterile filtration tubes	Ultrafree-CL or Ultrafree-MC (Cat.-No. UFC40GV02, UFC30GV0S), Merck KGaA, Darmstadt, Germany
T-25 cell culture flask	Cell culture flask, T-25, material: PS, surface: Suspension, for suspension cells, Sarstedt AG & Co. KG, Nümbrecht, Germany
T-75 cell culture flask	Cell culture flask, T-75, material: PS, surface: Cell+, for challenging adherent cells, Sarstedt AG & Co. KG, Nümbrecht, Germany
terminal disinfection reagent	Korsolex® basic, Paul Hartmann AG, Heidenheim, Germany
threeway stop-cock	Discofix C, B. Braun AG, Melsungen, Germany
Tubing	Precision Tubing, 0.8 mm inner diameter (913.A008.016), Watson-Marlow GmbH, Rommerskirchen, Germany
virucidal disinfectant	Sterillium® Virugard, Paul Hartmann AG, Heidenheim, Germany

4.1.6. Kits

Kit	Details and Manufacturer
CD34 MicroBead Kit UltraPure, human	Order-No.: 130-100-453, Miltenyi Biotec B.V. & Co. KG, Bergisch Gladbach, Germany
TaqMan™ RNA-to-CT™ 1-Step Kit	Cat.-No.: 4392653, Applied Biosystems® ThermoFisher Scientific, Waltham, MA, USA Stored at -15 to -25°C
QIAGEN RNase-Free DNase Set	Cat.-No.: 79254, QIAGEN GmbH, Hilden, Germany
QIAamp® MinElute® Virus Spin Kit	Cat.-No.: 57704, QIAGEN GmbH, Hilden, Germany

4.1.7. Reagents and Chemicals

Chemical or Reagent	Specifications and Company
Antibiotic-Antimycotic	Antibiotic-Antimycotic (100X), Gibco™ ThermoFisher Scientific, Waltham, MA, USA
ATP disodium salt	Adenosine 5'-triphosphate disodium salt hydrate, M = 551,14 g/mol, stored at -20°C Sigma-Aldrich®, Merck KGaA, Darmstadt, Germany
BSA	Bovine Serum Albumin, lyophilized powder, ≥96% Sigma-Aldrich®, Merck KGaA, Darmstadt, Germany

CoA	Coenzyme A sodium salt hydrate, M = 767,53 g/mol, stored at -20°C Sigma-Aldrich®, Merck KGaA, Darmstadt, Germany
Collagenase	Collagenase D from <i>Clostridium histolyticum</i> Sigma-Aldrich®, Merck KGaA, Darmstadt, Germany
Counting Beads for Flow Cytometry	CountBright™ Absolute Counting Beads, Invitrogen™, stored at 4°C and light protected, ThermoFisher Scientific, Waltham, MA, USA
DEAE-Dextran	Diethylaminoethyl-Dextran, M ~ 500,000 g/mol, Sigma-Aldrich®, Merck KGaA, Darmstadt, Germany
Dispase II	Protease from <i>Bacillus polymyxa</i> , Sigma-Aldrich®, Merck KGaA, Darmstadt, Germany
D-Luciferin	4,5-Dihydro-2-(6-hydroxy-2-benzothiazolyl)-4- thiazolecarboxylic acid sodium salt, LUCNA, Proven and Published®, Stored desiccated at -20°C, light-protected, GoldBio Inc., St. Louis, MO, USA
DMSO	Dimethyl sulfoxide, Hybri-Max™, sterile-filtered, ≥99.7%, Sigma-Aldrich®, Merck KGaA, Darmstadt, Germany
DNase I	Deoxyribonuclease I from bovine pancreas, Sigma-Aldrich®, Merck KGaA, Darmstadt, Germany
EDTA	Ethylenediaminetetraacetic acid, M = 292,25 g/mol, Carl Roth GmbH + Co. KG, Karlsruhe, Germany
<i>gag</i> specific primers for qPCR	forward primer: F 6F 5'- CATGTTTTTCAGCATTATCAGAAGGA-3' and reverse primer: 84R 5'-TGCTTGATGTCCCCCACT-3'
Gentamicin	Gentamicin, 10 mg/mL in deionized water Sigma-Aldrich®, Merck KGaA, Darmstadt, Germany
Glycine	Glycine, CELLPURE® ≥99 %, M = 75.07 g/mol, Carl Roth GmbH + Co. KG, Karlsruhe, Germany
HCl	Hydrochloric acid, 1 l ROTIPURAN® 37 % fuming, p.a. Carl Roth GmbH + Co. KG, Karlsruhe, Germany
Heparin	Heparin sodium salt from porcine intestinal mucosa, Sigma-Aldrich®, Merck KGaA, Darmstadt, Germany
IGEPAL® CA-630	Octylphenoxypoly(ethyleneoxy)ethanol, branched, Sigma-Aldrich®, Merck KGaA, Darmstadt, Germany
Instant Blue™	InstantBlue™ Ultrafast Protein Stain Sigma-Aldrich®, Merck KGaA, Darmstadt, Germany
Isoflurane 99,9%	Isoflurane Liquid Inhalation 99.9% Glass Bottle, Piramal Critical Care GmbH, Hallbergmoos, Germany
MgCl ₂	Magnesium Chlorid, M = 95,21 g/mol, ≥98%, Carl Roth GmbH + Co. KG, Karlsruhe, Germany
MOPS	3-(N-Morpholino)-propansulfonsäure, PUFFERAN® M = 209,27 g/mol, ≥99,5 %, Carl Roth GmbH + Co. KG, Karlsruhe, Germany
NaCl	Potassium chloride, M = 74,56 g/mol, ≥99 %, Carl Roth GmbH + Co. KG, Karlsruhe, Germany

NaOH	Potassium hydroxide, M = 39,997 g/mol, ≥99 %, in pellets, Carl Roth GmbH + Co. KG, Karlsruhe, Germany
Nuclease free water	Nuclease-free water (not DEPC-treated), Invitrogen™, ThermoFisher Scientific, Waltham, MA, USA
Paveron®	Papaverin hydrochloride PAVERON® N (25 mg/mL) LINDEN Arzneimittel-Vertrieb-GmbH, Heuchelheim, Germany
PEI	Polyethylenimine, branched, M ~ 25,000 g/mol, Sigma-Aldrich®, Merck KGaA, Darmstadt, Germany
Pen/Strep	Penicillin-Streptomycin (10.000 U/mL) Gibco™, Thermo Fisher Scientific, Waltham, MA, USA
Probe	qPCR_HIV-1_Gag_1_FAM-ZenDQ /56-FAM/CCACCCCACAAGATTTAAACACCATGCT AA /ZenDQ/ (double quench (IDT))
Protein G	Protein G Sepharose® 4 Fast Flow, Cytiva™ 17-0618-05, Cytiva Europe GmbH, Freiburg, Germany
SDS	Sodium dodecyl sulphate, ≥99,3 %, M = 288,38 g/mol, Carl Roth GmbH + Co. KG, Karlsruhe, Germany
Sucrose	D(+)-Saccharose, ≥99,5 %, p.a., M= 342,30 g/mol, Carl Roth GmbH + Co. KG, Karlsruhe, Germany
Tris	Tris-(hydroxymethyl)-aminomethane, PUFFERAN® ≥99,9 %, p.a., M = 121,14 g/mol, Carl Roth GmbH + Co. KG, Karlsruhe, Germany
Tris-HCl	TRIS Hydrochloride, PUFFERAN® ≥99 %, p.a., M = 157,60 g/mol, Carl Roth GmbH + Co. KG, Karlsruhe, Germany
Trypan-Blue	Trypan Blue solution, 0.4%, liquid, sterile-filtered, Sigma-Aldrich®, Merck KGaA, Darmstadt, Germany
virus Transfection reagent	FuGENE® 6 Transfection Reagent, Promega GmbH, Walldorf, Germany

4.1.8. Media, buffers and solutions

4.1.8.1. Purchased media, buffers and solutions

Medium, buffer or solution	Name, specifications and company
ACK Lysing Buffer	Ammonium Chloride Potassium lysing buffer Gibco™, Thermo Fisher Scientific, Waltham, MA, USA
DMEM (1X)	Dulbecco's Modified Eagle Medium, high glucose, no glutamine Gibco™, Thermo Fisher Scientific, Waltham, MA, USA
DPBS (1X)	1X Dulbecco's Phosphate-Buffered Saline, no calcium, no magnesium Gibco™, Thermo Fisher Scientific, Waltham, MA, USA
Ethanol ≥99,8 %	Rotipuran® ≥99,8 %, p.a. Carl Roth GmbH + Co. KG, Karlsruhe, Germany

Ethanol ≥70 %, denatured	Carl Roth GmbH + Co. KG, Karlsruhe, Germany
FBS	Fetal bovine serum, heat-inactivate, stored at -20°C Sigma-Aldrich®, Merck KGaA, Darmstadt, Germany
Formaldehyde	Thermo Scientific™ Pierce™ 16% Formaldehyde (w/v), Methanol-free ThermoFisher Scientific, Waltham, Massachusetts, USA Scientific
FreeStyle™ 293 Expression Medium	FreeStyle™ 293 Expression Medium Gibco™, Thermo Fisher Scientific, Waltham, MA, USA
HBSS	Hank's Balanced Salt Solution ThermoFisher Scientific, Waltham, MA, USA
HEPES, 1M	N-2-Hydroxyethylpiperazin-N-2-ethansulfonsäure, 1M Gibco™, Thermo Fisher Scientific, Waltham, MA, USA
Histopaque	Histopaque®-1077 Hybri-Max™ Sigma-Aldrich®, Merck KGaA, Darmstadt, Germany
Leukocyte Fixation Buffer	BD Cytotfix™ Fixation Buffer Becton, Dickinson and Company, Franklin Lakes, New Jersey, USA
L-Glutamine	Thermo Scientific™ L-Glutamine (200 mM) Thermo Fisher Scientific, Waltham, MA, USA
Nuclease free water	Invitrogen™ Nuclease-Free Water (not DEPC-Treated) Thermo Fisher Scientific, Waltham, MA, USA
PBS (1X)	1X Phosphate Buffered Saline Gibco™, Thermo Fisher Scientific, Waltham, MA, USA
RPMI 1640 GlutaMAX™	Gibco® Roswell Park Memorial Institute 1640 Medium, GlutaMAX™-I Supplement with Phenol Red, stored at 4°C light-protected Thermo Fisher Scientific, Waltham, MA, USA
Sodium Pyruvate	Sodium Pyruvate (100 mM) Gibco™, Thermo Fisher Scientific, Waltham, MA, USA
Trypsin	Trypsin-EDTA (0.05%), phenol red Gibco™, Thermo Fisher Scientific, Waltham, MA, USA

4.1.8.2. Self-made media, buffers and solutions

Medium, buffer or solution	composition
293T culture medium	50 mL FBS (10% (v/v)) 5 mL Pen/Strep (1% (v/v)) 5 mL of 100 mM sodium pyruvate (1 mM) 2,5 mL of 200 mM L-glutamine (1 mM) Adjusted to 500 mL with DMEM medium
EDTA 0.5 M, pH 8.0	146,125 g EDTA (0.5 M) in 1 L ultrapure water pH adjusted to 8.0 with 10 M NaOH autoclaved and stored at r.t.

FACS buffer	10 mL FBS (2% (v/v)) 2 mL of 0.5 M EDTA (2 mM) in 488 mL PBS (1X) sterile filtered and stored at 4°C
Freezing Medium	90% (v/v) FBS 10% (v/v) DMSO freshly prepared directly prior to usage
Glycine 0.1 M, pH 3.0	7.5 g Glycine (0.1 M) dissolved in 1 L ultrapure water pH adjusted to 3.0 with HCl sterile filtered and stored at r.t.
HBSS++++	1 mL of 5,000 U/mL Heparin (10 U/mL) 2 mL of 25 mg/mL PAVERON® (0.1 mg/mL) 0.5 mL of 0.5 M EDTA (0.5 mM) 2.8 mL of 10,000 U/mL Pen/Strep (56 U/mL) in 500 mL HBSS sterile filtered and stored at 4°C
Heparin Solution (HS)	0.2 mL of 5,000 U/mL Heparin (20 U/mL) 1 mL of 25 mg/mL PAVERON® (0.5 mg/mL) in 50 mL NaCl
Luciferase assay buffer (2X)	200 mM TrisHCl (pH 7.8) 10 mM MgCl 2500 µM Coenzyme A 300 µM ATP 300 µg/mL D-Luciferin (GoldBio) In Lysis buffer
Lysis Buffer for neutralization assay	50 mM TrisHCl 30 mM NaCl 1% IGPAL® In ultrapure water
MACS Buffer	0.5 g BSA (0.5%) 0.4 mL of 0.5M EDTA (2mM) In 100 mL PBS (1X)
MOPS (1X)	20X MOPS diluted in ultrapure water prior to usage (50mM MOPS, 50mM Tris, 0,1% SDS, 1mM EDTA)
MOPS (20X)	209.3 g MOPS (1 M) 6 g EDTA (20 mM) 121.2 g Tris (1 M) 20 g SDS (2%) Adjusted to 1 L with ultrapure water, stored at 4°C
NaOH 10 M	40 g NaOH in 100 mL ultrapure water
PBS/E	2 mL of 0.5 M EDTA (2 mM) in 500 mL PBS (1X)
Sucrose solution	30 g Sucrose (30%) Adjusted to 100 mL with DPBS

T cell medium	50 mL FBS (10% v/v) 5 mL of 10,000 U/mL Pen/Strep (1% v/v) Adjusted to 500 mL with RPMI 1640 GlutaMAX Medium
Tris-HCl 1 M , pH 8.0	78.8 g Tris-HCl (1 M) Dissolved in 500 mL ultrapure water pH 8.0, adjusted with NaOH sterile filtered and stored at r.t.
Tris-HCl 400 mM, pH 7,8	31.52 g Tris-HCl (400 mM) dissolved in 500 mL ultrapure water, pH 7,8, adjusted with HCl
TZM-bl medium	50 mL FBS (10% v/v) 450 mL DMEM (1X) 2.5 mL 10 mg/mL gentamicine (50 µg/mL)

4.1.9. Antibodies, nanobodies, interleukins and plasmids

Molecule	Details and company
Anti-Human CD16-Alexa Fluor® 700	Mouse CDF1 IgG ₁ , κ, Cat.No. 557920, BD Pharmingen™, BD (Becton Dickinson), Franklin Lakes, New Jersey, USA
Anti-Human CD19-APC	Mouse IgG ₁ , κ Cat.No. 555415, BD Pharmingen™, BD (Becton Dickinson), Franklin Lakes, New Jersey, USA
Anti-Human CD3- Pacific Blue™	Mouse BALB/c IgG ₁ , κ, Cat.No. 558117, BD Pharmingen™, BD (Becton Dickinson), Franklin Lakes, New Jersey, USA
Anti-Human CD4-PE	Mouse BALB/c IgG ₁ , κ, Cat.No. 340419, BD Pharmingen™, BD (Becton Dickinson), Franklin Lakes, New Jersey, USA
Anti-Human CD45-Pacific Orange™	Mouse IgG1 HI30, Cat.No. MHCD4530, ThermoFisher Scientific, Waltham, MA, USA Scientific
Anti-Human CD8-FITC	Mouse BALB/c IgG1,Kappa, Cat.No. 345772, BD Pharmingen™, BD (Becton Dickinson), Franklin Lakes, New Jersey, USA
Anti-Mouse CD45-PE/Cyanine7	Rat IgG2b, κ, Cat.No.103114, Biolegend®, San Diego, CA, United States
plasmids of HC and LC of bnAbs	SF12: Schoofs, T. et al. 2019 ¹²⁵ 3BNC117: Scheid, J.F. et al. 2011 ¹²⁶ 10-1074: Mouquet, H. et al. 2012 ¹²⁷
Recombinant Human IL-2	Cat.-No. 200-02, PeproTech, Hamburg, Germany
Recombinant Human IL-7	Cat.-No. 200-07, PeproTech, Hamburg, Germany
V _H H 6G2	provided by Dr. E. Geertsma, Max Planck Institute of Molecular Cell Biology and Genetics, Dresden, Germany
V _H H A6	provided by Ursula Dietrich, Georg-Speyer-Haus, Frankfurt, Germany

4.1.10. Software

Software	Company
Adobe Illustrator 2022	Adobe Inc., San Jose, CA, USA
applied biosystems™ standard curve analysis module, version 4.0	Life Technologies Corporation, Thermo Fisher Scientific, Waltham, MA, USA, available on https://apps.thermofisher.com/apps/spa/#/dashboard
BD FACSDiva™	BD (Becton Dickinson), Franklin Lakes, New Jersey, USA
BD FlowJo™	BD (Becton Dickinson), Franklin Lakes, New Jersey, USA
GraphPad Prism Version 9.0.0 for Windows	GraphPad Software, San Diego, CA, USA, www.graphpad.com
GraphPad Prism Version 9.5.0 for Mac OS	
Microsoft Office	Microsoft® for Microsoft Office 365 and Office 2019, Redmond, WA, USA

4.2. Methods

4.2.1. Determination of cell concentrations

Cell concentrations were determined using a double chambered Neubauer improved counting chamber. Therefore, a sample of the investigated cell suspension was mixed with Trypan-Blue 0.4% (Sigma-Aldrich®, Merck KGaA, Darmstadt, Germany) in a ratio of 1:1 to stain dead cells. When high cell concentrations were anticipated, an appropriate predilution was prepared in 1X PBS and stained respectively. The Neubauer chamber was prepared and checked for correct placement of the cover slip identified by the formation of Newton interference rings.

10 µL of the mixture were used to fill the prepared chamber, which was consecutively observed at 40 × magnification under a light microscope (Leica DM1000, Leica Mikrosysteme Vertrieb, Wetzlar, Germany). Viable unstained cells were counted in the four large corner squares of the 3 × 3 grid and the concentration in the sample was calculated using the following equation:

$$\text{cell concentration} \left(\frac{\text{cells}}{\text{mL}} \right) = \frac{\text{counted cells} \times \text{dilution factor}}{\text{counted squares} \times 0,1 \text{ mm}^3} \times 1000$$

Equation 4-1 Determination of cell concentrations utilizing a Neubauer improved counting chamber

Staining alone results in a dilution factor of 2. Predilutions were taken into account when used.

4.2.2. Virus production

All employed HIV-1 viral clones were produced by transfecting 293T cells with the different replication-competent molecular HIV-1 clones. The cells were cultured as described in 4.1.3.4. Transfection was performed using the FuGENE® 6 Transfection Reagent (Promega, Walldorf, Germany) according to the manufacturer's instructions. The virus culture was incubated at 38°C, 5% CO₂. Supernatant was harvested using a serological pipet at 48 h post infection and consecutively stored in aliquots at -80°C or -150°C.

4.2.3. Preparation of the luciferase assay buffer

The preparation of the Luciferase assay buffer (LUC-lysis mix) was done based on previous characterisation of the firefly luciferase by Yuichi Oba et al. 2003¹²⁸ and the protocol provided by GoldBio Inc., the D-Luciferin's manufacturer. Prior to mixture, the following solutions were prepared:

Solution	Concentration(s)	Storage and pH requirements
MgCl ₂ in H ₂ O	500 mM	stored at r.t.
Coenzyme A (CoA) in H ₂ O	25 mM	stored at -80°C
ATP in H ₂ O	15 mM	stored at -80°C
Tris-HCl in H ₂ O	400 mM	pH adjusted to 7,8
D-Luciferin in H ₂ O	15 mg/mL	
Lysis buffer	1% IGPAL® 50 mM TrisHCl 30 mM NaCl in H ₂ O	pH adjusted to 7,7

The prepared solutions were proportionally added together obtaining final concentrations of 200mM TrisHCl, 10mM MgCl₂, 500 µM CoA, 300 µM ATP and 300 µg/mL D-Luciferin in the corresponding volume of lysis buffer. 11 mL aliquots (for one assay plate each) were prepared and stored at -80°C for up to 6 months.

The buffer was regarded as 2X to be diluted to 1X final concentration when added 1:1 to the assay media.

4.2.4. Determination of infectivity of the produced viral stocks

In order to determine the infectivity of the virus stocks and consequentially administer viral doses of even infectivity to neutralization assays, we employed a TCID₅₀ assay based on the concept described by Montefiori et al. 2005 and optimised by Sarzotti-Kelsoe et al. 2014^{129,130}.

In brief, TZM-bl cells were utilized in a cell based assay on a 96-well plate in combination with a dilution series of the harvested virus stock, incubated for 48 h and consequentially incubated with the LUC-lysis mix in order to allow readout on a luminometer measuring luminescence in each well.

A 96-well flat-bottom culture plate was prefilled with 100 µL of TZM-bl cell medium per well. The virus dilution series was established by addition of 25 µL of the virus sample to the first column of the plate. To reduce assay based variation at least 4 replicates per sample were pipetted. A 1:5 dilution was established by transfer of 25 µL from column to column followed by mixing the resulting dilution each time. The last column (12) was left out in order to have a virus-free negative control. In the last dilution column (11), 25 µL were discarded to end up with equal volumes throughout the plate.

On top of the prefilled plate, the TZM-bl cells were added. Therefore they were trypsinized as described in 4.1.3.3. The concentration of viable cells was determined (4.2.1). A suspension of 100,000 cells/mL was prepared in TZM-bl medium supplemented with 20 µg/mL DEAE-Dextran (Sigma-Aldrich®, Merck, Darmstadt, Germany). 100 µL were added per well, starting at the cell control column and proceeding from most to least diluted sample in order to reduce carry-over. The plates were consecutively incubated for 48 h at 37°C and 5% CO₂.

Before performing the readout, plates were checked under the light microscope for regular cell growth to exclude relevant cell toxicity that would impair the result.

100 µL of culture medium were carefully discarded from each well. 100 µL of a prepared LUC-lysis mix was pipetted onto each well, again keeping the order from lowest to highest virus concentration. The mixture was incubated for 2 min at r.t. Subsequently, the solution was thoroughly mixed by pipetting multiple times and transferred into the corresponding wells of a flat-bottom 96 well black plate being then loaded onto a luminometer (TriStar² S LB 942,

BERTHOLD TECHNOLOGIES GmbH & Co. KG, Bad Wildbad, Germany). The relative light units (RLU) were obtained, measuring each well for 1 s.

TCID₅₀ values were calculated from the measured RLU raw data using the Microsoft Excel template *Calculation of TCID₅₀* provided by David C. Montefiori, Duke University Medical Center¹³¹.

4.2.5. Neutralization assay

Neutralisation assays for plasma samples, Ab and V_HH solutions were performed as described by Montefiori et al.¹²⁹ and Sarzotti-Kelsoe et al.¹³⁰ employing TZM-bl cells. Plasma samples were heat-inactivated at 56°C for 1 h prior to the assay in order to denature plasma complement.

In brief, a TZM-bl cell based assay on a 96 well plate was combined with a dilution series of the samples, incubated for 48 h with even amounts of virus aiming for around 200 TCID₅₀ per well. Readout was performed as for the TCID₅₀ assay (4.2.4). Per plate a virus only column (column 2) and a cell control column (column 1) were included in order to determine background signalling and signal range from 0 to 100% infection.

A 96-well flat-bottom culture plate was prefilled with 100 µL of TZM-bl medium per well, cell control wells received further 50 µL of medium. Row H of all sample columns received 40 µL of additional medium and 11 µL of the corresponding sample of interest. All samples were tested in duplicates. A 1:3 dilution series was established by mixture and transfer of 50 µL into the neighbouring row (direction from H to A respectively). 50 µL of Row A were discarded. Virus stock was thawed and the required volume was diluted in TZM-bl medium in order to obtain a 4,000 TCID₅₀/mL concentration. 50 µL of the prepared virus dilution were added to all columns except the cell control column 1 row-wise from A to H from lowest to highest sample concentration. The plate was incubated at 37°C, 5% CO₂ until addition of the TZM-bl cells. Cell suspension was prepared as described (4.2.4) in TZM-bl medium supplemented with 25 µg/mL of DEAE dextran (Sigma-Aldrich®, Merck, Darmstadt, Germany). 100 µL of cell suspension was added on-top of each well from A to H. The assay plate was incubated for further 48h at 37°C, 5% CO₂.

Prior to readout, plates were checked under the light microscope for regular cell growth to exclude relevant cell toxicity that would impair the result.

For the read-out, 150 μ L of medium were discarded from each well. 100 μ L of LUC-lysis mix were added onto each well and incubated at room temperature for 2 min, transferal to a black plate and read-out on the luminometer were performed as for the TCID₅₀ assay.

Data analysis was performed using the Microsoft Excel template *Measurement of Neutralization Titers* provided by David C. Montefiori, Duke University Medical Center¹³¹. Percentage of neutralization was determined as the reduction of RLU compared to the virus control mean after subtracting the background luminescence determined as the mean signal given by the cell control column. IC₅₀ and IC₈₀ values were calculated by extrapolating the Ab concentration, at which 50% and 80% neutralization would be achieved respectively. In case of plasma samples, inhibitory dose (ID)₅₀ and ID₈₀ values were calculated as the reciprocal of the corresponding plasma dilution.

4.2.6. Production of bnAbs

4.2.6.1. Transfection of 293-6E cells with plasmids containing human bnAb heavy and light chain sequence

293-6E cells (4.1.3.5) were used for the production of bnAbs. Plasmids containing the light and heavy chain sequences of the human bnAbs 3BNC117¹²⁶, 10-1074¹²⁷ and SF12¹²⁵ had previously been generated by single cell B cell cloning from blood samples of human HIV-1 positive individuals. Cells were transfected with a combination of the HC plasmid and the LC plasmid of the same Ab.

All reagents were brought to r.t., 293-6E cells were brought to a concentration of 0.8×10^6 cells/mL and the resulting culture volume was measured.

The following mixture was prepared in a sterile tube of suitable volume:

- 4.5 mL NaCl (150mM) x culture volume / 100 mL
- 50 μ g heavy chain DNA x culture volume / 100 mL
- 50 μ g light chain DNA x culture volume / 100 mL

The mixture was briefly vortexed and finally sterile-filtered Polyethylenimine (PEI, Sigma-Aldrich®, Merck KGaA, Darmstadt, Germany) at a volume of 0.34 mL per 100 mL culture from a stock of 0.45 mg/mL was added, resulting in a final concentration of 0.153 mg/mL. Immediately after the addition, the mixture was vortexed thoroughly for 15 s. It was consecutively added dropwise to the cell culture flask being gently rotated. The cells were then incubated for 7 days as described in 4.1.3.5.

4.2.6.2. Antibody purification from cell supernatant

The cells were spun down at 4,000 × g for 30 min, supernatant was harvested by transfer into fresh tubes through a 0.45 µm filter and stored at 4°C until proceeding.

Human IgG molecules were isolated using on-column Protein G binding (Protein G Sepharose® 4 Fast Flow in 20% EtOH, 17-0618-05, Cytiva Europe, Freiburg, Germany) followed by a pH change based elution and buffer exchange for storage. The required amount of protein G was estimated based on an anticipated IgG yield of about 40 µg/mL supernatant and the indicated binding capacity of protein G of 20 mg IgG/mL:

$$\text{protein G volume (mL)} = \frac{40 \mu\text{g/mL} \times \text{supernatant volume in mL}}{20 \text{ mg/mL}}$$

Equation 4-2 Estimation of required protein G for antibody purification

The protein G was thoroughly vortexed and the required volume was transferred into a new tube. Buffer exchange from EtOH to 1X PBS was performed by two rounds of centrifugation for 5 min at 300 × g without acceleration or brake, each round followed by careful removal of the supernatant and reconstitution in 1X PBS.

The washed protein G was added to the harvested supernatant and the solution was incubated on a shaker at 4°C for 12-24 hours. Subsequently, the mixture including the protein G bound IgG was filled onto chromatography columns and washed with 1X PBS. Finally the IgG was eluted by application of a 0.1 M glycine solution (pH 3.0). Eluate was collected into a fresh tube prefilled with 1M Tris-HCl (pH 8.0) at a ratio of 1:10 resulting in an immediate pH neutralization. Buffer was exchanged to 1X PBS utilizing 50 kDa Amicon® Ultra-15 spin columns (Merck Millipore, Merck, Darmstadt, Germany). In several rounds, the spin columns were centrifuged at 3,800 × g at 4°C, the ultrafiltrate was discarded and 1X PBS was added on top of the remaining fluid in the filter device. The process was repeated until the elution buffer was diluted by at least 1:200. The concentrated IgG was collected from the filter device into a fresh sterile tube of reasonable volume using a filter-tip pipet and performing side-wise pipetting movements to ensure most complete recovery. As a last step, the Ab suspension was sterile filtered using 0.22µm Ultrafree-CL columns (Cat.-No.: UFC40GV02, Merck, Darmstadt, Germany) and IgG concentration was measured using a microvolume spectrophotometer (NanoDrop). To avoid precipitation, a maximum storage concentration of 20 mg/mL was tolerated. If necessary, samples were diluted in 1XPBS and consecutively stored at 4°C.

4.2.6.3. Confirmation of the presence of IgG via gel electrophoresis

Before usage of the produced bnAbs, samples were run on an Invitrogen™ NuPAGE™ Bis-Tris gel (Thermo Fisher Scientific, Waltham, MA, USA) according to the manufacturer's instructions including a protein ladder on each gel and running a reduced and non-reduced sample per Ab. As running buffer, self-made 1X MOPS buffer was applied. Therefore a prepared stock of 20X MOPS buffer was diluted with ultrapure water.

The gel chamber was loaded and run for approximately 50 min at a constant voltage of 200 V. Protein bands were identified by performing Coomassie staining applying InstantBlue™ (Sigma-Aldrich®, Merck, Darmstadt, Germany) and incubation for at least 15 min at r.t. and continuous moderate shaking. Presence of human IgG was indicated by a visible band at approximately 150 kDa in the unreduced sample representing the whole Ab and two bands at 25kDa and 50kDa representing the single light and heavy chain in the reduced sample.

4.2.7. Humanization

4.2.7.1. Irradiation

Newborn pups no older than 5 days were irradiated using the MultiRad160 (Serial-No.: 2329A60113, Faxitron Bioptics, Tucson, AZ, USA). The machine setup was done in accordance to the company's recommendations and the laboratory's SOP. An aluminium filter was used for the Dose QA and exchanged by a copper filter for irradiation. Settings were set to "timed control" 60 sec, max. 129 kV, 19mA and Cu-Filter 0.3mm. A plastic box with 4 separate segments designated for this purpose was cleaned with Sterillium® Virugard (Paul Hartmann, Heidenheim, Germany) and pups were transferred into it, distributing them evenly into the segments with a maximum of two pups per segment. The box was placed onto the platform at the third level of the irradiator with its centre being slightly shifted from the centre point of the platform to improve evenness of radiation. The mice were irradiated with the aforementioned settings and consequentially transferred back into their cage. The total radiation dose was around 2 Gy. The MultiRad160 was switched off, platform position and filter were set back.

4.2.7.2. Haematopoietic stem cell injection

Four to six hours after irradiation, the new-born mice received a human stem cell injection of 2×10^5 CD34+ cells per mouse. The required volume of HCS suspension was taken out of the freezer and thawed by placing the aliquots into a 37°C water bath for 30 s. The aliquot content was taken out with a P1000 pipet and transferred into a tube prefilled with cold 1X DMEM medium (Gibco™, Thermo Fisher Scientific, Waltham, MA, USA) at a dilution of 1:14 cells to

medium. Only HSC suspensions of the same placenta donor were merged together. The tube containing the cell suspension was centrifuged at 4°C, 400 × g for 5 min and supernatant was removed with a serological pipet. The cell pellet was resuspended in an appropriate volume of DMEM to allow for injection of 2 × 10⁵ CD34+ cells per mouse, transferred into a 1.5 mL safe lock tube labelled with the placenta number and stored on ice until injection.

Pups were transferred from mother's cage into a new clean cage to allow definite allocation. 2 × 10⁵ of HSCs were drawn into an insulin syringe (B. Braun, Melsungen, Germany) and injected *i. h.* per mouse. Site of injection was determined by holding the pup with three fingers exposing the abdomen so that the liver became visible as a darker spot on the right flank. After injection, each pup was transferred back into mother's cage and observed for regular behaviour.

4.2.7.3. Flow cytometric measurement

Flow cytometry was used to measure the concentrations of different leukocyte populations in the peripheral blood and lymphoid tissues of the mice. Blood samples were gained by superficial temporal vein bleeding (4.1.1.1.2). Organ cells were isolated as described in 4.2.11. A staining master mix was prepared by adding the following antibodies to 14,5 µL of FACS buffer per sample (resulting in a total volume of 25 µL staining mix per sample):

Epitope	Conjugated fluorophore	Volume per sample	Final dilution
mCD45	PE-Cy7	0,005 µL	1:5000
hCD45	Pacific Orange	1,25 µL	1:20
hCD19	APC	2,5 µL	1:10
hCD3	Pacific Blue	1,25 µL	1:20
hCD4	PE	1,25 µL	1:20
hCD8	FITC	2,5 µL	1:10
hCD16	AF700	0,025 µL	1:1000

The master mix was kept at 4°C in the dark for a maximum of 2 h before usage.

30 µL of EDTA blood sample were pipetted onto a conical bottom 96 well plate and incubated with 200 µL ACK lysing buffer (Gibco™, Thermo Fisher Scientific, Waltham, MA, USA) for 5 min at r.t. in the dark to lyse erythrocytes. After incubation, the plate was centrifuged at 400 × g, 5 min, r.t. and gently flicked over a sink to discard supernatant. The samples were washed

once by resuspension in 200 μ L FACS buffer, centrifugation and flicking the plate as described to terminate the lysis reaction. In case of tissue derived cell suspensions as sample which had previously been treated with ACK lysis buffer, the staining preparation started at this point. 100 μ L of organ cell suspension were taken out into a conical bottom 96 well plate, centrifuged at 400 \times g for 5min, r.t. and the plate was flicked. All further steps were performed concordantly for tissue and blood derived samples. The prepared staining mix was mixed prior to usage. Each sample was resuspended in 25 μ L of staining mix and consequently incubated for 20 min at 4°C in the dark. Afterwards the sample was washed twice as described and eventually resuspended in 200 μ L FACS buffer. 20 μ L of well vortexed counting beads were added per sample. Resuspended sample solution was pipetted through a cell strainer cap into FACS tubes (Falcon®, Corning Inc., Corning, NY, USA). Additional 200 μ L of FACS buffer were added through the strainer cap. Sample tubes were kept on ice and light-protected until run on flow cytometer. A FACSAria™ Fusion (Becton, Dickinson and Company, Franklin Lakes, NJ, USA) was used in combination with BD FACSDiva™ software (Becton, Dickinson and Company, Franklin Lakes, NJ, USA) for data acquisition. Analysis and cell count calculations were done using BD FlowJo™ (Becton, Dickinson and Company, Franklin Lakes, NJ, USA) and Microsoft Excel 2019 (Microsoft®, Redmond, WA, USA).

4.2.8. Mononuclear cell injection

A treatment to improve human CD4+ cell reconstitution was performed in order to allow mucosal HIV-1 infection¹³². Therefore mice received an *i.p.* cell injection. Two different cell populations were tested:

- a) PBMCs (4.1.3.1)
- b) UCBCs (4.1.3.2)

Cells were stored at -150°C and thawed quickly by placing the required amount of aliquots in a pre-heated 37°C water bath. Vial content was transferred with a P1000 pipet into a tube prefilled with T cell medium (RPMI 1640 GlutaMAX Medium, Gibco®, Thermo Fisher Scientific, Waltham, MA, USA, supplemented with 10% FBS and 1% Pen/Strep) diluting the cell suspension by at least 1:4. Only vial contents of the same donor were merged together in one tube. Cell suspension was spun down by centrifugation (400 \times g, 4°C, 6 min) to eliminate cytotoxic freezing medium. Supernatant was taken off with a serological pipet and the cell pellet was resuspended in fresh T cell medium. If clotting was visible, the cell suspension was pipetted through a 40 μ m cell strainer (Cat.-No. 734-0002, Corning Inc., Corning, NY, USA). The cell concentration was determined as described in 4.2.1. Cells were recentrifuged with the

same settings and resuspended in the required volume of T cell medium supplemented with 100 U/mL Il-2 (Cat.-No. 200-02, PeproTech, Hamburg, Germany) and 0.05 µg/mL Il-7 (Cat.-No. 200-07, PeproTech, Hamburg, Germany).

20 to 40 × 10⁶ cells were used per mouse throughout the modification of the mouse model. Single mouse aliquots were prepared for the corresponding amount of mice and stored on ice prior to injection.

Mice were anesthetized as described (4.1.1.1.1). The content of one aliquot was taken up with one insulin syringe (B. Braun, Melsungen, Germany). For the *i.p.* injection, the anesthetized mouse was restrained and slightly tilted head-down, exposing the abdomen with the left hind leg held in abduction and external rotation in order to minimize the risk of organ or blood vessel injury. The syringe was inserted in a 30°- 40° angle in the lateral lower abdomen. Smooth injection without resistance was possible when correctly injecting into the peritoneal cavity. If resistance was felt, repositioning of the needle was required.

After injection, the mouse was held in the described position for some seconds to control for leaking or bleeding from the puncture site.

4.2.9. Injection of interleukin 7 (Il-7)

Single injection aliquots of 250 ng Il-7 in 1X DPBS were prepared. Therefore 50 µg recombinant human Il-7 (Cat.-No. 200-07, PeproTech, Hamburg, Germany) were dissolved in 1 mL 1X DPBS and well mixed. The solution was transferred into a 50 mL tube and 4 mL DPBS were added leading to a stock concentration of 10 µg/mL. Aliquots of 25 µL Il-7 were prepared from the stock by appropriate dilution in 1X DPBS. The aliquots were immediately frozen and stored at -80°C.

The required amount of aliquots was thawed one hour prior to usage. The content of one aliquot was drawn with an insulin syringe (B. Braun, Melsungen, Germany). Anesthetized (4.1.1.1.1) mice were restrained and subcutaneous (*s.c.*) injection was done in a flat angle at the base of a lifted skin fold above the neck. The needle was left in position for some additional seconds after to prevent leaking due to elevated tissue pressure.

4.2.10. Mucosal HIV-1 challenge

A solution of HIV-1 and the different compounds to be tested for their preventive potency was administered intrarectally (*i.r.*) to the mice to model mucosal transmission. Therefore aliquots of HIV-1 and aliquots of the compound solutions were prepared in advance and kept frozen

(HIV-1 aliquots at -150°C, compound aliquots at -20°C). They were thawed and stored on ice prior to challenge and mixed together 30 min before application.

Mice were anesthetized as described (4.1.1.1.1). The mice were held upside down by holding the tail and supporting the body with the back of the hand in such a way that the anus was exposed. The HIV-1 compound mixture was taken up from the aliquot with a P200 pipet using a filtered pipet tip and applied *i.r.* with slow and even pressure to minimize local trauma. Mice were held in this position for some seconds to prevent leaking and thereupon placed back into the cage being observed for regular gain of consciousness.

4.2.11. Isolation of cells from the murine spleen and gut-associated lymphoid tissue

Mice were sacrificed by cervical dislocation. The body was dissected using a clean dissection set. The spleen, small and large intestine were excised and transferred into T cell medium (RPMI 1640 GlutaMAX Medium, Gibco®, Thermo Fisher Scientific, Waltham, MA, USA, supplemented with 10% FBS and 1% Pen/Strep) at 4°C until further procedure.

For the isolation of splenic cells the spleen was initially cut into several pieces in the medium. The pieces were pressed through a cell strainer using the plunger of a syringe and the resulting cell suspension was passed through a 18G syringe needle (Sterican® Safety, B. Braun, Melsungen, Germany). The suspension was mixed with ACK lysis buffer (Gibco™, Thermo Fisher Scientific, Waltham, MA, USA) and incubated for 5 min at r.t. Afterwards, the sample was washed by centrifugation at 400 × g, 5 min, r.t., taking off of the supernatant and resuspension of the cell pellet in 200 µL FACS buffer. 100 µL of cell suspension are taken up to stain for flow cytometric measurement (4.2.7.3).

For the intestinal tissue samples, two distinct cell fractions were aimed for: the intra-epithelial layer (IEL) lymphocytes and the lymphocytes located in the lamina propria (LP). In order to isolate those cell fractions, the intestine was initially flushed with 1X PBS and cut into approximately 1 cm long sections.

One fraction was incubated in the T cell medium supplemented with 25 mM EDTA at 37°C for 15 min to break down extracellular matrix followed by vortexing the suspension and passing it through a 70 µm cell strainer. This procedure was performed twice to improve the yield which was regarded as containing the IEL lymphocytes.

The other fraction was incubated for 20 min at 37°C in T cell medium supplemented with 1.0 mg/mL Collagenase D (from *Clostridium histolyticum*, Sigma-Aldrich®, Merck, Darmstadt, Germany), 0.1 mg/mL DNase I (Sigma-Aldrich®, Merck, Darmstadt, Germany), 0.5 mg/mL Dispase II (from *Bacillus polymyxa*, Sigma-Aldrich®, Merck, Darmstadt, Germany).

Consecutively the suspension was vortexed and passed through a 70 µm cell strainer. The digestion treatment was performed twice and the resulting suspension was regarded as containing the LP lymphocyte fraction.

Both fractions were washed in T cell medium and strained in two steps, primarily through a 70 µm (Cat.-No. 352350, Corning Inc., Corning, NY, USA) and finally through a 40 µm (Cat.-No. 352340, Corning Inc., Corning, NY, USA) sterile Falcon® Cell Strainer.

From the three different tissues investigated (spleen, intestinal LP and intestinal intraepithelial cells), lymphocytes were isolated by density gradient based separation utilizing Histopaque®-1077 (Sigma-Aldrich®, Merck KGaA, Darmstadt, Germany) solution at 30% (v/v). The resulting cell suspensions were consecutively stained and measured via flow cytometry (4.2.7.3).

4.2.12. Immunofluorescence imaging and In-Situ Hybridisation for HIV-1-RNA on murine tissue samples

Mice were sacrificed and dissected (4.2.11). The spleen was transferred into 1X DPBS on ice. The small and large intestine were flushed carefully with 1X DPBS using a 200 µL filter tip put onto a syringe. The intestine was cut open longitudinally, washed in 1X DPBS and sliced into pieces of approximately 2 cm length. All harvested tissue was placed into distinct safe-lock tubes containing fixation buffer (1X DPBS supplemented with 4% PFA) overnight. Afterwards, the tissue was washed in cold 1X DPBS and transferred into sucrose solution (1X DPBS containing 30 g/100 mL sucrose) and stored at 4°C. Further processing of the samples including all staining, immunofluorescence imaging and image processing were performed by the collaborating researcher group “Infection and Immunity”, led by Dr Kathrin Held and PD Dr Christof Geldmacher, Division of Infectious Diseases and Tropical Medicine, University Hospital, LMU Munich, Germany¹³².

4.2.13. Viral load determination

4.2.13.1. Sample acquisition and RNA isolation

Samples for the viral load measurement were peripheral blood samples obtained from the mice as described (4.1.1.1.2). Blood was collected in EDTA microtubes and centrifuged at 2,000 ×

g at r.t. for 10 min. Plasma was transferred into new sterile tubes under the hood by carefully pipetting off the plasma phase from above the cell pellet. Per sample, 100 μ L of plasma were used, potential excess was stored at -20°C.

For the RNA extraction, a viral standard (STD) and negative control (NEG) consisting of nuclease free water were included and treated concordantly and in parallel to the samples for each step. The STD with a pre-determined concentration of 6 million viral copies per 100 μ L (measured in a clinical assay using the Roche Cobas HIV-1 quantitative nucleic acid test) was kindly provided by Kanika Vanshylla. The QIAamp MinElute virus spin kit (QIAGEN, Hilden, Germany) was used in combination with the QIAcube classic (QIAGEN, Hilden, Germany). The required reagents were reconstituted according to the manufacturer's instructions, including the protease reconstituted in buffer AVE, carrier RNA dissolved in buffer AVE, the washing buffers referred to as buffer AW1 and buffer AW2 by the manufacturer, both diluted in 100% ethanol.

Samples were chemically lysed and consequently heat-inactivated in the presence of the lysis buffer composed of 200 μ L Buffer AL, 100 μ L nuclease free water, 5.6 μ L of 1 mg/mL Carrier RNA and 25 μ L of reconstituted protease volumes per reaction.

Each plasma sample of 100 μ L as well as STD and NEG received 325 μ L of lysis buffer. The tubes were thoroughly vortexed for 15 s under the hood and subsequently inactivated at 56°C for 15 min on a heating block (hlc Block Thermostat HBT130, HLC, Bovenden, Germany).

To remove proviral DNA, a DNase on-column step was included. Therefore lyophilized RNase-free DNase (QIAGEN GmbH, Hilden, Germany) was dissolved in nuclease free water.

The QIAcube was loaded with the columns, collection tubes and rotor adapters of the MinElute Virus Spin Kit and the buffers AW1, AW2 and ethanol (100%, non-denaturated). The DNase was diluted in buffer RDD (10 μ L of reconstituted DNase in 70 μ L buffer RDD per sample) and placed into the QIAcube at loading position A. At position B a tube with buffer AVE was loaded. The program was set to differential manual lysis from body fluid and the elution volume was set to 55 μ L. The eluate containing the isolated RNA was immediately frozen and stored at -80°C until set-up of the qPCR.

4.2.13.2. Quantitative real-time PCR (q-RT PCR)

In order to determine the viral load, the TaqMan™ RNA-to-CT™ 1-Step Kit (Applied Biosystems®, ThermoFisher Scientific, Waltham, MA, USA) was used to set up a qPCR⁴⁷.

A 1:5 dilution series of the co-extracted STD was prepared in clean tubes in order to generate a standard curve. For the first dilution 10 µL of the RNA isolated STD were diluted in 40 µL of buffer AVE. This was sequentially repeated to obtain 7 serial dilutions, thereby 8 different STD concentrations.

The master mix (MM) for the qPCR was prepared under a clean hood. A secondary mix (MM no-RT) was prepared for one reaction to include an internal control consisting of an STD sample without the RT enzyme.

Component	MM per reaction	MM no-RT per reaction
TaqMan RT-PCR mix (2X)	25 µL	25 µL
Primer/probe solution	2.5 µL	2.5 µL
TaqMan RT enzyme	1.25 µL	0 µL
Nuclease-free water	1.25 µL	2.5 µL

The primer/probe solution used in the qPCR contains a forward and reverse *gag* primer and a corresponding probe used for detection¹³³.

component	name	Sequence
Forward primer	qPCR_HIV-1_Gag_region_F	CATGTTTTTCAGCATTATCAGAAGGA
Reverse primer	qPCR_HIV-1_Gag_region_R	TGCTTGATGTCCCCCCT
probe	qPCR_HIV-1_Gag_1_FAM-ZenDQ	/56-FAM/CCACCCCACAAGATTTAAACACCATGCT AA /ZenDQ/ (<i>double quench (IDT)</i>)

Primers and probe were reconstituted in nuclease-free water to a stock solution of 100 µM each and stored at -20°C. The primer/probe solution was prepared using the stock solutions:

Component	Volume	Concentration in Primer/probe solution	Final concentration per qPCR reaction
Forward primer	90 µL	9.0 µM	450 nM
Reverse primer	90 µL	9.0 µM	450 nM
Probe	25 µL	2.5 µM	125 nM

Nuclease-free H₂O 795 µL

30 µL of PCR master mix were added per sample well onto a qPCR plate (LightCycler® 480 Multiwell Plates 96, Roche Molecular Systems, F. Hoffmann-La Roche, Basel, Switzerland) working on a 96 well cooler. 20 µL of sample were added to the corresponding well and mixed by pipetting 3 times. The plate was sealed using LightCycler® 480 sealing foil (Roche Molecular Systems, F. Hoffmann-La Roche, Basel, Switzerland) and spun down briefly at 4°C. A QuantStudio5 (QuantStudio™ 5 Real-Time PCR System, 96-well 0.2 mL, ThermoFisher Scientific, Waltham, MA, USA) qPCR cycler was used with the following run setting:

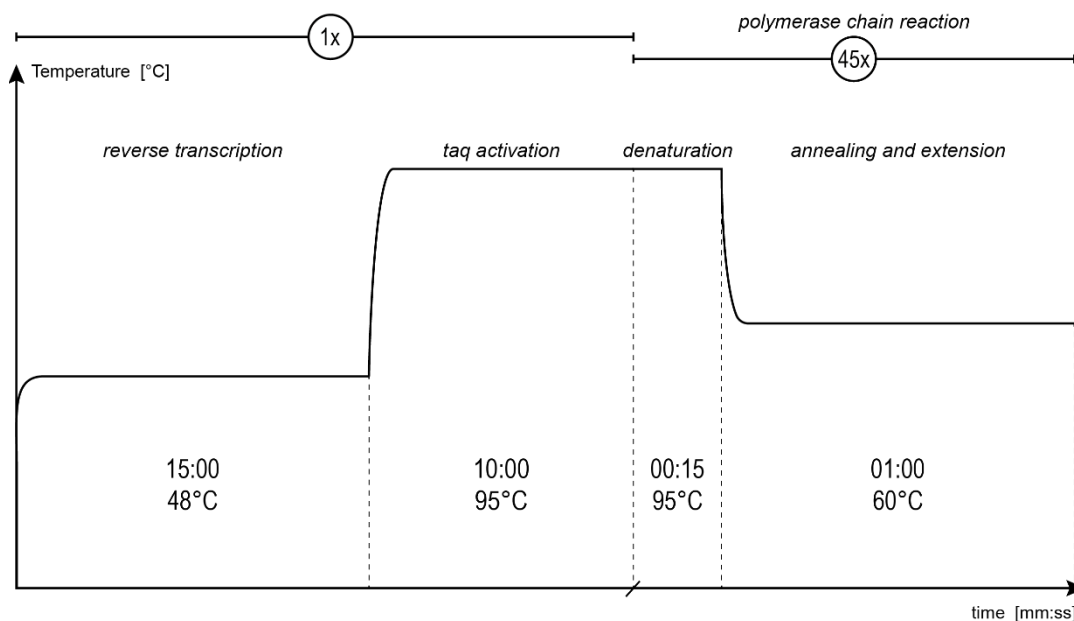


Figure 4.1 outline of the settings for the viral load determining qPCR

For data analysis, the applied biosystems™ standard curve online tool (standard curve analysis module, version 4.0, Life Technologies Corporation, Thermo Fisher Scientific, Waltham, MA, USA, available on <https://apps.thermofisher.com/apps/spa/#/dashboard>) was used. Out of the 8 standard curve measurement points only the first 7 were considered for analysis to minimize variation due to the low viral copy numbers. FAM-ZenDQ was indicated as target for all sample wells and the generated curves were checked for plausibility. The lowest standard dilution integrated in the calculation ($6,000,000 \text{ copies}/5^6 = 384 \text{ copies}$) was consequently regarded as detection limit.

4.2.14. Statistical analysis and result interpretation

The BD FACSDiva™ software was used for data acquisition when performing flow cytometric measurements. Analysis and cell count calculations were done using BD FlowJo™ and Microsoft Excel. Statistical analysis from the calculated cell counts was performed using Microsoft Excel and GraphPad Prism. Wilcoxon matched-pairs signed-rank test was used to analyse statistical significance between cell count measurements from two different timepoint within the same group. Mann-Whitney test was used to compare two unrelated groups. Two-tailed P values were calculated and significance level α was set to 0.05 if not mentioned otherwise.

When comparing HIV-1 infection rates between groups, measurements with a viral load above or equal to the detection limit of 384 copies/ μ L were regarded as positive whilst those lower as negative respectively. A qualitative comparison between groups was performed since the primary endpoint was determined as protection from infection defined as a sustained viral load below detection limit throughout the observation period.

5. Results

5.1. A novel mouse model with improved T cell reconstitution is highly susceptible to mucosal HIV-1 infection

5.1.1. The hCD34T+ model displays a significant increase in human T cell reconstitution in the peripheral blood

A novel mouse model harbouring a human immune system was created to study mucosal HIV-1 infection and potential inhibitors. Various mouse models with human immune reconstitution, being referred to as humanized mice have already been established. All of these models are based on two major components, an immunodeficient mouse strain and a human xenograft.

The hCD34T+ model is a modification of the pre-existing hCD34+ model especially designed to improve susceptibility to mucosal HIV-1 infection.

In brief, the hCD34+ mice are NOD-Rag1^{null} IL2rg^{null} (NRG) mice that received a sublethal irradiation followed by an *i.h.* injection of 2×10^5 hCD34+ cells isolated from placenta donors. After 12 weeks, different peripheral blood lymphocyte concentrations were measured via flow cytometry. Since the human CD4+ cells are critical for maintenance of HIV-1 infection, this

fraction was used to determine positive humanization and mice with a hCD4 cell blood level above 1/ μ L were regarded as humanized hCD34+ mice onwards.

During the isolation of human hematopoietic stem cells from umbilical cord blood via MACS selection for hCD34+ cells, the flow-through of hCD34 negative mononuclear cells was collected as a second fraction. HCD34+ cells represent hHSCs while mononuclear cells without this surface marker are leukocytes in further maturation and differentiation stages including lymphocytes, monocytes and granulocytes being referred to as umbilical cord blood mononuclear cells (UCBCs). For the CD34T+ mouse model we employed this cell fraction with respect to the placenta donor, so that UCBCs were always only administered to mice that had received HSCs from the corresponding placenta donor previously.

The modification of the hCD34T+ model consisted of a donor-matched *i.p.* application of UCBCs to CD34+ mice older than 12 weeks accompanied by four subcutaneous administrations of human IL-7, once 4 h in advance (on day 0), as well as on the consecutive days 1 and 2 and on day 7. After two weeks on day 14 flow cytometric analysis was repeated. The generation method for hCD34T+ mice is outlined in Figure 5.1.

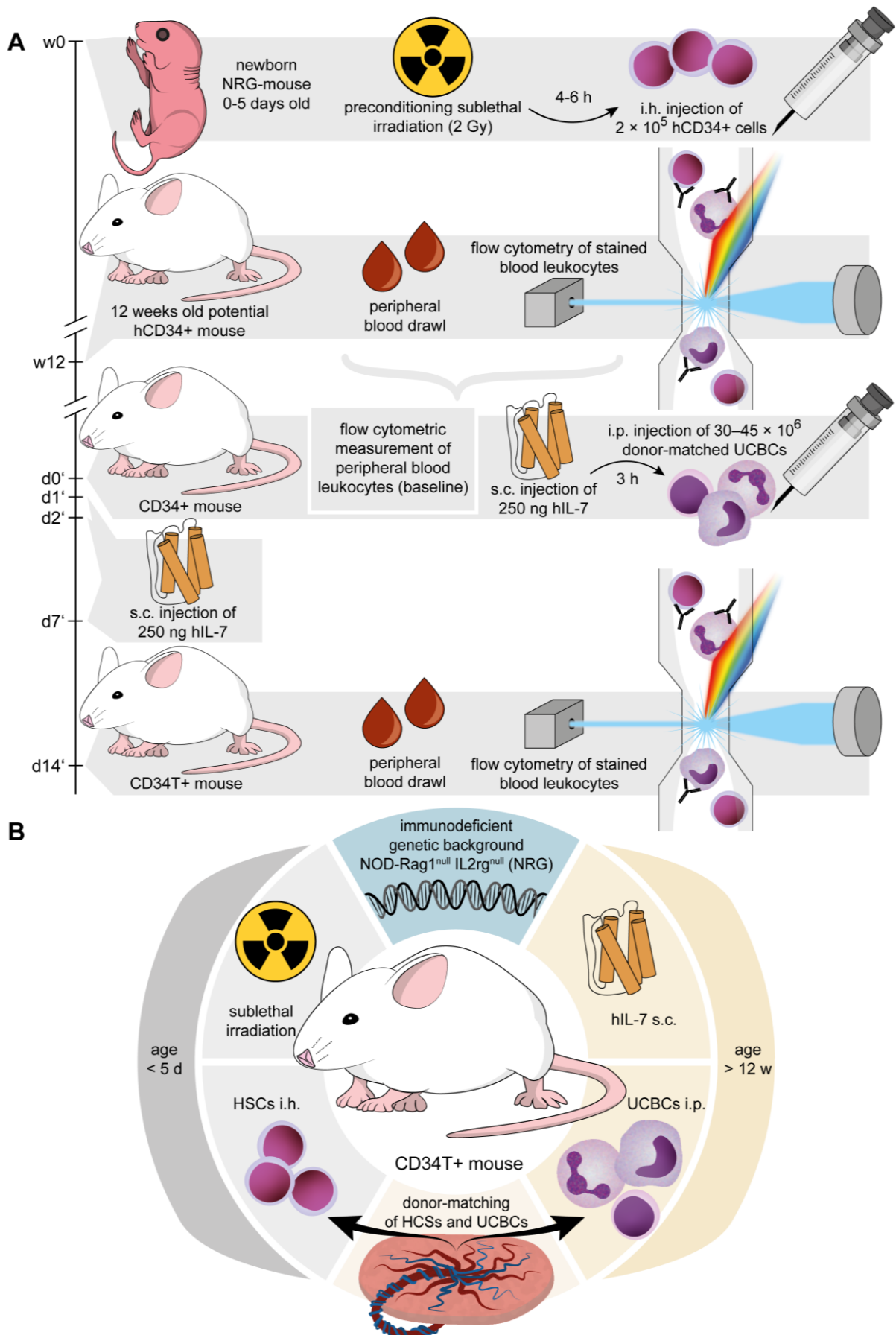


Figure 5.1 generation of the novel CD34T+ mouse model

A schematic outline of the generation method of CD34T⁺ mice: Newborn NRG mice were irradiated with a sublethal radiation dose of 2 Gy, 4-6 h later they received an *i.h.* injection of 2×10^5 hCD34⁺ cells isolated from umbilical cord blood. At 12 weeks of age, the mice were checked for their human reconstitution by surface staining of peripheral blood leukocytes and flow cytometric measurement of the cell populations. Before the T⁺ treatment, hCD34⁺ mice were once again measured for their peripheral blood human leukocyte concentrations as a baseline value and consecutively treated with a *s.c.* injection of 250 ng human IL-7, followed by an *i.p.* injection of $30-45 \times 10^6$ UCBCs from the corresponding placenta donor after 3 h. IL-7 administration was repeated on the consecutive days 1,2 and 7 in the same way. After 2 weeks, indicated as d14', mice were finally checked for their human reconstitution by flow cytometric analysis as performed before. Axis on the left indicates timepoints.

B illustration of the key features of the novel CD34T⁺ mouse model: The model is based on the NRG genetic background. As human graft, cells obtained from umbilical cord blood of placenta donors, were introduced into the host on two distinct occasions: Aged less than 5 days, pups received a sublethal irradiation followed by an *i.h.* injection of HSCs. As adult and positively humanized mice (CD34 mice) older than 12 weeks, mice received a second human cell injection consisting of UCBCs intraperitoneally accompanied by *s.c.* injection of human IL-7.

The CD34T⁺ model incorporates four key features, whose relevance we wanted to evaluate distinctly. We compared the CD34T⁺ mouse model therefore to four different control groups. The model consists of immunodeficient mice that received human HSCs as new-borns to humanize them (3), they received a donor-matched (2) injection of leukocytes (1) from umbilical cord blood (4). So, we compared the model to

- (1) CD34⁺ mice that did not receive further leukocytes in the mean time
- (2) CD34⁺ mice that received non-donor-matched PBMCs from adult blood donors instead
- (3) non-humanized NRG mice receiving the same UCBC injection accompanied by administration of human IL-7
- (4) To compare the reconstitution after administration of UCBCs to PBMCs from adult human blood donors, we compared a group of non-humanized NRG mice that received PBMCs to the group of NRG mice receiving UCBCs (3).

5.1.2. Human T leukocyte reconstitution is significantly higher in CD34T⁺ in comparison to CD34⁺ mice

To address the relevance of the additional *i.p.* UCBC injection, we used age-matched CD34⁺ mice as a control group, that did not receive any treatment in the meantime. Peripheral blood leukocyte levels were measured via flow cytometry in both groups on day 0 and day 14 (Figure 5.2, Table 5.1, Table 5.2).

In comparison to the control group, we observed an increase in absolute levels of human CD45⁺ cells in the CD34T⁺ group. The lymphocyte population with the most significant increment were the hCD3⁺ T lymphocytes. Both subpopulations we gated for, hCD4⁺ and hCD8⁺ T lymphocytes, expanded significantly. A further observation was the expansion of the hCD16⁺ cells while hCD19⁺ cells, representing the human B lymphocyte population as well

as murine CD45+ cells did not change significantly. The control group of untreated CD34+ mice on the other hand remained stable throughout all measured cell populations.

We analysed a total of 111 mice, 42 in the control CD34+ group and 69 in the CD34T+ group by the end of the study. Human cells from 18 different placenta donors were utilized. Our data indicates that the generation of CD34T+ mice is possible from a variety of human donors and results are consistent throughout the different human grafts.

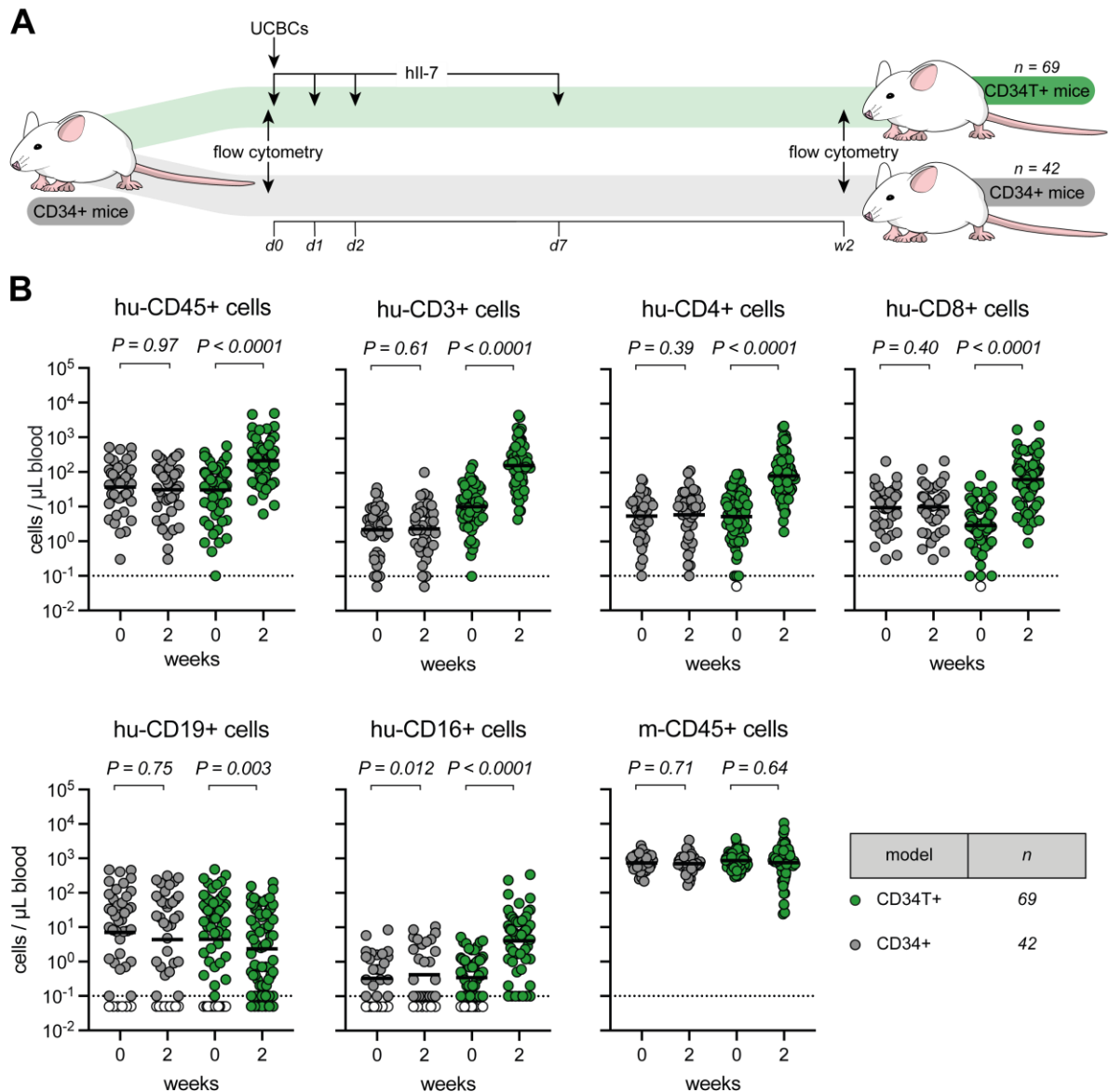


Figure 5.2 Comparison of leukocyte concentrations of the CD34T+ and the CD34+ control group at w0 and w2¹³²

A schematic overview of the experiment timeline. CD34+ mice either received T+ treatment (CD34T+ group) or remained without intervention (CD34 group), at timepoints d0 and after 2 weeks, leukocyte concentrations in the blood were measured. **B** Cell concentrations in the peripheral blood were determined by flow cytometry, see Table 5.1 and Table 5.2 for the raw values. Measurements for CD34+ mice displayed in grey, for CD34T+ mice in green, values below detection limit indicated in white. Concentrations at baseline (w0) and after 2 weeks (w2) were compared and significance was calculated using a two-tailed Wilcoxon matched-pairs signed rank test. This figure is adopted from Figure 1B from Vanshylla et al. 2021¹³².

Table 5.1 Leukocyte concentrations of the CD34T+ group at w0 and w2

$n=69$, mouse ID given in left column, human CD45+, CD3+, CD3+CD4+, CD3+CD8+, CD19+ and CD16+ as well as murine CD45+ cell concentrations were determined via flow cytometry at baseline (w0) and after the described procedure on d14 (w2). Measuring of hCD16+ cell populations was not carried out for all individuals, indicated by the note nd (not done). This table is adopted from Supplementary Table 1 from Vanshylla et al. 2021¹³².

	x < 10		10 ≤ x < 100		100 ≤ x		nd							
Mouse ID	hu-CD45+		hu-CD3+		hu-CD4+		hu-CD8+		hu-CD19+		hu-CD16+		m-CD45+	
	w0	w2	w0	w2	w0	w2	w0	w2	w0	w2	w0	w2	w0	w2
1317	13,2	977,9	4,9	927,1	4,0	446,3	0,8	439,1	6,3	0,7	nd	nd	846,6	801,9
1320	41,3	1019,3	38,1	977,6	31,7	507,3	3,3	417,7	1,0	0,7	nd	nd	876,3	3291,4
1344	373,2	542,3	32,1	472,4	18,0	198,2	12,7	204,5	323,6	11,0	nd	nd	793,1	45,1
1550	98,1	632,7	54,8	615,6	32,7	202,0	19,1	354,6	38,4	9,2	nd	nd	719,4	201,3
1571	4,0	229,4	3,8	225,7	2,9	162,1	0,4	54,2	0,1	0,5	nd	nd	652,6	981,2
1618	0,9	22,2	0,7	21,5	0,1	9,9	0,5	8,8	0,0	0,1	nd	nd	673,3	911,8
1800	65,7	181,0	23,1	170,5	9,7	56,1	3,8	88,8	33,2	5,4	nd	nd	524,1	24,0
1551	78,5	260,0	62,9	256,2	31,9	79,8	27,1	156,8	10,6	1,7	nd	nd	538,6	219,3
1578	5,7	87,0	4,7	85,2	1,2	33,7	2,7	44,1	0,3	0,3	nd	nd	1874,5	1078,5
1614	32,2	140,4	31,9	139,1	26,3	87,9	4,2	45,4	0,0	0,0	nd	nd	1329,2	2288,0
1782	46,0	490,5	44,2	486,2	18,1	244,5	3,5	155,7	0,7	0,2	nd	nd	842,1	1930,3
1502	3,8	348,7	3,8	340,5	2,4	171,5	0,8	136,0	0,0	0,1	0,0	4,2	1052,2	1454,1
1508	63,8	141,0	63,2	139,7	59,4	100,0	2,9	32,7	0,0	0,1	0,1	1,2	1550,3	1322,3
1529	2,9	135,8	2,8	131,6	0,6	43,1	1,9	72,2	0,0	0,1	0,0	1,8	670,3	865,0
1534	2,1	1039,1	2,1	1014,1	1,4	406,3	0,7	470,8	0,0	0,4	0,0	23,0	1101,6	786,0
1539	0,5	260,9	0,4	256,1	0,1	135,3	0,2	109,3	0,0	0,0	0,0	2,8	510,3	2004,4
1542	12,5	289,6	12,5	282,8	8,8	174,9	3,5	99,1	0,0	0,2	0,0	4,4	1239,9	2861,7
1901	0,1	39,1	0,1	16,3	0,0	7,1	0,1	7,1	0,0	0,1	0,0	17,4	462,7	1184,8
1915	7,5	134,9	7,5	89,9	6,0	38,8	1,5	44,4	0,0	0,2	0,0	32,0	999,0	1774,1
2021	37,5	73,2	11,6	56,8	8,6	29,4	2,5	21,8	18,5	11,0	0,2	1,2	373,5	312,8
2039	13,2	97,2	0,6	94,2	0,3	33,8	0,1	44,7	10,6	0,4	0,1	1,8	553,4	418,4
2047	15,9	2065,4	9,6	2026,4	6,4	1197,6	2,1	723,4	1,8	0,0	0,9	32,2	301,3	1075,9
1930	16,8	64,7	6,5	23,1	5,4	17,6	0,9	3,6	7,4	29,7	0,3	5,3	342,3	1122,0
1931	50,8	164,6	29,7	117,9	22,3	81,3	6,3	31,8	14,1	35,6	2,2	7,1	547,8	764,7
1956	43,5	41,8	4,8	8,0	2,2	3,8	2,1	3,7	33,8	21,6	0,4	1,0	2004,9	10542,0
1958	36,9	44,8	10,1	19,7	7,3	13,4	2,2	5,0	22,4	19,9	0,8	2,3	1369,7	808,1
1959	50,0	127,2	12,8	45,8	9,2	32,7	2,5	10,8	29,3	54,7	3,7	20,1	657,2	812,5
1960	29,9	49,6	16,5	28,2	11,9	17,8	3,4	7,3	9,9	15,8	1,1	2,5	654,0	589,1
1961	60,8	139,2	36,4	121,3	19,8	65,3	14,6	48,6	14,6	7,3	5,2	10,1	287,3	95,6
1962	85,2	210,1	30,7	128,2	23,8	70,5	5,2	48,7	43,1	58,7	2,7	17,0	320,0	226,2
2071	43,7	43,3	42,8	42,4	0,1	13,8	39,6	26,4	0,0	0,0	0,1	0,1	3089,6	2544,1
2098	1,6	6,1	0,9	4,4	0,4	1,9	0,4	2,2	0,4	0,8	0,0	0,2	1153,0	1186,1
2099	0,9	15,3	0,9	14,8	0,9	10,4	0,0	4,1	0,0	0,0	0,0	0,1	1120,4	1237,4
2109	3,7	73,6	3,7	73,0	1,0	28,3	2,7	42,0	0,0	0,2	0,0	0,1	3764,3	5449,2
2149	102,4	288,0	32,2	204,6	16,0	105,7	15,3	88,7	57,7	63,6	1,3	7,5	702,7	690,1
2150	65,7	50,9	61,1	48,8	39,5	28,2	18,4	19,4	3,3	0,7	0,1	0,1	422,8	397,1
2154	258,6	199,6	176,1	179,2	90,3	149,9	82,1	26,7	73,3	16,6	1,2	0,5	986,5	768,7
2168	70,9	132,8	11,1	50,5	7,9	32,7	2,7	14,7	52,7	55,9	0,9	11,2	472,2	684,0
2169	31,6	37,5	30,8	37,0	18,6	20,6	11,3	14,7	0,2	0,1	0,1	0,1	528,0	797,8
2242	1,2	10,9	1,1	8,0	0,9	6,5	0,1	0,9	0,0	2,7	0,0	0,1	938,9	2610,6
2372	28,7	62,4	7,6	23,8	6,0	17,1	1,4	6,1	17,7	32,6	0,4	1,7	560,2	877,8
2381	211,7	305,5	3,8	54,2	1,2	34,4	2,5	11,0	191,6	201,5	1,4	29,5	1054,7	619,5
2373	51,2	1924,0	48,7	1906,8	30,2	1159,6	15,3	684,5	1,4	0,4	0,5	2,0	810,4	1742,6
2376	61,5	513,5	17,2	499,4	11,9	273,9	3,4	199,9	36,2	1,1	1,1	8,9	1263,2	542,6
2405	282,0	444,6	49,9	278,5	41,7	167,0	7,1	105,8	211,8	127,1	3,7	20,4	610,9	249,3
2410	55,2	146,0	54,1	143,0	41,1	35,8	8,6	101,6	0,9	0,0	0,0	0,2	1237,9	1215,2
2412	69,5	155,1	17,8	146,1	5,6	78,7	10,4	59,6	44,9	2,5	3,4	1,2	1307,0	963,7

2415	88,7	1101,7	81,3	1081,6	65,7	741,4	10,3	306,1	5,6	0,0	0,1	14,8	1907,1	607,1
2417	81,0	1762,5	9,5	1634,3	7,4	949,5	1,8	595,1	63,9	5,7	0,7	69,9	876,5	551,8
2418	159,1	4613,0	9,6	4093,2	7,0	2064,8	2,5	1769,1	136,3	29,8	0,5	338,3	1766,9	1445,9
2419	200,7	939,5	7,0	597,8	2,3	180,7	4,3	372,7	172,1	45,3	1,0	232,0	804,3	26,4
2422	79,3	1621,1	5,2	1489,8	2,5	892,5	2,6	476,9	70,5	3,2	0,7	91,0	1153,6	372,7
2424	52,1	238,4	19,2	176,6	13,8	73,2	5,2	85,3	30,4	44,3	0,7	14,4	1743,1	620,6
2425	32,6	301,6	5,4	281,9	3,4	95,4	1,3	157,8	24,9	5,6	0,2	8,7	882,2	949,5
2426	37,7	339,9	14,5	336,0	12,2	171,0	1,1	146,1	22,1	0,3	0,1	0,6	975,7	1846,7
2429	51,5	209,2	6,3	173,3	4,1	75,3	2,0	76,8	39,1	24,0	0,3	5,6	611,9	776,6
2431	91,2	787,3	23,6	755,1	10,5	244,8	9,6	462,9	58,5	4,4	1,2	14,1	1010,1	824,5
2433	285,0	384,4	6,7	246,8	1,0	75,0	2,8	138,3	262,1	75,5	2,2	49,7	722,5	94,5
2434	563,8	409,6	58,8	235,7	20,9	62,3	27,2	157,4	482,9	154,4	4,1	11,5	541,4	45,9
2435	60,8	322,2	5,4	263,0	3,1	64,7	2,0	182,5	50,2	49,2	0,4	6,0	1184,5	156,9
2436	35,8	230,0	2,9	221,1	1,6	53,9	1,0	128,7	29,9	3,5	0,2	1,7	1071,0	1344,2
2438	22,3	437,5	2,6	419,5	1,0	213,5	1,5	169,0	18,2	2,7	0,2	5,5	854,5	1775,7
2439	12,0	215,1	4,0	200,6	2,0	117,7	1,8	63,4	6,7	0,5	0,1	7,6	1854,1	993,7
2443	94,0	251,2	5,1	205,9	2,7	84,0	2,4	103,8	85,6	24,8	0,7	6,8	1361,4	841,0
2444	133,9	4889,2	44,0	4759,8	16,9	2260,5	16,9	2296,9	86,5	70,1	1,1	8,4	959,4	676,9
2551	118,1	172,1	7,4	78,1	4,3	52,1	2,9	20,2	104,8	71,7	1,1	15,8	914,2	672,9
2571	18,6	160,0	15,2	149,3	11,4	100,2	3,7	40,4	0,0	0,7	2,4	8,2	432,4	1202,3
2575	10,3	31,4	9,9	30,5	3,4	16,6	5,9	11,1	0,0	0,1	0,0	0,1	877,1	6681,7
2649	142,4	591,6	136,7	578,6	89,8	446,8	40,0	108,9	2,4	3,2	0,2	6,0	1077,0	1671,3

Table 5.2 Leukocyte concentrations of the CD34+ control group at w0 and w2¹³²

$n=42$, mouse ID given in left column, human CD45+, CD3+, CD3+CD4+, CD3+CD8+, CD19+ and CD16+ as well as murine CD45+ cell concentrations were determined via flow cytometry at baseline (w0) and after the described procedure on d14 (w2). Measuring of hCD 16+ cell populations was not carried out for all individuals, indicated by the note nd (not done). This table is adopted from Supplementary Table 2 from Vanshylla et al. 2021¹³².

$x < 10$	$10 \leq x < 100$	$100 \leq x$	nd
----------	-------------------	--------------	----

Mouse ID	hu-CD45+		hu-CD3+		hu-CD4+		hu-CD8+		hu-CD19+		hu-CD16+		m-CD45+	
	w0	w2	w0	w2	w0	w2	w0	w2	w0	w2	w0	w2	w0	w2
1300	447,3	258,2	4,5	7,1	12,2	24,8	17,4	33,5	408,2	193,4	nd	nd	641,4	255,0
1306	493,7	235,6	6,6	6,9	14,2	10,6	23,3	18,5	456,9	209,5	nd	nd	524,2	195,2
1321	42,2	134,3	5,7	10,6	24,2	113,0	31,0	124,9	9,9	0,4	nd	nd	803,2	773,2
1337	4,2	3,9	0,5	0,1	0,8	0,8	1,5	0,9	1,7	0,9	nd	nd	2340,8	3357,8
1548	45,2	54,6	23,8	21,5	19,3	30,3	44,9	54,4	0,1	0,0	nd	nd	804,5	591,7
1576	60,7	86,5	4,7	6,7	14,1	30,0	19,4	37,3	33,9	38,2	nd	nd	899,1	694,7
1620	7,0	17,1	0,0	0,6	1,6	3,0	1,7	3,9	4,5	11,5	nd	nd	945,5	936,8
1802	26,8	64,9	2,4	2,3	2,6	4,5	5,4	7,7	16,3	49,9	nd	nd	485,3	619,3
1549	115,6	161,9	14,8	24,9	27,0	50,3	43,7	78,4	64,6	71,6	nd	nd	427,0	382,9
1617	21,3	9,8	2,2	1,1	15,5	6,7	18,9	8,6	1,0	0,7	nd	nd	1809,4	840,0
1619	0,3	0,6	0,1	0,3	0,1	0,2	0,3	0,6	0,0	0,0	nd	nd	1300,3	1041,1
1803	213,3	38,6	36,9	9,4	57,5	13,9	210,2	38,2	0,7	0,1	nd	nd	381,1	1096,2
1506	1,9	1,5	0,4	0,5	1,3	0,6	1,8	1,4	0,0	0,0	0,0	0,1	956,8	935,7
1535	18,8	0,3	0,3	0,1	0,2	0,1	0,7	0,3	15,1	0,0	0,1	0,0	466,9	338,9
1541	3,3	2,1	1,5	0,9	1,2	0,8	3,3	1,8	0,0	0,0	0,0	0,0	838,2	648,9
1996	14,2	18,4	1,9	1,6	1,5	2,7	3,7	4,8	7,8	10,6	0,0	0,0	510,1	636,7
2035	18,6	7,3	3,0	0,7	5,9	0,9	8,9	1,7	7,5	4,8	0,0	0,0	1004,8	547,8
2040	23,2	15,2	0,4	2,7	13,4	11,1	14,7	14,6	7,6	0,5	0,1	0,1	247,8	695,7
2044	1,7	2,4	0,1	0,2	0,3	0,2	0,4	0,5	0,9	1,0	0,0	0,1	544,6	1150,6
2048	5,6	2,2	1,9	0,7	3,5	1,2	5,6	2,1	0,0	0,0	0,0	0,1	875,3	1518,0
2049	74,9	20,0	4,4	2,8	63,8	16,1	74,5	19,7	0,1	0,0	0,1	0,1	617,4	1724,6
2050	17,3	47,0	0,1	0,5	2,6	19,3	3,2	20,4	8,3	19,1	0,6	1,2	274,4	164,9

1929	78,5	120,0	10,2	10,6	16,6	32,7	29,0	45,3	37,3	63,8	1,6	5,2	400,2	416,9
1964	91,6	115,3	9,4	12,8	28,7	27,1	40,3	42,8	33,3	54,5	8,4	8,5	480,0	477,4
2070	23,0	16,8	0,2	0,0	22,6	16,4	22,9	16,5	0,0	0,0	0,0	0,0	1043,7	1917,9
2151	86,8	266,9	26,0	104,0	34,9	99,0	65,5	217,6	8,5	21,4	1,8	10,5	617,1	789,3
2156	12,1	11,0	3,2	3,8	8,4	6,3	12,1	10,8	0,0	0,1	0,0	0,1	983,1	814,6
2171	47,8	89,2	10,0	22,4	9,3	27,2	19,7	51,6	21,2	21,2	0,6	3,2	215,4	261,1
2371	54,6	60,6	2,2	2,1	3,4	3,6	6,3	5,9	42,7	48,8	0,3	0,3	1123,7	852,4
2382	115,0	112,9	5,1	7,6	2,9	5,9	9,2	14,6	90,6	80,0	1,4	2,3	612,7	473,3
2375	158,3	133,2	1,5	1,8	15,1	7,6	17,6	10,4	127,6	110,0	2,0	2,0	1263,5	742,7
2378	513,2	340,8	1,4	0,8	8,0	5,0	9,8	6,5	468,2	311,6	5,8	6,9	521,0	329,6
2397	297,6	308,7	3,9	3,9	3,7	6,0	9,0	11,2	264,7	272,6	1,7	4,5	864,1	858,5
2398	132,0	208,5	3,1	3,0	5,8	13,3	10,3	17,5	111,6	171,7	0,6	3,8	1215,0	876,2
2400	247,1	284,7	4,2	2,2	4,1	15,7	9,4	19,4	213,9	237,1	2,0	4,5	1180,1	693,8
2421	50,4	26,8	10,4	11,4	8,5	9,5	21,1	22,9	26,2	2,0	1,2	0,1	695,1	1313,5
2430	70,4	72,1	7,8	4,1	5,9	6,4	13,7	10,9	50,8	53,0	0,3	1,0	610,8	986,5
2442	234,5	33,9	11,1	6,6	14,8	10,0	27,0	18,8	189,3	13,3	1,4	0,3	739,4	1138,2
2549	47,4	31,2	2,0	2,1	11,2	10,1	13,6	12,2	29,6	17,8	0,3	0,1	556,2	660,9
2550	84,7	84,6	0,3	1,0	0,6	0,4	1,2	1,8	78,6	79,1	0,9	1,0	1022,1	665,6
2573	3,9	4,5	1,7	2,2	1,0	1,5	2,8	4,3	0,6	0,0	0,0	0,0	1083,7	1105,9
2647	22,4	18,2	8,3	5,2	10,3	10,4	20,2	16,5	1,2	1,0	0,2	0,1	1433,4	501,7

5.1.3. The prior humanization with donor-matched HSCs is essential for an enhanced human leukocyte reconstitution post UCBC administration

Next, we addressed the prior humanization as a key feature of the novel CD34T+ model and wanted to evaluate the human cell reconstitution of non-humanized (NRG) mice, that receive the same regime of human Il-7 applications and either the UCBCs (NRG-UCBC group) or PBMCs (NRG-PBMC group) derived from adult blood donors instead of the donor-matched UCBC injection. Absolute cell numbers administered were consistent with the CD34T+ model, by that meaning $30-45 \times 10^6$ cells per mouse. Flow cytometric measurement of peripheral blood human leukocyte concentrations was performed 14 days after the *i.p.* cell injection (Figure 5.3).

We employed 13 mice in this experiment, 4 mice in the NRG-PBMC group and 9 mice in the NRG-UCBC group.

The NRG-UCBC group showed significantly lower human T lymphocyte levels compared to the NRG-PBMC group as well as to the overall mean observed in the CD34T+ model. The NRG-PBMC group on the other hand was found to possess similar human immune cell concentrations as the CD34T+ mice. However they rapidly developed symptoms of impaired health, including fur loss, bent posture and visible weight loss, that can be interpreted as features of GvHD in mice which has previously been shown^{97,113}.

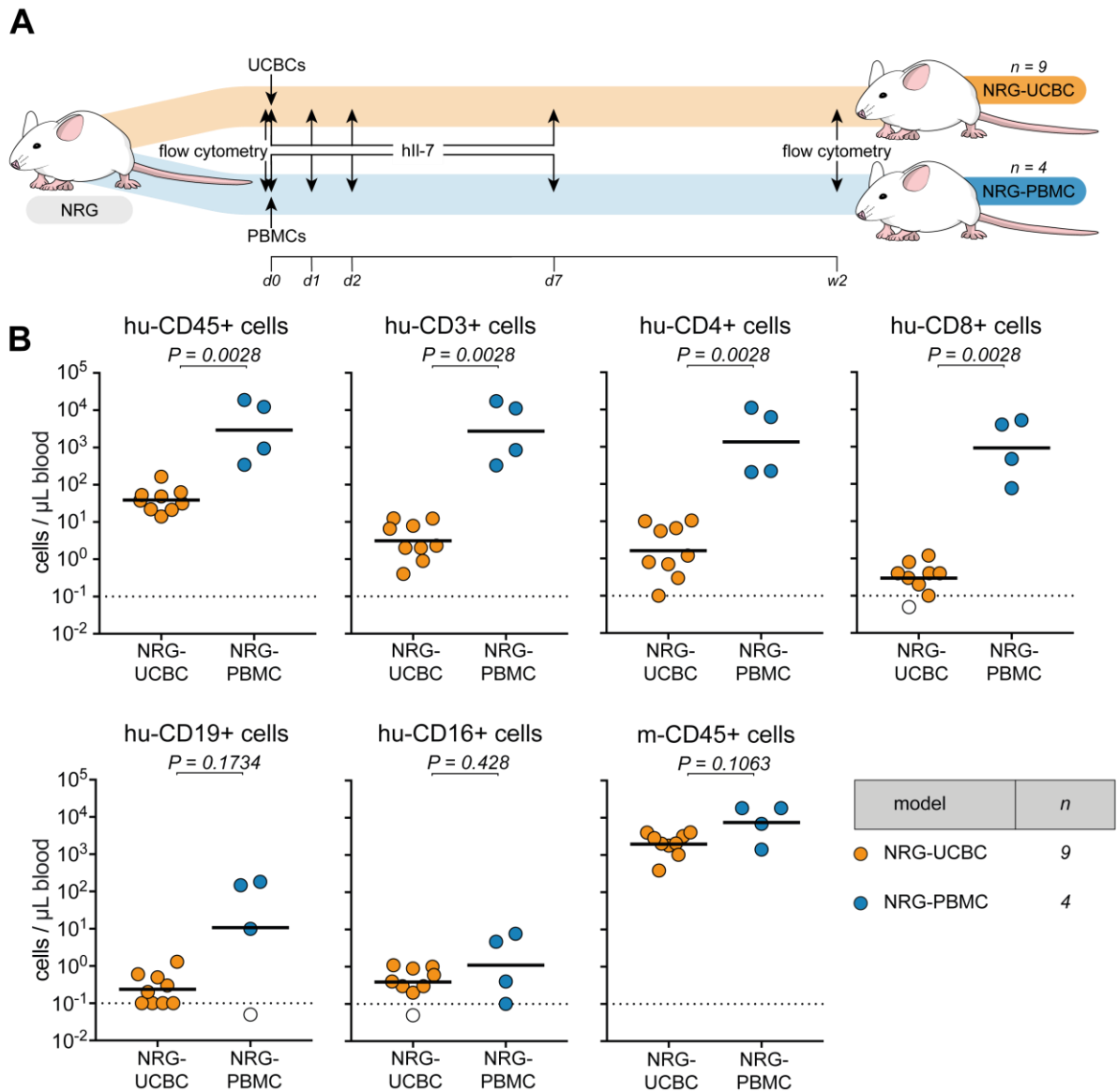


Figure 5.3 comparison of leukocyte concentrations in the peripheral blood in NRG-UCBC and NRG-PBMC mice¹³²

A schematic overview of the experiment timeline. Adult NRG mice either received UCBCs (NRG-UCBC group) or PBMCs (NRG-PBMC group), both accompanied by Il-7 injections on days 0, 1, 2 and 7 post cell-injection. After 2 weeks, leukocyte concentrations in the blood were measured. **B** Depicted are the cell concentrations after 2 weeks. NRG-UCBC mice exhibit significantly less hCD45+ cells which is majorly attributable to the hCD3+ cell population including both CD4+ and CD8+ cells. Statistical analysis was done using a Wilcoxon–Mann–Whitney test. This figure is Supplementary Figure 2B from Vanshylla et al. 2021¹³².

We further addressed the donor-matching as key feature of the novel model. Therefore, we compared CD34T+ mice (CD34T+ group) to humanized mice, that were then treated with PBMCs from adult blood donors instead of the donor-matched UCBCs (CD34+-PBMC group) (Figure 5.4). In conclusion, the administered cells did not match with the previously engrafted HSCs that were derived from placenta donors. We employed a total of 20 mice, equally

distributed into the two groups regarding age and sex. 3 different placenta donors were used for the HSCs as well as the UCBCs and we chose even numbers per placenta and group. Mice were distributed in order to obtain a similar geometric mean of baseline human CD4+ cell concentrations in the flow cytometric measurement from peripheral blood. In the CD34+-PBMC group we administered PBMCs from three different blood donors with the maximum possible variation in placenta donor PBMC donor combinations.

The two groups displayed a similar human cell reconstitution in the peripheral blood after 2 weeks. This experiment indicates that UCBCs are not inferior to PBMCs in enhancing human cell reconstitution and particularly hCD4+ TC levels in the peripheral blood in CD34+ engrafted mice. Mice in the CD34+-PBMC group did however develop clinical features of GvHD including fur loss and hunched posture more rapidly than mice that received donor-matched UCBCs instead.

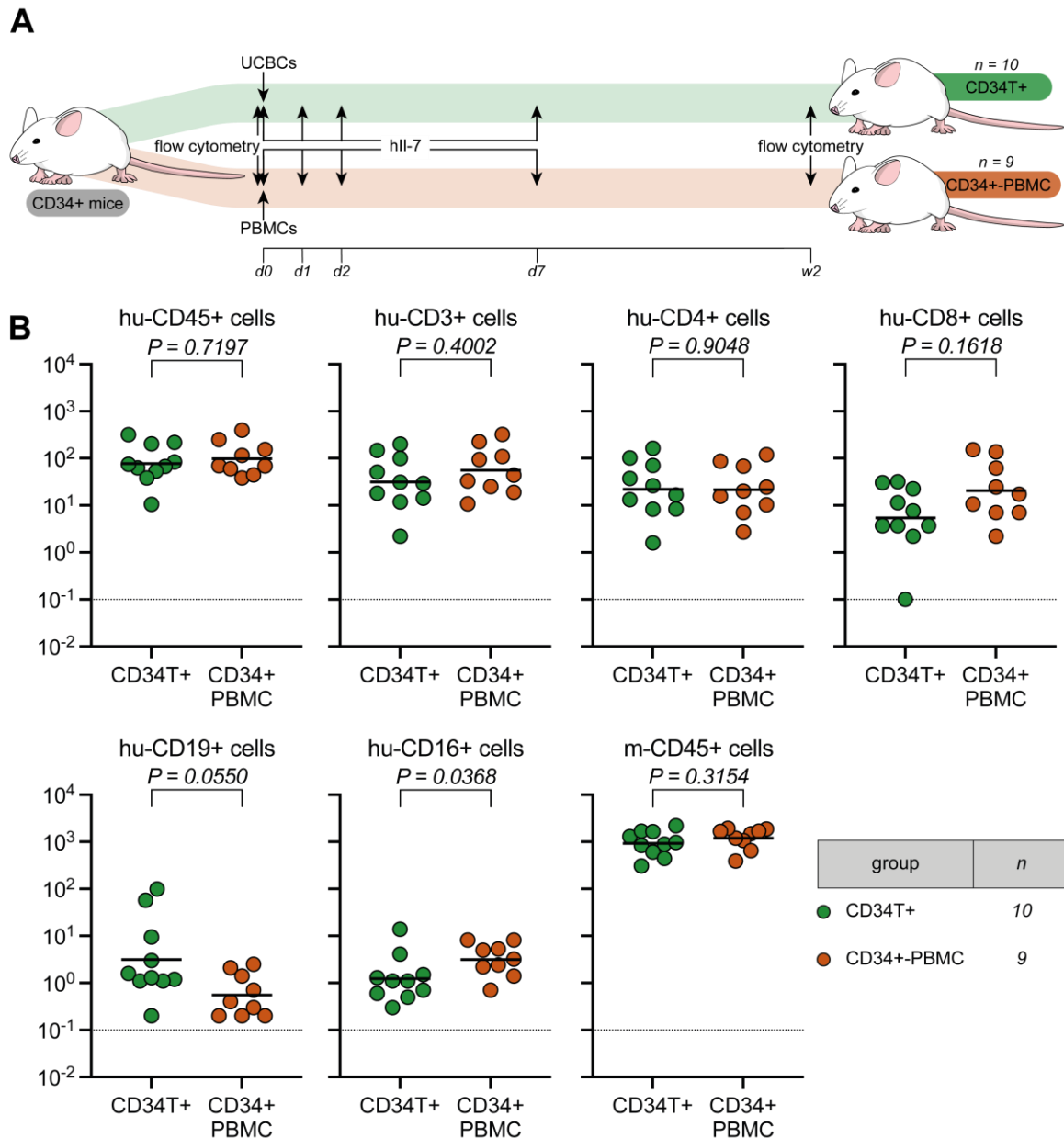


Figure 5.4 Leukocyte concentrations of CD34T+ mice compared to CD34+-PBMC mice

A schematic overview of the experiment timeline. Adult CD34+ mice either received UCBCs (CD34T+ group) or PBMCs (CD34+-PBMC group), both accompanied by Il-7 injections on days 0, 1, 2 and 7 post cell injection. After 2 weeks, leukocyte concentrations in the blood were measured. **B** Depicted are the cell concentrations after 2 weeks. Total human cell reconstitution, concentration of human CD3+, CD4+, CD8+ and CD19+ did not differ significantly. CD34+-PBMC mice only exhibited significantly higher levels of human CD16+ cells. Statistical analysis was done using a Wilcoxon–Mann–Whitney test.

In summary, the CD34T+ mouse model was superior to the compared alternatives in terms of the peripheral blood human TC reconstitution.

5.1.4. The CD34T+ model displays a significant increase in the human T cell presence in the gut mucosal tissue

Since a mucosal HIV-1 infection requires contact to susceptible human cells at the site of infection, the presence of human CD4+ cells is regarded a critical factor in susceptibility for this route of transmission. To evaluate the human cell reconstitution in different lymphoid tissues we isolated cells from the spleen and gut from CD34T+ mice and CD34+ mice serving as comparison (Figure 5.5). Via flow cytometry we measured the proportions of human leukocytes in the murine spleen, the LP and IEL of the intestine. In both the LP and the IEL CD34T+ mice exhibited significantly higher proportions of human CD4+ TCs while the difference in the splenic leukocytes was not significant. In parallel we measured the murine CD45+ cells, which represent the total of murine leukocytes. Since their proportions were similar across the two compared groups, a similar level of purification can be assumed. Furthermore, hCD3+ cell proportions were significantly higher in all three regarded tissues and hCD8+ cell proportions in the LP and spleen.

All other regarded human leukocyte subpopulations did not exhibit significant differences between the groups in neither regarded tissue.

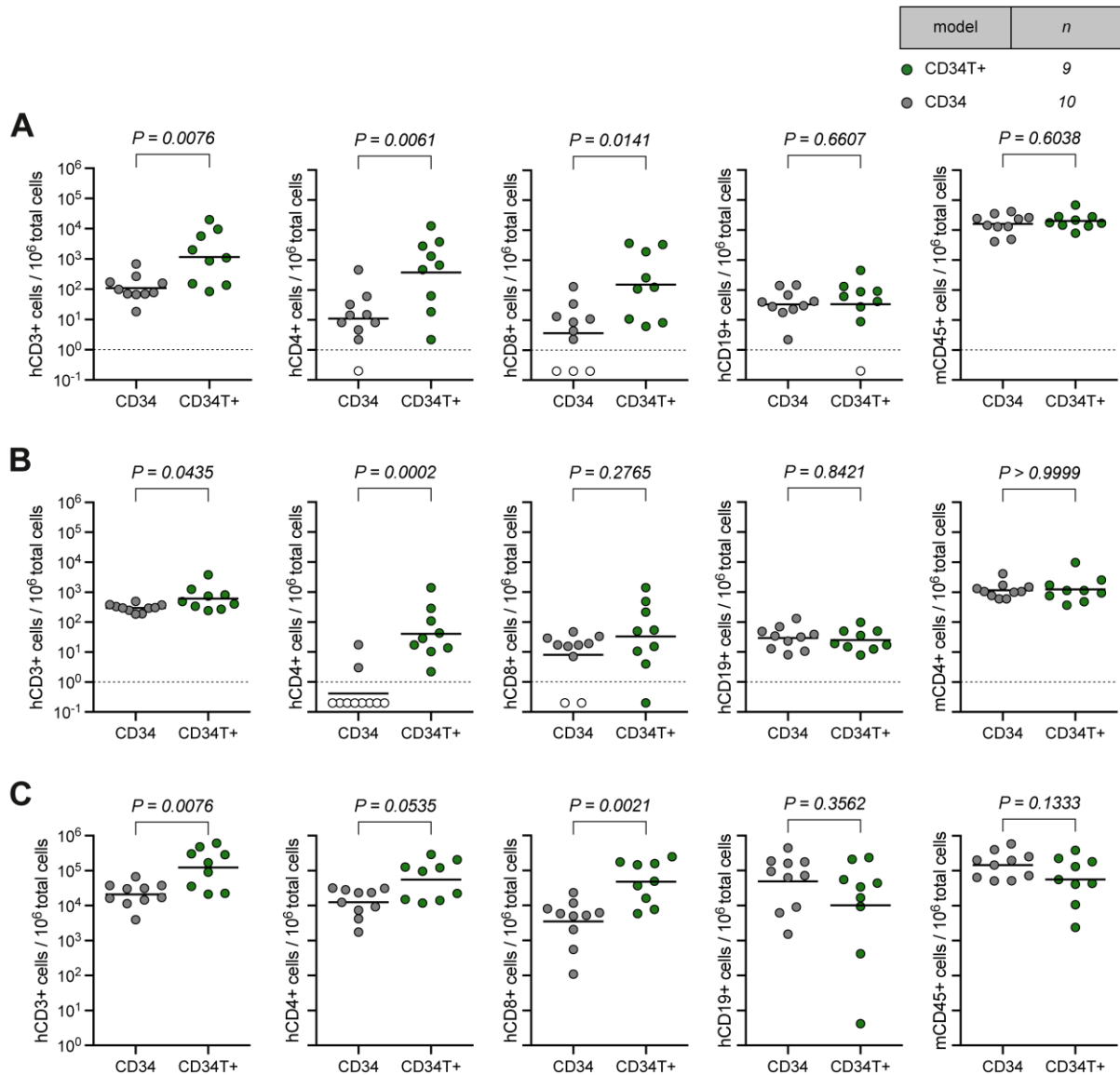


Figure 5.5 comparison of leukocyte concentrations in secondary lymphoid tissue of the CD34T+ and the CD34+ control group ¹³²

Depicted are cell concentrations in the intestinal lamina propria (**A**), the intra-epithelial layer of the intestine (**B**) and the spleen (**C**) for 9 mice of the CD34T+ (green) and 10 mice of the CD34+ control group (grey). Values below detection limit are displayed in white. Statistical analysis was done using an Wilcoxon–Mann–Whitney test and two-tailed P values are indicated above two compared data sets. This figure is derived from figures 1C and S3A from Vanshylla et al. 2021¹³².

Immunofluorescence staining of intact tissue slices allowed for further investigation of the origins of the detected cell populations (Figure 5.6). In the gut samples we primarily wanted to rule out that the cells were only located intravascularly but also present in the mucosa. The immunofluorescence analysis confirmed that human TCs were present in the gut sections of CD34T+ mice while none were identified in those from CD34+ mice. The cells were located in the LP, exhibiting an uneven distribution with accumulation around crypts and rarefication in

the villi. Of the human T lymphocytes in the stained slices, CD4+ cells were more frequent than CD8+ ones. No formed secondary lymphoid organs were found in the gut. In the splenic tissue slices, neither mouse model exhibited the defined zone-wise arranged organization known from immunocompetent mice or humans. However in some of the analysed CD34T+ mice, structures imitating the microscopic image of periarteriolar lymphoid sheaths (PALS) were found which was not the case for the CD34+ group respectively.

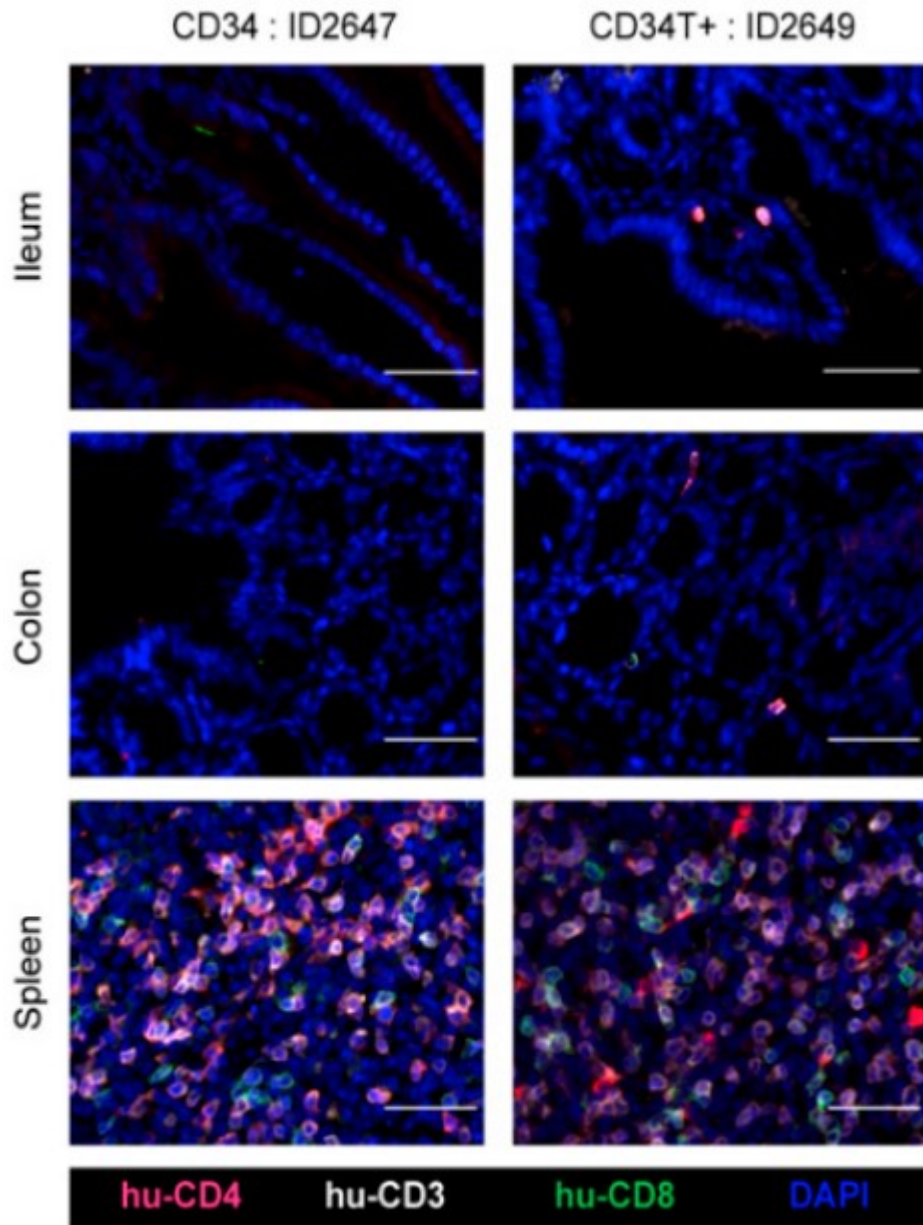


Figure 5.6 IF analysis of human T cells in the ileum, colon and spleen of CD34 and CD34T+ mice at week 2.¹³²

Human CD3+ (white), CD4+ (red), CD8+ (green) cells were labelled for detection along with DAPI for visualizing the nucleus. Scale bar is 50 μ m. Three mice per group were analysed with at least three different slices from different areas of each mouse tissue being analysed. Representative images were selected for display. This figure is equivalent to figure 1D from Vanshylla et al. 2021¹³². Imaging was performed by the Research group of Dr Kathrin Held and PD Dr Christof Geldmacher from the Division of Infectious Diseases and Tropical Medicine, University Hospital, LMU, Munich, Germany.

When plotting the hCD4+ TC proportions measured via flow cytometry in the LP, IEL and spleen against the hCD4+ TC levels derived from the peripheral blood sample flow cytometry, a positive linear correlation with Pearson correlation coefficient values $> 0,7$ (Figure 5.7) was found. The correlation for the IEL and LP pointed out that in the CD34T+ model, in addition to

an increased human CD4+ cell reconstitution also an efficient homing of these cells to the gut-associated lymphoid tissue (GALT) was present. Furthermore, this qualified the peripheral blood hCD4+ cell levels could serve as surrogate parameter for the mucosal reconstitution in the CD34T+ model.

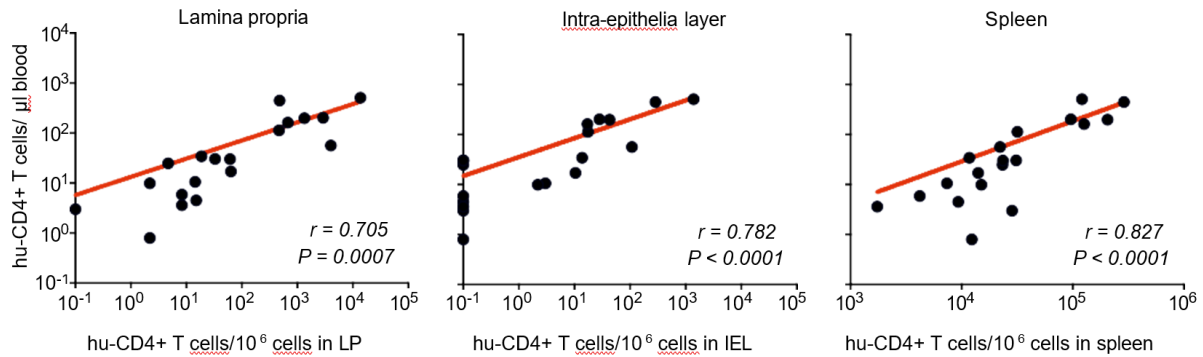


Figure 5.7 correlation of hCD4+ cell concentrations in peripheral blood and regarded secondary lymphoid tissue

We plotted the determined hCD4+ cell concentrations in the analysed tissue (LP, IEL and spleen) against the measured hCD4+ cell concentrations in the peripheral blood for all animals we performed organ leukocyte measurement on (CD34T+ and CD34+ group), $n = 19$. Combined Pearson correlation curves are plotted and correlation coefficients are displayed, a strong correlation ($r > 0,7$) was noted for all regarded tissues. This figure is Supplementary Figure 3C from Vanshylla et al. 2021¹³².

5.1.5. The CD34T+ mouse model is highly susceptible to mucosal HIV-1 infection

Since the main goal of the novel CD34T+ model was to facilitate the study of mucosal HIV-1 transmission, we wanted to address the susceptibility of this model to a mucosal HIV-1 exposure. Again, the CD34+ model was employed as control group. We compared a group of 5 CD34T+ mice to 17 CD34+ mice. All mice were challenged intrarectally with NL4-3_{YU2} HIV-1 on two consecutive days (day 0 and 1) and viral load measurements from peripheral blood were performed on days 14, 21, 28, 35 and 42.

In the CD34+ group, 2 mice died before viral loads were measured. Out of the remaining 15, only 5 mice developed detectable viremia. To verify the general ability of these mice to establish a productive HIV-1 viremia, the uninfected 11 mice were challenged with an *i.p.* application of NL3-4_{YU2} HIV-1 after 42 days of absence of viremia after the first *i.r.* challenge. On 2 consecutive days, NL3-4_{YU2} HIV-1 was administered *i.p.* and on days 14 and 21, the HIV-1 viral load from peripheral blood was measured via qPCR. All 11 mice developed detectable viremia until day 21 confirming their systemic susceptibility.

In the CD34T+ group on the other hand, all 5 mice developed detectable viremia within 21 days post *i.r.* challenge. Furthermore, HIV-1 RNA copies per mL plasma were significantly higher than in the fraction of CD34+ mice that became viraemic after mucosal challenge.

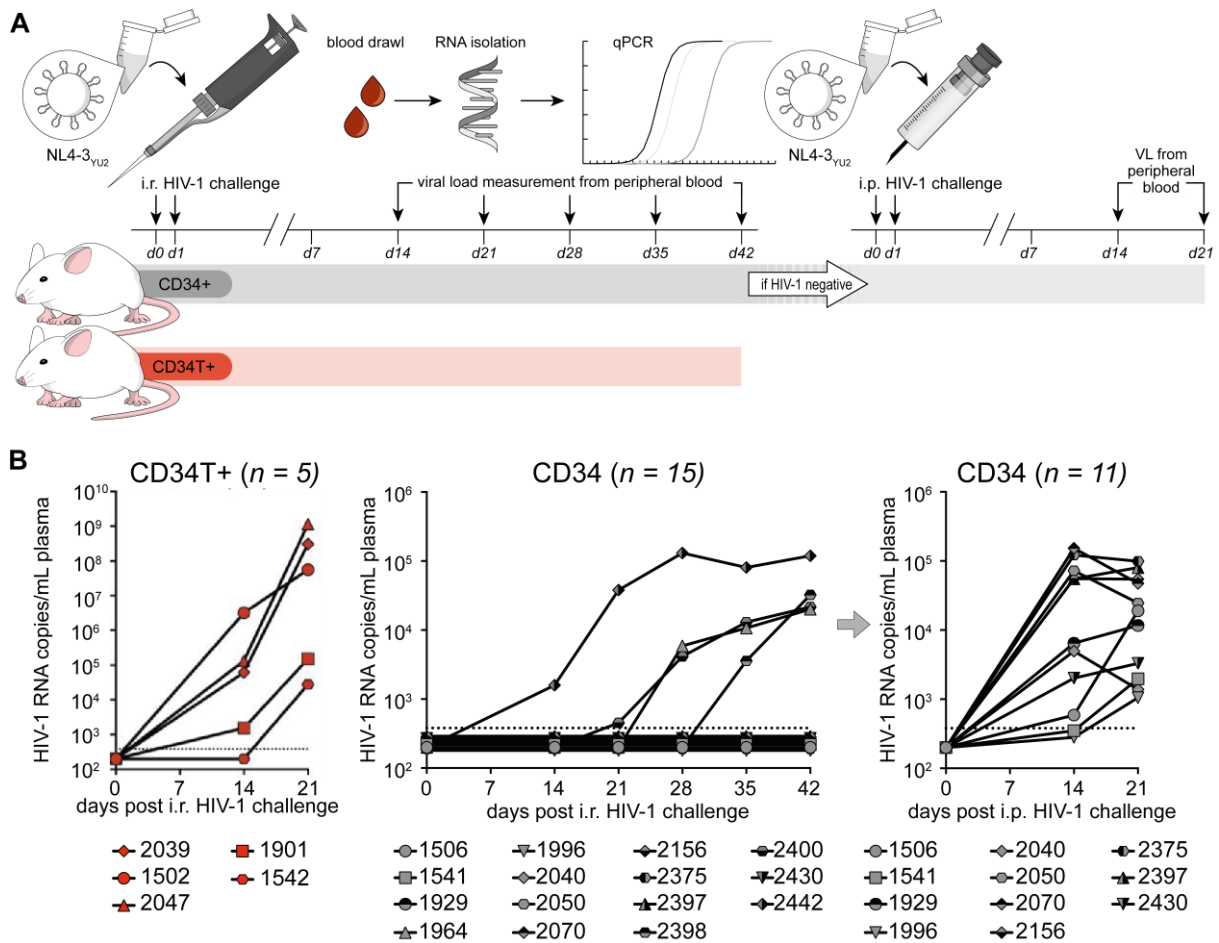


Figure 5.8 CD34T+ mice are highly susceptible to mucosal HIV-1 transmission

A schematic overview of the experimental design: CD34+ mice (grey) in parallel with CD34T+ mice (red) were exposed to HIV-1 NL4-3_{YU2} via *i.r.* application on 2 consecutive days (d0, d1). Consecutively, viral loads were determined via qPCR from RNA isolated from peripheral blood on d14, d21, d28, d35 and d42. Mice, that did not exhibit viraemia by day d42 post challenge were challenged with HIV-1 NL4-3_{YU2} intraperitoneally. Only mice from the CD34+ group fulfilled this criteria and were rechallenged respectively. **B** HIV-1 RNA copies/mL blood plasma are represented for each mouse (mouse ID given below). The detection limit of 384 copies/mL is represented by a dotted line. This figure is adopted from Figure 2B and Supplementary Figure 4B from Vanshylla et al. 2021¹³².

5.1.6. Highly potent bnAbs can prevent mucosal HIV-1 infection in CD34T+ mice

We wanted to finally evaluate the potential of the CD34T+ mouse model in the testing of novel molecules for their capabilities to prevent mucosal HIV-1 infection. BnAbs against HIV-1 had already been shown to prevent *i.p.* HIV-1 infection in CD34 mice and suppress viremia in humans¹³⁴.

Here we applied a triple combination of bnAbs, that are highly efficient in neutralizing NL4-3_{YU2} HIV-1 each possessing a different target epitope on the virion: 3BNC117 that targets the CD4-binding site, 10-1074 targeting the V3 loop and SF12 which recognizes the silent face¹²⁵⁻¹²⁷. Neutralizing activity against the infectious molecular HIV-1 clone of use, NL4-3_{YU2} was determined *in vitro* using a TZM-bl assay for each bnAb separately as well as for the equimolar combination (Tri-mix). The Tri-mix exhibited an IC₅₀ of 0.107 µg/mL and IC₈₀ of 0.320 µg/mL.

We set up an experiment with 5 CD34T+ mice that received the Tri-mix as an *i.p.* infusion a day prior to an intrarectal HIV-1 challenge whereas 6 CD34T+ mice without bnAb application served as control and were challenged *i.r.* in the same manner. On days 14 and 21 post HIV-1 exposure, viral loads were determined.

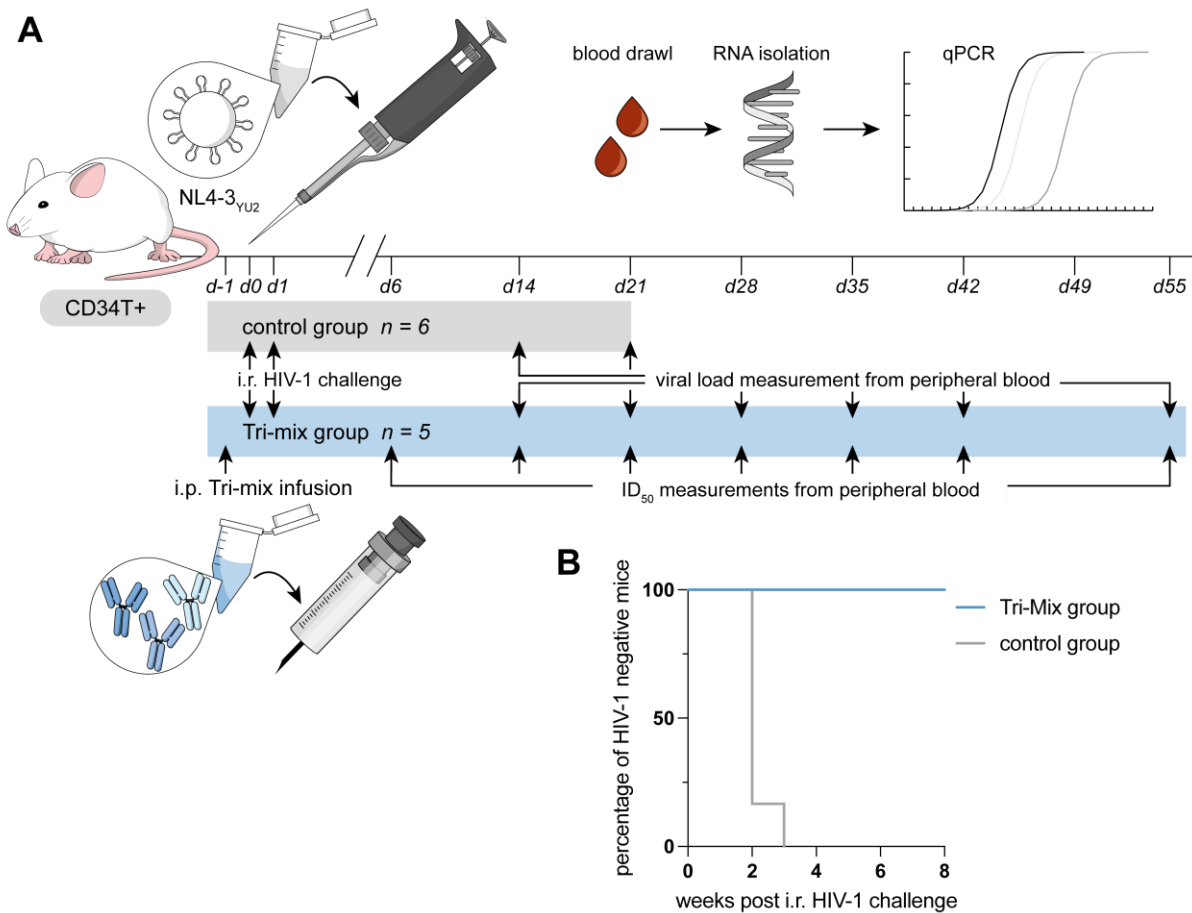


Figure 5.9 protective potential of bnAbs against intrarectal HIV-1 challenge in CD34T+ mice

A schematic overview of the experiment. CD34T+ mice were distributed into a control group (grey) and the bnAb Tri-mix (Tri-mix group) (blue). The Tri-mix group received the *i.p.* bnAb infusion 1 day prior to HIV-1 challenge (d-1), both groups were challenged *i.r.* with HIV-1 NL4-3_{YU2} on two consecutive days (d0, d1) and followed up for viral loads on days 14 and 21. Further viral load measurements were only conducted for the Tri-mix group since all mice in the control group were viraemic by d21. In the Tri-mix group, additional determination of plasma ID₅₀ was performed in order to calculate antibody concentrations in the plasma. **B** Kaplan-Meier curves of the viraemia free survival in both groups. Curves significantly differ (P = 0.0009) in a Log-rank (Mantel-Cox) test. This figure is adopted from Figure 4 from Vanshylla et al. 2021¹¹⁹.

In the control group, all animals developed detectable viremia whereas in the Tri-mix group, no infection was detected. The group was followed up by weekly viral load measurements from peripheral blood until day 55 post challenge and all mice remained aviraemic (Figure 5.9). In parallel we followed up on the plasma concentrations of the administered Abs in the Tri-mix group. Therefore 50% inhibitory dilutions (ID₅₀) against NL4-3_{YU2} were measured from the heat-inactivated mouse plasma in a TZM-bl assay and by correlation to the IC₅₀ of the tri-mix, active antibody concentrations in the plasma were determined. On d35, Ab levels dropped below detection limit for all 5 mice, one of whom exhibited low detectable neutralizing activity again on d42 and d55 (Table 5.3).

Table 5.3 Pharmacokinetics of the bnAb Tri-mix in the CD34T+ mice

Depicted above are the plasma inhibitory dilutions against NL4-3_{YU2} and below the corresponding antibody concentrations calculated from ID₅₀ and tri-mix IC₅₀ value against NL4-3_{YU2}. Grey backgrounds signifies values below detection limit. This table is adopted from Supplementary figure 5 D and E from Vanshylla et al. 2021¹³².

timepoint	d0	d1	d6	d14	d21	d28	d35	d42	d55
mouse ID	Plasma ID50 levels against NL4-3 _{YU2}								
1960	6308	2788	1068	240	<45	<45	<45	<45	<45
2242	1330	849	250	45	<45	<45	<45	<45	<45
2169	6091	3361	622	144	<45	<45	<45	<45	<45
2410	8155	4432	1412	480	113	157	<45	56	70
2412	6819	3901	854	152	<45	<45	<45	<45	<45
	calculated plasma antibody concentrations in the mouse plasma (µg/mL)								
1960	857.89	379.17	145.25	32.64	<6.12	<6.12	<6.12	<6.12	<6.12
2242	180.88	115.46	34.00	6.12	<6.12	<6.12	<6.12	<6.12	<6.12
2169	828.38	457.10	84.59	19.58	<6.12	<6.12	<6.12	<6.12	<6.12
2410	472.99	257.06	81.90	27.84	6.55	9.11	<2.61	3.25	4.06
2412	395.50	226.26	49.53	8.82	<2.61	<2.61	<2.61	<2.61	<2.61

Despite the decline of Ab titres in the peripheral blood of the mice, none developed detectable HIV-1 infection, indicating the successful prevention and ruling out any latent infection that would have been revealed by the time of Ab clearance.

5.2. HIV-1 specific nanobody A6 can prevent mucosal HIV-1 infection *in vitro* and *in vivo*

In this work, we assessed the *in vivo* preventive potential of the V_HH A6⁵⁸ against HIV-1. We employed the novel CD34T+ model which we challenged intrarectally with a mixture of HIV-1 NL4-3_{BAL} and V_HH A6. We included a control group receiving equal viral doses and an HIV-1 unrelated nanobody, V_HH 6G2¹³⁵ (selected against a bacterial transporter protein, kindly provided by Dr E. Geertsma, Max Planck Institute of Molecular Cell Biology and Genetics, Dresden, Germany).

5.2.1. V_HH A6 neutralizes HIV-1_{BAL} in TZM-bl assay

Prior to the *in vivo* experiment, we assessed the *in vitro* neutralization capacity of both nanobodies in a TZM-bl assay. Both nanobodies were added at a maximum concentration of 1,250 µg/mL and a 1:5 dilution series was performed in order to cover both the expected IC₅₀ of V_HH A6 and high concentrations to reveal any potential unspecific interference. It is known, that a broad variety of factors can interfere with the TZM-bl assay, including anticoagulants, traces or cytotoxic drugs and undetermined factors from plasma or serum¹²⁹, which we wanted to rule out for the employed nanobody.

IC₅₀ of V_HH A6 was determined at 0.032 µg/mL, IC₈₀ at 0.124 µg/mL respectively. The unrelated V_HH 6G2 did not exhibit significant neutralization activity at any concentration, ensuring its suitability as control nanobody.

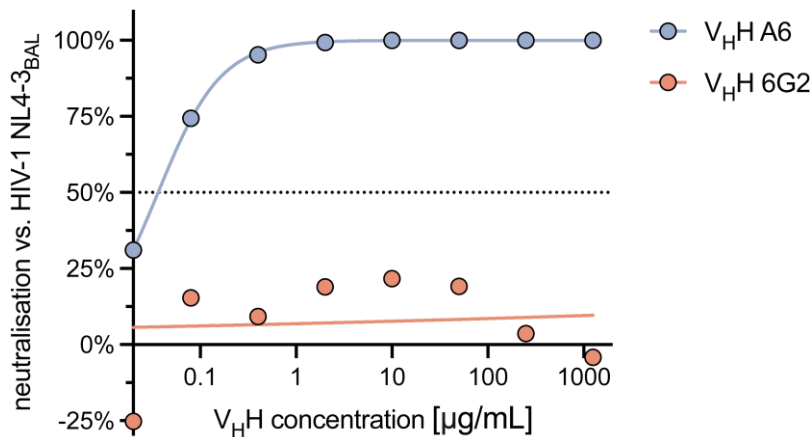
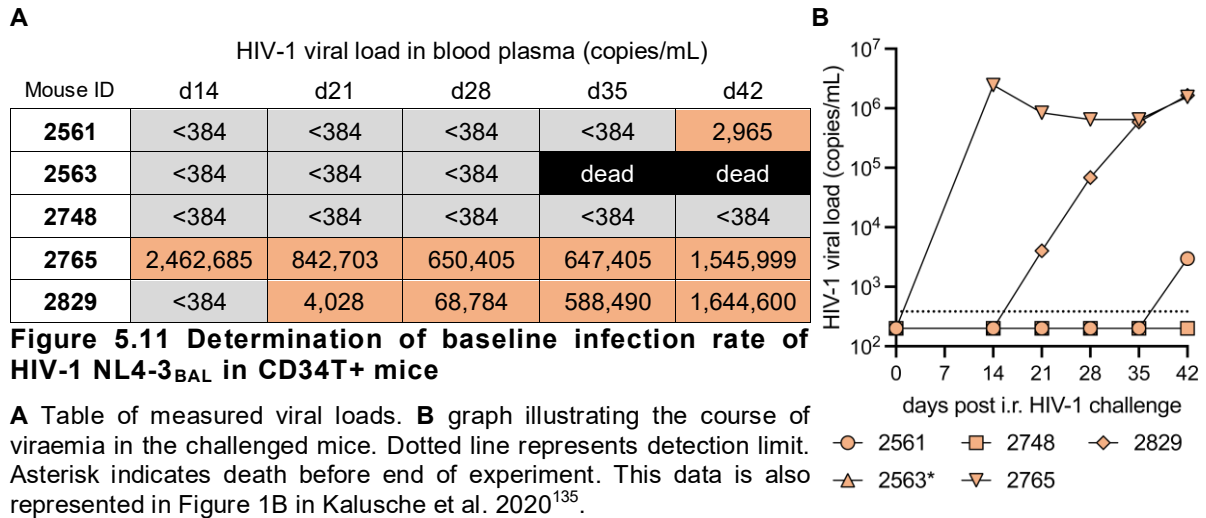


Figure 5.10 TZM-bl assay of V_HH A6 and V_HH 6G2 against HIV-1 NL4-3_{BAL}

Calculated neutralisation rates are depicted as data points. A dose-response inhibition curve was plotted to illustrate the neutralisation activity. This figure is equivalent to Figure 1A from Kalusche et al. 2020¹³⁵.

5.2.2. HIV-1_{BAL} has a high infection rate in intrarectal exposure to CD34T+ mice

In order to determine the susceptibility of the CD34T+ mice to intrarectal exposure with the HIV-1 NL4-3_{BAL} infectious molecular clone (IMC env from HIV-1_{BAL} in pNL4-3) we wanted to apply, we performed a baseline experiment. We used a total of 5 mice that were engrafted with cells from three different placenta donors (2 mice from P141, 2 from P153 and 1 from P157). Their peripheral blood hCD4+ cell concentration was determined via flow cytometry one day prior to challenging. It ranged from 1.1 to 84.1 cells/μL. The mice were challenged on two consecutive days with 1.2×10^5 TCID₅₀ HIV-1_{BAL} per challenge, delivered intrarectally by atraumatic pipetting. We measured viral loads from peripheral blood on days 14, 21, 28, 35 and 42 and determined detectable viraemia (>384 copies/mL) as primary endpoint. One mouse (2563) died before the end of the observation period without becoming infected. A second animal did not develop detectable viraemia throughout the entire experiment whilst 3 mice became HIV-1 positive. Overall infection rate was thereby 70% in a Kaplan-Meier analysis of viraemia-free survival. Once positive, high viral loads were maintained.



5.2.3. HIV-1_{BAL} infection in humanized mice in a combined mucosal administration with V_HH A6 is inhibited

An experiment was designed to investigate the potential of V_HH A6 against HIV-1 *in vivo*. In the experiment, CD34T⁺ mice were employed and generated as described above in 5.1. We included a total of 24 mice engrafted with cells from 4 different placenta donors (4 from P157, 9 from P171, 7 from P179A and 4 from P184). Mice received a donor-matched *i.p.* injection of $\sim 9 \times 10^6$ UCBCs as part of the T⁺ modification.

They were distributed into 3 groups, based on hCD4⁺ cell concentration, cord blood donor and age. Blood hCD4⁺ cell concentration served as a surrogate for the mucosal hCD4⁺ reconstitution as previously shown. Hence, it was assumed to decisively contribute to the susceptibility to HIV-1 by mucosal challenge.

The mice consecutively received an *i.r.* application of an HIV-1 nanobody mixture or HIV-1 only on three successive days. Figure 5.12 gives an overview of the experimental design and viral load results. The applied mixture consisted of either V_HH A6 and HIV-1 (group A6), V_HH 6G2 and HIV-1 (control group 6G2) or HIV-1 only (control group HIV only). In consideration of the TZM-bl assay results we determined to use a concentration of 1.25 $\mu\text{g}/\mu\text{L}$ V_HH, which was also the maximum administered in the neutralization assay, at which no unspecific interference of the V_HH with cell infectivity was observed. Nanobody volume was replaced by the corresponding volume of 1X DPBS in the HIV-1 only group.

The first day of challenge was determined as day 0 (d0) resulting in the nomenclature used below. From d14 to d42, weekly viral load measurements from peripheral blood were carried out. Probability of HIV-1 infection significantly differed between the A6 group and both control groups using a pair-wise Log-rank test while there was no significant difference between the 6G2 and the HIV-1 only control group (Figure 5.12).

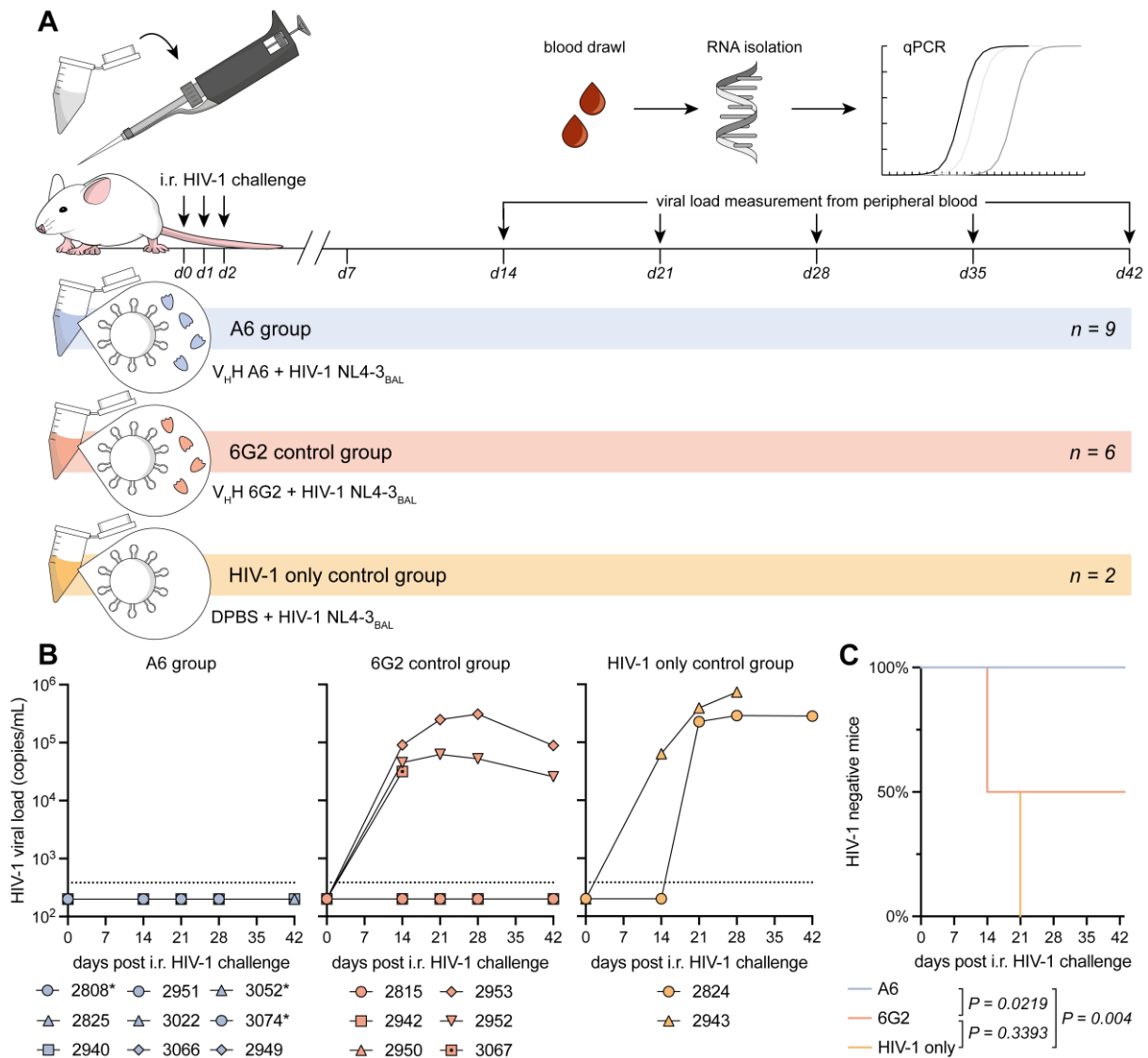


Figure 5.12 $V_{H}H A6$ mucosal prevention experiment in $CD34T+$ mice

A schematic outline of the experimental set-up. Performed procedures common for all 3 experimental groups are depicted above the timeline, the single altered factor was the challenge mixture administered as noted below. Each tube followed by a bar represents one experimental group. $V_{H}H A6$ is illustrated as a blue particle, $V_{H}H 6G2$ in red. Mice were challenged *i.r.* on consecutive days d0, d1 and d2, indicated by arrows above these timepoints. On d14, 21 and 28 respectively, viral loads from peripheral blood were measured in all animals, consisting of the three major steps illustrated: peripheral blood draw, RNA isolation and a qPCR to quantify HIV-1 RNA. **B** course of viral loads depicted per group. Asterisks identify mice that died before d42 without becoming viraemic. Measured viral loads are given in Table 5.4 **C** Kaplan-Meier curve of viraemia free survival. P values were calculated in a pair-wise Log-rank (Mantel-Cox) test. This figure is adopted from Figure 1 from Kalusche et al. 2020¹³⁷.

Table 5.4 V_HH A6 mucosal prevention experiment, table of measured viral loads

Group	Mouse ID	Viral loads in blood plasma (copies/mL)			
		d14	d21	d28	d42
A6	2808	<384	<384	<384	dead
A6	2825	<384	<384	<384	<384
A6	2940	<384	<384	<384	<384
A6	2949	<384	<384	<384	<384
A6	2951	<384	<384	<384	<384
A6	3022	<384	<384	<384	<384
A6	3066	<384	<384	<384	<384
A6	3074	<384	<384	<384	dead
A6	3052	<384	<384	<384	dead
6G2	2815	<384	<384	<384	<384
6G2	2942	<384	<384	<384	<384
6G2	2950	<384	<384	<384	<384
6G2	2952	44,943	62,144	52,334	25,744
6G2	2953	90,306	248,537	307,172	88,838
6G2	3067	31,529	dead	dead	dead
HIV only	2824	<384	226,508	288,071	282,491
HIV only	2943	63,489	390,932	734,618	dead

6. Discussion

6.1. Discussion of the novel CD34T+ Mouse Model

In the ongoing HIV-1 pandemic that still remains without cure or the ability to establish long-lasting immunity by vaccination, *in vivo* research is crucial. Of the two predominant animal platforms, humanized mice are favourable compared to NHPs with regard to legal and ethical restrictions, feasibility of incorporating large group sizes and shorter experiment durations⁶¹. Importantly, in huMice actual infectious HIV-1 from lab derived strains or isolates from infected humans can be used while NHP models require the use of SIV, SHIV or HSIV respectively^{69,70,75}. The inter-individual difference is minimized in huMice by identical genetic background. As human graft, material from one donor is usually administered to multiple mice so that the inter-donor-variability is still well evaluable.

Despite having been helpful in a broad range of settings, huMice still bear multiple limitations, especially regarding the human cell reconstitution in the mucosa as predominant site of infection. Only the BLT model exhibits a stable human mucosal reconstitution including detectable GALT and has consequentially been the model of choice for mucosal HIV-1 studies⁷⁰. However, it relies on foetal tissue limiting its usage legally and ethically. There are reports about HCS-only engrafted humanized mice susceptible to mucosal HIV-1 transmission.

However, a high percentage of human cell reconstitution is required, which is only achieved by a small proportion of CD34+ mice¹⁰⁷.

This work sought to establish and evaluate the novel foetal-tissue-independent CD34T+ mouse model which is especially suitable for studies addressing the mucosal HIV-1 prevention *in vivo*. We could demonstrate, that it is reliably infectable with HIV-1 by intrarectal inoculation.

CD34T+ mice can be generated with only a few procedures, that are both technically less demanding and less invasive for the mice compared to the BLT model. Instead of foetal tissue they only require cord blood derived cells that can easily be obtained from placenta donors. Noteworthy, another replacement of foetal tissue might lie in the utilization of superfluous thymic tissue obtained during neonatal cardiac surgeries¹³⁶. However, its availability is limited due to the nature of its origin.

Modifications to pre-existing mouse models improving aspects of their reconstitution have been the course of humanized mice research ever since their first description. In accordance with this idea, we sought to use the well-established and widespread CD34+ mouse model⁸⁹ and focus on the mucosal TC reconstitution by additionally administering UCBCs accompanied by human IL-7.

A major contributing factor to the poor human reconstitution in peripheral tissue of humanised mice may lie in the absence of human cytokine signalling (3.5.3.2). We decided for the administration of exogenous human IL-7, which has been demonstrated to be crucially involved in both TC lymphopoiesis and the homing of TC into the GALT^{70,93,137-139} and was thereby regarded as the one single interleukin with the highest individual potential to increase GALT TC reconstitution.

The CD34T+ model exhibits an increased human TC reconstitution in the peripheral blood and GALT. Correlation of these two parameters renders peripheral blood measurements a reasonable surrogate for GALT reconstitution *in vivo* in this model. When intrarectally inoculated with HIV-1, CD34T+ were highly susceptible. We observed a 100% infectivity rate in the study population. Our findings about the CD34T+ mouse model were consistent throughout 18 different donors indicating it as a robust method with limited variability.

The suitability of this model for mucosal prevention studies was demonstrated by successful transmission inhibition by a systemically administered highly potent bnAb mixture.

In this study we have only assessed the intrarectal HIV-1 susceptibility whilst other common routes of mucosal transmission, most importantly through the female genital tract (FGT) have

not been investigated. It is critical to note that some differences in the microenvironment and homeostasis, for instance the pH milieu might significantly alter the course of infection between these two sites^{20,135,140}. Therefore it would be advantageous to further investigate the model and characterise the vaginal human reconstitution of CD34T+ mice and HIV-1 susceptibility of their FGT.

In the CD34T+ mice, we sporadically observed development of anaemia about 4 to 6 weeks post the injection of UCBCs. GvHD is a common and critical problem in humanized mice^{97,98}. Rapid-onset GvHD in mice is normally observed when mature TCs are engrafted as in the hu-PBL-mouse model whereas late-onset or chronic GvHD is a common feature of BLT mice, in which the TC maturation is located in human-derived thymic tissue¹¹³. Furthermore a human phagocyte mediated murine erythrocyte depletion has been described for MISTRG and MITRG mice, which are immunodeficient mice in whose genetic background several murine interleukin genes are exchanged by the corresponding human gene sequences¹⁴¹. Those mice are reported to develop anaemia after 2-3 weeks, the incidence of which was directly associated with their human CD45+ cell engraftment¹⁴¹. Suggestions made in the corresponding publication include the omission of the sublethal irradiation in order to not additionally affect the murine erythropoiesis. This on the other hand is known to significantly reduce the human engraftment as described for human PBMCs in NOD-SCID-IL2 γ ^{null} mice⁹⁷.

Probably the administration of UCBCs without human phagocytes, predominantly represented by the CD16+ cell population, would be an option to reduce the development of anaemia since the direct phagocytosis of murine erythrocytes by human cells has been reported in humanized mice¹⁴¹.

Several advances have been made recently to reduce GvHD in humanized mice. For example murine genetic backgrounds harbouring an MHC I and II knockout, by that eliminating the major targets for the human CD3+ cell mediated Graft-versus-host reactions, have been published¹⁴². Those were reported to have an extended GvHD-free survival compared to NSG mice when engrafted with human PBMCs.

In the CD34T+ mouse model we promoted the utilization of UCBCs instead of PBMCs aiming for a better and more sustainable graft tolerance. It is known that cord blood derived mononuclear cells have a tendency towards a more tolerant immune response compared to adult leukocytes^{143,144}. On a functional level this can be explained by the required tolerance towards maternal cells and surface markers during the foetal development. Regarding the cell population characteristics, UCBCs are at least partially less mature and less differentiated than

PBMCs¹⁴³. Our speculations about UCBCs being advantageous over PBMCs were supported by the observation of a high rate of GvHD characteristic symptoms in those mice treated with PBMCs. In accordance with previous characterisation of hu-PBL-mice, we observed a high potential for TC expansion in the NRG-PBMC group compared to the NRG-UCBC group, indicating that the engraftment of PBMCs predominantly consists of TCs, which have been shown to be xenoreactive and therefore activated by murine antigens¹⁰².

We used NRG mice, a widely used and available mouse strain. Practical implications remain a critical aspect in facilitating research, especially with humanized mice. Setting up a new humanized mouse population is challenging and time-consuming whereas the CD34T+ method can easily be adopted to pre-existing NRG mice in different laboratories. Other genetic backgrounds have not been investigated.

The occurrence of GvHD and impaired healthy survival of the mice is a drawback but also eventually tolerable in experimental designs addressing preventive questions that only require experiment durations of less than 5 to 6 weeks.

As for all animal models, it becomes clear that the novel CD34T+ mouse model is not a complete model of the human organism suitable for every scientific question. Rather, the model has its advantages when employing it for the right aspects of the wide spectrum of HIV-1 research. It facilitates the *in vivo* testing of novel anti-HIV-1 molecules or substances that are administered locally or systemically to prevent a mucosal HIV-1 infection, which is the most common and critical route of infection in humans regarding the ongoing pandemic. Further investigations into the suitability for studies of the vaginal transmission route would be required.

In the broad field of humanized mice, a variety of new approaches are under current development. Whilst research addressing the immune response and active vaccination against HIV-1 requires a functional and competent human immune system, the passive prevention research relies on mimicking the site of infection as good as possible. This might include cell populations involved in maintaining and promoting the initial infection, microbiota and other pathogens that interfere with HIV-1 or even facilitate its transmission as known for several co-infections¹.

New approaches include the concept of “dual-reconstitution” referring to a reconstitution of gnotobiotic humanized mice with human microbiota to the gut. In the future, these models would probably enable the close study of microbial influence on the HIV-1 transmission and maybe identify novel preventive targets. Other improvements of humanized mice might lay in

further knock-in mutations of human genes for crucial cytokines as readily demonstrated for a variety of examples^{70,145}.

6.2. Conclusions of this work for the potential of V_HH A6

In this project we tested the preventive *in vivo* potential of the V_HH A6 against HIV-1 NL4-3_{BAL} compared to a non-HIV-1-specific V_HH (6G2). V_HH A6 had previously presented a broad neutralizing spectrum regarding different HIV-1 strains *in vitro*. This project intended to investigate the transferability of the V_HH's anti-HIV-1-activity into an *in vivo* setting.

We carried out a baseline experiment to determine the infection rate of HIV-1 NL4-3_{BAL} in the CD34T+ mouse model, which we used to apply the nanobody to. The infection rate was 70% (Figure 5.11). Due to low group size and a broad variation in potential mediator parameters (CD4+ cell concentration, placenta donors), the quantitative power of this result was regarded as rather limited. However, two conclusions were drawn: Primarily, the data suggest that HIV-1 NL4-3_{BAL} can efficiently infect CD34T+ mice via mucosal routes. But, secondarily, it does not show complete transmissibility.

Based on these observations, the actual prevention experiment employing V_HH A6 was performed. Here, the observation interval was from day 14 until day 42 post-challenge and the primary endpoint was HIV-1 infection, indicated by a detectable viraemia (>384 copies/ μ L blood). The group sizes in this experiment did not allow a quantitative statement about the preventive potential of V_HH A6 against HIV-1 NL4-3_{BAL} in this mouse model (Figure 5.12). However the difference between infection rates in mice that received V_HH A6 together with the infectious virus and those that received V_HH 6G2 instead, was significant. The infection rate in the group receiving V_HH 6G2 on the other hand was in accordance with the previously observed transmission rate with this HIV-1 strain. A qualitative conclusion can therefore be drawn despite the small group sizes. V_HH A6 prevents mucosal infection of CD34T+ mice with HIV-1 NL4-3_{BAL} in comparison to the non-related V_HH 6G2 in a rectal challenge setting.

It is important to note that we employed a rectal challenge model to assess V_HH A6 *in vivo*. A different microenvironment and pH are known to account for relevant differences between transmission through the FGT and the gut^{20,135,140}. The novel CD34T+ model has not yet been evaluated for its human leukocyte reconstitution in the FGT nor its vaginal HIV-1 susceptibility. However, these would be reasonable next steps in the preclinical testing of V_HH A6 and add on to the transferability of generated data into a clinical setting.

To sum up, the results of this first *in vivo* experiment qualify V_HH A6 as a promising candidate for further analysis and development of clinical application routes.

6.3. Perspectives for V_HH A6 in clinical use

When regarding the clinical potential of V_HHs, their usage as passive HIV-1 immunisation at the side of infection seems elaborate. Since V_HHs are only encoded by a single gene sequence and do not require posttranscriptional modifications as Abs do, they can in contrast be expressed by bacterial cells transfected with the encoding plasmid^{135,146}.

This has already been accomplished for V_HH expression in a *Lactocaseibacillus rhamnosus* (*L. rhamnosus*) strain. Both a surface anchored and a soluble V_HH A6 expression have been established and exhibited *in vitro* neutralization activity against a selection of HIV-1 strains¹³⁵.

L. rhamnosus is a highly qualified bacterium for this purpose since it is part of the physiological vaginal microbiome. Applied as intravaginal capsules, it initiates vaginal colonization remaining stable for up to 3 months after application which is already approved in the treatment of bacterial vaginosis¹⁴⁷. Furthermore *L. rhamnosus* contributes to a healthy vaginal flora that intrinsically reduces HIV-1 susceptibility^{135,140}.

The transferability of the lactobacilli-expressed V_HH A6 into an *in vivo* setting remains to be investigated and could be part of ensuing animal experiments.

When evaluating the current situation of preventive tools, it is critical to distinguish between routes of transmission and consider resulting implications especially for women.

Regarding PrEP, a pharmacological model hints at substantial differences between colorectal and cervicovaginal tissue²⁰, suggesting that at least 6 oral out of 7 doses per week would be required to achieve vaginal protection, whilst 2 would suffice for colorectal protection. PrEP efficacy was found to be highly moderated by treatment adherence²⁵ with a variety of social and structural factors restricting access especially for women in SSA¹⁴⁸. Notably, a clinical phase I/II trial employing a prolonged administration of PrEP by s.c. implants is ongoing¹⁴⁹. Although no significant adverse effects of PrEP were found in multiple large RCTs, subclinical decrease in renal or liver function and bone mineralization have been observed²⁵. Long-term effects remain to be investigated. Noteworthy, it remains uncertain, whether an up-scaling of PrEP would impact the global genetic HIV-1 diversity also because PrEP usage might increase risk behaviour, eventually enhancing transmission of drug resistant strains and compromising both PrEP and ART efficacy¹⁵⁰.

BnAbs isolated from elite neutralizers could be a further component in HIV-1 prevention³⁸. They have been tested in animal models and clinical trials proofing their safety as well as their capability in HIV-1 infected individuals^{46,151}. Two randomised trials (HVTN 704/HPTN 085 and HVTN 703/HPTN 081⁵⁰) assessed the preventive potential of the bnAb VRC01 through repeated *i.v.* infusions. The bnAb did not significantly alter HIV-1 acquisition likelihood which was mainly attributed to viral escape and insensitivity to the bnAb⁵⁰. These results illustrate that, in analogy to the therapeutic setting, a single bnAb alone does not mediate protection. Complementary bnAb combinations remain to be assessed further in a preventive setting⁵¹. Limited tissue penetration of Abs require high systemic concentrations in order to achieve sufficient local activity in the mucosa¹⁵¹. The healthy vaginal environment is characterized by an acidic pH around 4-5¹⁴⁰, which extremely reduces affinity of IgG to HIV-1 *in vitro*¹³⁵. A further drawback of bnAbs is the requirement of parenteral administration¹⁵². While *i.v.* infusions are only feasible in a clinical or outpatient setting, *s.c.* applications can be learned and carried out independently. However, the tolerated volume per *s.c.* injection is limited, which might be a restricting factor¹⁵³.

To obtain a long-lasting prevention, continuous bnAb delivery is required which could either be achieved by repeated administration or induction of a durable Ab expression. The half-life ($t_{1/2}$) of bnAbs is around 11-24 days in healthy individuals^{45,153} but can be significantly increased through introduction of an LS mutation in the Ab's Fc region, which increases affinity to the neonatal Fc receptor¹⁵⁴ ($t_{1/2} = 71 \pm 18$ days for VRC01LS versus $t_{1/2} = 15 \pm 3.9$ days for VCR01¹⁵⁵). Noteworthy the Ab $t_{1/2}$ in infected patients alters from the one in healthy individuals and it remains to be investigated whether this also stands true for mere contact with the virus^{45,46}. An alternative to periodical bnAb administration consists of a vector-mediated gene delivery resulting in a stable expression in the host organism itself. While employing adeno-associated viral (AAV) vectors to mediate protein expression¹⁵⁶ is a proven concept¹⁵⁷, concordant approaches mediating anti-HIV-1 bnAb delivery have not resulted in consistent stable bnAb titres yet. Anti-drug responses including anti-drug antibodies (ADA) were determined as a major obstacle in both NHPs^{158,159} and humans¹⁶⁰. Distance from germline identity of the mAb and extent of ADA correlated^{158,159} which is especially precarious in anti-HIV-1 bnAbs regarding their high rates of somatic hypermutation⁴¹. ADA might be enhanced by the vector, since they have not yet been detected after repeated bnAb administrations¹⁵⁵. Novel gene editing techniques offer new perspectives but would in any case require time to be implemented and approved.

BnAbs are an elaborate tool to mimic intrinsic immunity. They target antigens on the viral surface highly specifically and with high affinity, so that adverse effects are minimal^{45,46,153,155}.

Whilst administration of a single bnAb did not protect from HIV-1 acquisition in first large scale clinical trials, bnAb combinations have not been clinically investigated in prevention yet. So far, repeated infusions are the only option for an enduring effect. A central shortcoming of preventive bnAbs is their impaired function in an acidic pH as present in the FGT which appears especially delicate with females in SSA being the largest and most precarious population at risk.

Nanobodies might be advantageous regarding some of the shortcomings of bnAbs in mucosal HIV-1 prevention. They are not only stable in acidic pH but also maintain their affinity to HIV-1 in that environment¹³⁵. In an ELISA based measurement all tested nanobodies did not exhibit significant reduction of binding at pH 4.2 vs. 7.4 and only one showed significantly reduced binding at pH 3.7 vs. 7.4, which might be of minor clinical implications since the physiological pH of the vaginal mucus is around 4-5 and an increase of the pH comes along with higher HIV-1 transmission rates while a decrease might even be protective against HIV-1 intrinsically^{135,140}.

Notably V_HHs do not possess an F_c domain lacking any F_c-F_cR interaction mediated cellular responses IgGs can initiate. However, the importance of F_c signalling in bnAb function against HIV-1 remains controversial and appears at least to some extent dispensable¹⁶¹.

As seen in the clinic for bnAbs with rational combinations of antibodies with complimentary targets⁴⁷, there are *in vitro* data suggesting a potential broadening of the neutralizing capacity of V_HHs when administered combined⁵⁸.

Finally, V_HHs exhibit some advantageous characteristics with regard to the currently established preventive tools especially for females. The investigation of their potential is still in its early stages and further research is required. Potential questions arising from this work include the *in vivo* functionality of lactobacilli-expressed V_HH, the prevention of infection through the FGT and the *in vivo* neutralization breadth of single as well as combinations of V_HHs.

7. References

- 1 Lara LM de, Parthasarathy RS, Rodriguez-Garcia M. Mucosal Immunity and HIV Acquisition in Women. *Curr Opin Physiol* 2021; **19**: 32–38. <https://doi.org/10.1016/j.cophys.2020.07.021>.
- 2 Coffin J, Haase A, Levy JA, et al. What to call the AIDS virus? *Nature* 1986; **321**: 10. <https://doi.org/10.1038/321010a0>.
- 3 Fauci AS, Desrosiers RC. Pathogenesis of HIV and SIV. In: Coffin JM, Hughes SH, Varmus HE, eds. *Retroviruses*. Cold Spring Harbor Laboratory Press, 1997.
- 4 Taylor BS, Sobieszczyk ME, McCutchan FE, Hammer SM. The challenge of HIV-1 subtype diversity. *N Engl J Med* 2008; **358**: 1590–602. <https://doi.org/10.1056/NEJMra0706737>.
- 5 Eisinger RW, Dieffenbach CW, Fauci AS. HIV Viral Load and Transmissibility of HIV Infection: Undetectable Equals Untransmittable. *JAMA* 2019; **321**: 451–52. <https://doi.org/10.1001/jama.2018.21167>.
- 6 Wagh K, Hahn BH, Korber B. Hitting the sweet spot: exploiting HIV-1 glycan shield for induction of broadly neutralizing antibodies. *Curr Opin HIV AIDS* 2020; **15**: 267–74. <https://doi.org/10.1097/COH.0000000000000639>.
- 7 Korber B, Gaschen B, Yusim K, Thakallapally R, Kesmir C, Detours V. Evolutionary and immunological implications of contemporary HIV-1 variation. *British medical bulletin* 2001; **58**: 19–42. <https://doi.org/10.1093/bmb/58.1.19>.
- 8 Clapham PR, McKnight A. HIV-1 receptors and cell tropism. *British medical bulletin* 2001; **58**: 43–59. <https://doi.org/10.1093/bmb/58.1.43>.
- 9 Apetrei C, Hahn B, Rambaut A, et al. HIV Sequence Compendium 2021. Los Alamos, New Mexico 87545 U.S.A.: Theoretical Biology and Biophysics Group, Los Alamos National Laboratory, 2021.
- 10 Gottlieb MS. Pneumocystis pneumonia--Los Angeles. *MMWR* 1981; **30**: 250–52.
- 11 Hymes KB, Greene JB, Marcus A, et al. Kaposi's sarcoma in homosexual men - a report of eight cases. *The Lancet*. 1981; **318**: 598–600. [https://doi.org/10.1016/S0140-6736\(81\)92740-9](https://doi.org/10.1016/S0140-6736(81)92740-9).

- 12 Center for Disease Control. Update on acquired immune deficiency syndrome (AIDS)-- United States. *MMWR* 1982; **31**: 507-8, 513-4.
- 13 Barré-Sinoussi F, Chermann JC, Rey F, et al. Isolation of a T-lymphotropic retrovirus from a patient at risk for acquired immune deficiency syndrome (AIDS). *Science* 1983; **220**: 868–71. <https://doi.org/10.1126/science.6189183>.
- 14 Karch CP, Matyas GR. The current and future role of nanovaccines in HIV-1 vaccine development. *Expert review of vaccines* 2021; **20**: 935–44. <https://doi.org/10.1080/14760584.2021.1945448>.
- 15 Ceccarelli G, Giovanetti M, Sagnelli C, et al. Human Immunodeficiency Virus Type 2: The Neglected Threat. *Pathogens*. 2021; **10**: 1377. <https://doi.org/10.3390/pathogens10111377>.
- 16 UNAIDS. Latest global and regional statistics on the status of the AIDS epidemic. [Fact Sheet]. Geneva, Switzerland, 2023.
- 17 Sharp PM, Hahn BH. Origins of HIV and the AIDS pandemic. *CSH perspectives* 2011; **1**: a006841. <https://doi.org/10.1101/cshperspect.a006841>.
- 18 Hemelaar J, Elangovan R, Yun J, et al. Global and regional molecular epidemiology of HIV-1, 1990–2015: a systematic review, global survey, and trend analysis. *The Lancet. Infectious Diseases*. 2019; **19**: 143–55. [https://doi.org/10.1016/S1473-3099\(18\)30647-9](https://doi.org/10.1016/S1473-3099(18)30647-9).
- 19 Karim SSA, Baxter C. HIV incidence rates in adolescent girls and young women in sub-Saharan Africa. *The Lancet. Global Health*. 2019; **7**: e1470-e1471. [https://doi.org/10.1016/S2214-109X\(19\)30404-8](https://doi.org/10.1016/S2214-109X(19)30404-8).
- 20 Cottrell ML, Yang KH, Prince HMA, et al. A Translational Pharmacology Approach to Predicting Outcomes of Preexposure Prophylaxis Against HIV in Men and Women Using Tenofovir Disoproxil Fumarate With or Without Emtricitabine. *J Infect Dis* 2016; **214**: 55–64. <https://doi.org/10.1093/infdis/jiw077>.
- 21 World Health Organization. Global Health Estimates 2020: Deaths by Cause, Age, Sex, by Country and by Region, 2000-2019. <https://www.who.int/data/gho/data/themes/mortality-and-global-health-estimates/ghle-leading-causes-of-death> (accessed Aug 06, 2022).
- 22 Shaw GM, Hunter E. HIV transmission. *CSH perspectives* 2012; **2**. <https://doi.org/10.1101/cshperspect.a006965>.

- 23 Rodger AJ, Cambiano V, Bruun T, et al. Sexual Activity Without Condoms and Risk of HIV Transmission in Serodifferent Couples When the HIV-Positive Partner Is Using Suppressive Antiretroviral Therapy. *JAMA* 2016; **316**: 171–81. <https://doi.org/10.1001/jama.2016.5148>.
- 24 Attia S, Egger M, Müller M, Zwahlen M, Low N. Sexual transmission of HIV according to viral load and antiretroviral therapy: systematic review and meta-analysis. *AIDS* 2009; **23**: 1397–404. <https://doi.org/10.1097/QAD.0b013e32832b7dca>.
- 25 Fonner VA, Dalglish SL, Kennedy CE, et al. Effectiveness and safety of oral HIV preexposure prophylaxis for all populations. *AIDS* 2016; **30**: 1973–83. <https://doi.org/10.1097/QAD.0000000000001145>.
- 26 U.S. Food and Drug Administration. FDA encourages ongoing education of HIV PrEP treatment. <https://www.fda.gov/news-events/fda-brief/fda-brief-fda-continues-encourage-ongoing-education-about-benefits-and-risks-associated-prep> (accessed Apr 28, 2021).
- 27 Weller SC, Davis-Beaty K. Condom effectiveness in reducing heterosexual HIV transmission. *Cochrane library* 2012; **2012**. <https://doi.org/10.1002/14651858.CD003255>.
- 28 Chan DC, Kim PS. HIV entry and its inhibition. *Cell* 1998; **93**: 681–84. [https://doi.org/10.1016/S0092-8674\(00\)81430-0](https://doi.org/10.1016/S0092-8674(00)81430-0).
- 29 Klasse PJ. Neutralization of Virus Infectivity by Antibodies: Old Problems in New Perspectives. *Adv Biol* 2014; **2014**. <https://doi.org/10.1155/2014/157895>.
- 30 Vidarsson G, Dekkers G, Rispens T. IgG subclasses and allotypes: from structure to effector functions. *Front Immunol* 2014; **5**: 520. <https://doi.org/10.3389/fimmu.2014.00520>.
- 31 Woof JM, Burton DR. Human antibody-Fc receptor interactions illuminated by crystal structures. *Nat Rev Immunol* 2004; **4**: 89–99. <https://doi.org/10.1038/nri1266>.
- 32 Muyldermans S. Nanobodies: natural single-domain antibodies. *Annu Rev Biochem* 2013; **82**: 775–97. <https://doi.org/10.1146/annurev-biochem-063011-092449>.
- 33 Murphy KM, Weaver C. Janeway Immunologie. Berlin, Germany: Springer Spektrum, 2018.
- 34 Caskey M, Klein F, Nussenzweig MC. Broadly neutralizing anti-HIV-1 monoclonal antibodies in the clinic. *Nat Med* 2019; **25**: 547–53. <https://doi.org/10.1038/s41591-019-0412-8>.

- 35 Geiß Y, Dietrich U. Catch Me If You Can--The Race Between HIV and Neutralizing Antibodies. *AIDS Rev* 2015; **17**: 107–13.
- 36 Wyatt R, Sodroski J. The HIV-1 envelope glycoproteins: fusogens, antigens, and immunogens. *Science* 1998; **280**: 1884–88. <https://doi.org/10.1126/science.280.5371.1884>.
- 37 Walker LM, Huber M, Doores KJ, et al. Broad neutralization coverage of HIV by multiple highly potent antibodies. *Nature* 2011; **477**: 466–70. <https://doi.org/10.1038/nature10373>.
- 38 Simek MD, Rida W, Priddy FH, et al. Human immunodeficiency virus type 1 elite neutralizers: individuals with broad and potent neutralizing activity identified by using a high-throughput neutralization assay together with an analytical selection algorithm. *J Virol* 2009; **83**: 7337–48. <https://doi.org/10.1128/JVI.00110-09>.
- 39 Navarrete-Muñoz MA, Restrepo C, Benito JM, Rallón N. Elite controllers: A heterogeneous group of HIV-infected patients. *Virulence* 2020; **11**: 889–97. <https://doi.org/10.1080/21505594.2020.1788887>.
- 40 Combadière B, Beaujean M, Chaudesaigues C, Vieillard V. Peptide-Based Vaccination for Antibody Responses Against HIV. *Vaccines (Basel)* 2019; **7**. <https://doi.org/10.3390/vaccines7030105>.
- 41 Scheid JF, Mouquet H, Feldhahn N, et al. Broad diversity of neutralizing antibodies isolated from memory B cells in HIV-infected individuals. *Nature* 2009; **458**: 636–40. <https://doi.org/10.1038/nature07930>.
- 42 Tiller T, Tsuiji M, Yurasov S, Velinzon K, Nussenzweig MC, Wardemann H. Autoreactivity in human IgG+ memory B cells. *Immunity* 2007; **26**: 205–13. <https://doi.org/10.1016/j.immuni.2007.01.009>.
- 43 McLellan JS, Pancera M, Carrico C, et al. Structure of HIV-1 gp120 V1/V2 domain with broadly neutralizing antibody PG9. *Nature* 2011; **480**: 336–43. <https://doi.org/10.1038/nature10696>.
- 44 Montefiori DC, Roederer M, Morris L, Seaman MS. Neutralization tiers of HIV-1. *Curr Opin HIV AIDS* 2018; **13**: 128–36. <https://doi.org/10.1097/COH.0000000000000442>.

- 45 Caskey M, Klein F, Lorenzi JCC, et al. Viraemia suppressed in HIV-1-infected humans by broadly neutralizing antibody 3BNC117. *Nature* 2015; **522**: 487–91. <https://doi.org/10.1038/nature14411>.
- 46 Caskey M, Schoofs T, Gruell H, et al. Antibody 10-1074 suppresses viremia in HIV-1-infected individuals. *Nat Med* 2017; **23**: 185–91. <https://doi.org/10.1038/nm.4268>.
- 47 Klein F, Halper-Stromberg A, Horwitz JA, et al. HIV therapy by a combination of broadly neutralizing antibodies in humanized mice. *Nature* 2012; **492**: 118–22. <https://doi.org/10.1038/nature11604>.
- 48 Sneller MC, Blazkova J, Justement JS, et al. Combination anti-HIV antibodies provide sustained virological suppression. *Nature* 2022; **606**: 375–81. <https://doi.org/10.1038/s41586-022-04797-9>.
- 49 Garber DA, Adams DR, Guenther P, et al. Durable protection against repeated penile exposures to simian-human immunodeficiency virus by broadly neutralizing antibodies. *Nat Commun* 2020; **11**: 3195. <https://doi.org/10.1038/s41467-020-16928-9>.
- 50 Corey L, Gilbert PB, Juraska M, et al. Two Randomized Trials of Neutralizing Antibodies to Prevent HIV-1 Acquisition. *N Engl J Med* 2021; **384**: 1003–14. <https://doi.org/10.1056/NEJMoa2031738>.
- 51 Bar-On Y, Gruell H, Schoofs T, et al. Safety and antiviral activity of combination HIV-1 broadly neutralizing antibodies in viremic individuals. *Nat Med* 2018; **24**: 1701–07. <https://doi.org/10.1038/s41591-018-0186-4>.
- 52 Hamers-Casterman C, Atarhouch T, Muyldermans S, et al. Naturally occurring antibodies devoid of light chains. *Nature* 1993; **363**: 446–48. <https://doi.org/10.1038/363446a0>.
- 53 Ma H, O’Kennedy R. The Structure of Natural and Recombinant Antibodies. In: Houen G, ed. Peptide Antibodies. Methods and Protocols. Humana Press, New York, NY, 2015: 7–11.
- 54 Blanc MR, Anouassi A, Ahmed Abed M, et al. A one-step exclusion-binding procedure for the purification of functional heavy-chain and mammalian-type gamma-globulins from camelid sera. *Biotechnology and applied biochemistry* 2009; **54**: 207–12. <https://doi.org/10.1042/BA20090208>.

- 55 Holliger P, Hudson PJ. Engineered antibody fragments and the rise of single domains. *Nature biotechnology* 2005; **23**: 1126–36. <https://doi.org/10.1038/nbt1142>.
- 56 Conrath K, Vincke C, Stijlemans B, et al. Antigen binding and solubility effects upon the veneering of a camel VHH in framework-2 to mimic a VH. *JMB* 2005; **350**: 112–25. <https://doi.org/10.1016/j.jmb.2005.04.050>.
- 57 Vu KB, Ghahroudi MA, Wyns L, Muyldermans S. Comparison of llama VH sequences from conventional and heavy chain antibodies. *Molecular Immunology* 1997; **34**: 1121–31. [https://doi.org/10.1016/S0161-5890\(97\)00146-6](https://doi.org/10.1016/S0161-5890(97)00146-6).
- 58 Koch K, Kalusche S, Torres JL, et al. Selection of nanobodies with broad neutralizing potential against primary HIV-1 strains using soluble subtype C gp140 envelope trimers. *Sci Rep* 2017; **7**: 8390. <https://doi.org/10.1038/s41598-017-08273-7>.
- 59 Forsman A, Beirnaert E, Aasa-Chapman MMI, et al. Llama antibody fragments with cross-subtype human immunodeficiency virus type 1 (HIV-1)-neutralizing properties and high affinity for HIV-1 gp120. *J Virol* 2008; **82**: 12069–81. <https://doi.org/10.1128/JVI.01379-08>.
- 60 Lauwereys M, Arbabi Ghahroudi M, Desmyter A, et al. Potent enzyme inhibitors derived from dromedary heavy-chain antibodies. *European Molecular Biology Organization journal* 1998; **17**: 3512–20. <https://doi.org/10.1093/emboj/17.13.3512>.
- 61 Hatzioannou T, Evans DT. Animal models for HIV/AIDS research. *Nat Rev Microbiol* 2012; **10**: 852–67. <https://doi.org/10.1038/nrmicro2911>.
- 62 Spertzel RO. Animal models of human immunodeficiency virus infection. Public Health Service Animal Models Committee. *Antiviral Research* 1989; **12**: 223–30. [https://doi.org/10.1016/0166-3542\(89\)90050-8](https://doi.org/10.1016/0166-3542(89)90050-8).
- 63 Warren CJ, Meyerson NR, Stabell AC, Fattor WT, Wilkerson GK, Sawyer SL. A glycan shield on chimpanzee CD4 protects against infection by primate lentiviruses (HIV/SIV). *Proc Natl Acad Sci U S A* 2019; **116**: 11460–69. <https://doi.org/10.1073/pnas.1813909116>.
- 64 Perelman P, Johnson WE, Roos C, et al. A molecular phylogeny of living primates. *PLOS genetics* 2011; **7**: e1001342. <https://doi.org/10.1371/journal.pgen.1001342>.
- 65 Chahroudi A, Bosinger SE, Vanderford TH, Paiardini M, Silvestri G. Natural SIV hosts: showing AIDS the door. *Science* 2012; **335**: 1188–93. <https://doi.org/10.1126/science.1217550>.

- 66 Liao C-H, Kuang Y-Q, Liu H-L, Zheng Y-T, Su B. A novel fusion gene, TRIM5-Cyclophilin A in the pig-tailed macaque determines its susceptibility to HIV-1 infection. *AIDS* 2007; **21 Suppl 8**: S19-26. <https://doi.org/10.1097/01.aids.0000304692.09143.1b>.
- 67 Wetzel KS, Yi Y, Yadav A, et al. Loss of CXCR6 coreceptor usage characterizes pathogenic lentiviruses. *PLOS pathogens* 2018; **14**: e1007003. <https://doi.org/10.1371/journal.ppat.1007003>.
- 68 Pandrea IV, Gautam R, Ribeiro RM, et al. Acute loss of intestinal CD4+ T cells is not predictive of simian immunodeficiency virus virulence. *J Immunol* 2007; **179**: 3035–46. <https://doi.org/10.4049/jimmunol.179.5.3035>.
- 69 Nath BM, Schumann KE, Boyer JD. The chimpanzee and other non-human-primate models in HIV-1 vaccine research. *Trends Microbiol* 2000; **8**: 426–31. [https://doi.org/10.1016/S0966-842X\(00\)01816-3](https://doi.org/10.1016/S0966-842X(00)01816-3).
- 70 Shultz LD, Brehm MA, Garcia-Martinez JV, Greiner DL. Humanized mice for immune system investigation: progress, promise and challenges. *Nat Rev Immunol* 2012; **12**: 786–98. <https://doi.org/10.1038/nri3311>.
- 71 International Union for Conservation of Nature and Natural Resources. The IUCN Red List of Threatened Species. <https://www.iucnredlist.org/> (accessed Feb 04, 2024).
- 72 Daniel MD, Desrosiers RC, Letvin NL, et al. Simian models for AIDS. *Cancer Detect Prev Suppl* 1987; **1**: 501–07.
- 73 Apetrei C, Lerche NW, Pandrea I, et al. Kuru experiments triggered the emergence of pathogenic SIVmac. *AIDS* 2006; **20**: 317–21. <https://doi.org/10.1097/01.aids.0000206498.71041.0e>.
- 74 Riddick NE, Hermann EA, Loftin LM, et al. A novel CCR5 mutation common in sooty mangabeys reveals SIVsmm infection of CCR5-null natural hosts and efficient alternative coreceptor use in vivo. *PLOS pathogens* 2010; **6**: e1001064. <https://doi.org/10.1371/journal.ppat.1001064>.
- 75 Sui Y, Gordon S, Franchini G, Berzofsky JA. Nonhuman primate models for HIV/AIDS vaccine development. *Curr Protoc Immunol* 2013; **102**: 12.14.1-12.14.30. <https://doi.org/10.1002/0471142735.im1214s102>.

- 76 Feinberg MB, Moore JP. AIDS vaccine models: challenging challenge viruses. *Nat Med* 2002; **8**: 207–10. <https://doi.org/10.1038/nm0302-207>.
- 77 Ziani W, Bauer A, Lu H, et al. Immune Responses and Viral Persistence in Simian/Human Immunodeficiency Virus SHIV.C.CH848-Infected Rhesus Macaques. *J Virol* 2021; **95**. <https://doi.org/10.1128/JVI.02198-20>.
- 78 Hatzioannou T, Ambrose Z, Chung NPY, et al. A macaque model of HIV-1 infection. *Proc Natl Acad Sci U S A* 2009; **106**: 4425–29. <https://doi.org/10.1073/pnas.0812587106>.
- 79 Schmidt F, Keele BF, Del Prete GQ, et al. Derivation of simian tropic HIV-1 infectious clone reveals virus adaptation to a new host. *Proc Natl Acad Sci U S A* 2019; **116**: 10504–09. <https://doi.org/10.1073/pnas.1818059116>.
- 80 Morrow WJ, Wharton M, Lau D, Levy JA. Small animals are not susceptible to human immunodeficiency virus infection. *J Gen Virol* 1987; **68 (Pt 8)**: 2253–57. <https://doi.org/10.1099/0022-1317-68-8-2253>.
- 81 Keppler OT, Welte FJ, Ngo TA, et al. Progress toward a human CD4/CCR5 transgenic rat model for de novo infection by human immunodeficiency virus type 1. *JEM online* 2002; **195**: 719–36. <https://doi.org/10.1084/jem.20011549>.
- 82 Gruell H, Bournazos S, Ravetch JV, Ploss A, Nussenzweig MC, Pietzsch J. Antibody and antiretroviral preexposure prophylaxis prevent cervicovaginal HIV-1 infection in a transgenic mouse model. *J Virol* 2013; **87**: 8535–44. <https://doi.org/10.1128/JVI.00868-13>.
- 83 Mariani R, Chen D, Schröfelbauer B, et al. Species-Specific Exclusion of APOBEC3G from HIV-1 Virions by Vif. *Cell* 2003; **114**: 21–31. [https://doi.org/10.1016/S0092-8674\(03\)00515-4](https://doi.org/10.1016/S0092-8674(03)00515-4).
- 84 Shultz LD, Ishikawa F, Greiner DL. Humanized mice in translational biomedical research. *Nat Rev Immunol* 2007; **7**: 118–30. <https://doi.org/10.1038/nri2017>.
- 85 Bosma GC, Custer RP, Bosma MJ. A severe combined immunodeficiency mutation in the mouse. *Nature* 1983; **301**: 527–30. <https://doi.org/10.1038/301527a0>.
- 86 van der Burg M, van Dongen JJM, van Gent DC. DNA-PKcs deficiency in human: long predicted, finally found. *Curr Opin Allergy Clin Immunol* 2009; **9**: 503–09. <https://doi.org/10.1097/ACI.0b013e3283327e41>.

- 87 Shultz LD, Schweitzer PA, Christianson SW, et al. Multiple defects in innate and adaptive immunologic function in NOD/LtSz-scid mice. *J Immunol* 1995; **154**: 180–91.
- 88 Spear GT, Sullivan BL, Takefman DM, Landay AL, Lint TF. Human immunodeficiency virus (HIV)-infected cells and free virus directly activate the classical complement pathway in rabbit, mouse and guinea-pig sera; activation results in virus neutralization by virolysis. *Immunology* 1991; **73**: 377–82.
- 89 Shultz LD, Keck J, Burzenski L, et al. Humanized mouse models of immunological diseases and precision medicine. *Mammalian genome* 2019; **30**: 123–42. <https://doi.org/10.1007/s00335-019-09796-2>.
- 90 Barclay AN, Brown MH. The SIRP family of receptors and immune regulation. *Nat Rev Immunol* 2006; **6**: 457–64. <https://doi.org/10.1038/nri1859>.
- 91 Mombaerts P, Iacomini J, Johnson RS, Herrup K, Tonegawa S, Papaioannou VE. RAG-1-deficient mice have no mature B and T lymphocytes. *Cell* 1992; **68**: 869–77. [https://doi.org/10.1016/0092-8674\(92\)90030-G](https://doi.org/10.1016/0092-8674(92)90030-G).
- 92 Pearson T, Shultz LD, Miller D, et al. Non-obese diabetic-recombination activating gene-1 (NOD-Rag1 null) interleukin (IL)-2 receptor common gamma chain (IL2r gamma null) null mice: a radioresistant model for human lymphohaematopoietic engraftment. *CEI* 2008; **154**: 270–84. <https://doi.org/10.1111/j.1365-2249.2008.03753.x>.
- 93 Sugamura K, Asao H, Kondo M, et al. The interleukin-2 receptor gamma chain: its role in the multiple cytokine receptor complexes and T cell development in XSCID. *Annu Rev Immunol* 1996; **14**: 179–205. <https://doi.org/10.1146/annurev.immunol.14.1.179>.
- 94 Cao X, Shores EW, Hu-Li J, et al. Defective lymphoid development in mice lacking expression of the common cytokine receptor gamma chain. *Immunity* 1995; **2**: 223–38. [https://doi.org/10.1016/1074-7613\(95\)90047-0](https://doi.org/10.1016/1074-7613(95)90047-0).
- 95 Ito M, Kobayashi K, Nakahata T. NOD/Shi-scid IL2ry (NOG) Mice More Appropriate for Humanized Mouse Models. In: *Curr Top Microbiol Immunol*. 2008.324:53–76.
- 96 Dr. Cynthia Smith, Dr. Stanley Lauderkind. MGI-Guidelines for Nomenclature of Genes, Genetic Markers, Alleles, & Mutations in Mouse & Rat. <http://www.informatics.jax.org/mgihome/nomen/gene.shtml> (accessed Jul 12, 2022).

- 97 King MA, Covassin L, Brehm MA, et al. Human peripheral blood leucocyte non-obese diabetic-severe combined immunodeficiency interleukin-2 receptor gamma chain gene mouse model of xenogeneic graft-versus-host-like disease and the role of host major histocompatibility complex. *CEI* 2009; **157**: 104–18. <https://doi.org/10.1111/j.1365-2249.2009.03933.x>.
- 98 Brehm MA, Shultz LD, Luban J, Greiner DL. Overcoming current limitations in humanized mouse research. *J Infect Dis* 2013; **208 Suppl 2**: S125-30. <https://doi.org/10.1093/infdis/jit319>.
- 99 Marsden MD, Zack JA. Humanized Mouse Models for Human Immunodeficiency Virus Infection. *Annu Rev Virol* 2017; **4**: 393–412. <https://doi.org/10.1146/annurev-virology-101416-041703>.
- 100 Lavender KJ, Pang WW, Messer RJ, et al. BLT-humanized C57BL/6 Rag2-/-γc-/-CD47-/- mice are resistant to GVHD and develop B- and T-cell immunity to HIV infection. *Blood* 2013; **122**: 4013–20. <https://doi.org/10.1182/blood-2013-06-506949>.
- 101 Pearson T, Greiner DL, Shultz LD. Creation of "humanized" mice to study human immunity. *Curr Protoc Immunol* 2008; **Vol 81**: 15.21.1-15.21.21. <https://doi.org/10.1002/0471142735.im1521s81>.
- 102 Brehm MA, Bortell R, Verma M, Shultz LD, Greiner DL. Humanized Mice in Translational Immunology. In: Josep Bassagany-Riera, ed. *Translational Immunology. Mechanisms and Pharmacologic Approaches*. Elsevier, 2016: 285–326.
- 103 D'Cruz OJ, Uckun FM. Limitations of the human-PBL-SCID mouse model for vaginal transmission of HIV-1. *Am J Reprod Immunol* 2007; **57**: 353–60. <https://doi.org/10.1111/j.1600-0897.2007.00478.x>.
- 104 Ishikawa F, Yasukawa M, Lyons B, et al. Development of functional human blood and immune systems in NOD/SCID/IL2 receptor {gamma} chain(null) mice. *Blood* 2005; **106**: 1565–73. <https://doi.org/10.1182/blood-2005-02-0516>.
- 105 Brehm MA, Cuthbert A, Yang C, et al. Parameters for establishing humanized mouse models to study human immunity: analysis of human hematopoietic stem cell engraftment in three immunodeficient strains of mice bearing the IL2rgamma(null) mutation. *Clin Immunol* 2010; **135**: 84–98. <https://doi.org/10.1016/j.clim.2009.12.008>.

- 106 Hofer U, Baenziger S, Heikenwalder M, et al. RAG2^{-/-} gamma(c)^{-/-} mice transplanted with CD34⁺ cells from human cord blood show low levels of intestinal engraftment and are resistant to rectal transmission of human immunodeficiency virus. *J Virol* 2008; **82**: 12145–53. <https://doi.org/10.1128/JVI.01105-08>.
- 107 Gillgrass A, Wessels JM, Yang JX, Kaushic C. Advances in Humanized Mouse Models to Improve Understanding of HIV-1 Pathogenesis and Immune Responses. *Front Immunol* 2020; **11**: 617516. <https://doi.org/10.3389/fimmu.2020.617516>.
- 108 Namikawa R, Weilbaecher KN, Kaneshima H, Yee EJ, McCune JM. Long-term human hematopoiesis in the SCID-hu mouse. *JEM online* 1990; **172**: 1055–63. <https://doi.org/10.1084/jem.172.4.1055>.
- 109 Honeycutt JB, Wahl A, Archin N, Choudhary S, Margolis D, Garcia JV. HIV-1 infection, response to treatment and establishment of viral latency in a novel humanized T cell-only mouse (TOM) model. *Retrovirology* 2013; **10**: 121. <https://doi.org/10.1186/1742-4690-10-121>.
- 110 Kollmann TR, Pettoello-Mantovani M, Zhuang X, et al. Disseminated human immunodeficiency virus 1 (HIV-1) infection in SCID-hu mice after peripheral inoculation with HIV-1. *JEM online* 1994; **179**: 513–22. <https://doi.org/10.1084/jem.179.2.513>.
- 111 Bundesrepublik Deutschland, vertreten durch den Bundesminister der Justiz. Gesetz zum Schutz von Embryonen. ESchG, 1990.
- 112 Melkus MW, Estes JD, Padgett-Thomas A, et al. Humanized mice mount specific adaptive and innate immune responses to EBV and TSST-1. *Nat Med* 2006; **12**: 1316–22. <https://doi.org/10.1038/nm1431>.
- 113 Greenblatt MB, Vrbanac V, Vrbanac V, et al. Graft versus host disease in the bone marrow, liver and thymus humanized mouse model. *Public Library of Science one* 2012; **7**: e44664. <https://doi.org/10.1371/journal.pone.0044664>.
- 114 Yahata T, Ando K, Nakamura Y, et al. Functional human T lymphocyte development from cord blood CD34⁺ cells in nonobese diabetic/Shi-scid, IL-2 receptor gamma null mice. *J Immunol* 2002; **169**: 204–09. <https://doi.org/10.4049/jimmunol.169.1.204>.
- 115 ssniff Spezialdiäten GmbH. ssniff Spezialdiäten GmbH Produktkatalog. <https://www.ssniff.de/index.php?pcid=1&pdid=1> (accessed Mar 10, 2024).

- 116 Dr. André Dülsner, Dr. Rüdiger Hack, Dr. Christine Krüger, et al. Recommendation for blood sampling in laboratory animals, especially small laboratory animals, 2017.
- 117 Zhang Y-J, Hatzioannou T, Zang T, et al. Envelope-dependent, cyclophilin-independent effects of glycosaminoglycans on human immunodeficiency virus type 1 attachment and infection. *J Virol* 2002; **76**: 6332–43. <https://doi.org/10.1128/jvi.76.12.6332-6343.2002>.
- 118 Vanshylla K, Di Cristanziano V, Kleipass F, et al. Kinetics and correlates of the neutralizing antibody response to SARS-CoV-2 infection in humans. *Cell host and microbe* 2021; **29**: 917-929.e4. <https://doi.org/10.1016/j.chom.2021.04.015>.
- 119 Derdeyn CA, Decker JM, Sfakianos JN, et al. Sensitivity of human immunodeficiency virus type 1 to the fusion inhibitor T-20 is modulated by coreceptor specificity defined by the V3 loop of gp120. *J Virol* 2000; **74**: 8358–67. <https://doi.org/10.1128/jvi.74.18.8358-8367.2000>.
- 120 Platt EJ, Wehrly K, Kuhmann SE, Chesebro B, Kabat D. Effects of CCR5 and CD4 cell surface concentrations on infections by macrophagetropic isolates of human immunodeficiency virus type 1. *J Virol* 1998; **72**: 2855–64. <https://doi.org/10.1128/JVI.72.4.2855-2864.1998>.
- 121 Wei X, Decker JM, Liu H, et al. Emergence of resistant human immunodeficiency virus type 1 in patients receiving fusion inhibitor (T-20) monotherapy. *Antimicrob Agents Chemother* 2002; **46**: 1896–905. <https://doi.org/10.1128/aac.46.6.1896-1905.2002>.
- 122 Jeeninga RE, Hoogenkamp M, Armand-Ugon M, Baar M de, Verhoef K, Berkhout B. Functional differences between the long terminal repeat transcriptional promoters of human immunodeficiency virus type 1 subtypes A through G. *J Virol* 2000; **74**: 3740–51. <https://doi.org/10.1128/jvi.74.8.3740-3751.2000>.
- 123 F.L. Graham, van der Eb A. A new technique for the assay of infectivity of human adenovirus 5 DNA. *Virology* 1973; **52**: 456–67. [https://doi.org/10.1016/0042-6822\(73\)90341-3](https://doi.org/10.1016/0042-6822(73)90341-3).
- 124 DuBridges RB, Tang P, Hsia HC, Leong PM, Miller JH, Calos MP. Analysis of mutation in human cells by using an Epstein-Barr virus shuttle system. *Mol Cell Biol* 1987; **7**: 379–87. <https://doi.org/10.1128/mcb.7.1.379>.

- 125 Schoofs T, Barnes CO, Suh-Toma N, et al. Broad and Potent Neutralizing Antibodies Recognize the Silent Face of the HIV Envelope. *Immunity* 2019; **50**: 1513-1529.e9. <https://doi.org/10.1016/j.immuni.2019.04.014>.
- 126 Scheid JF, Mouquet H, Ueberheide B, et al. Sequence and structural convergence of broad and potent HIV antibodies that mimic CD4 binding. *Science* 2011; **333**: 1633–37. <https://doi.org/10.1126/science.1207227>.
- 127 Mouquet H, Scharf L, Euler Z, et al. Complex-type N-glycan recognition by potent broadly neutralizing HIV antibodies. *Proc Natl Acad Sci U S A* 2012; **109**: E3268-77. <https://doi.org/10.1073/pnas.1217207109>.
- 128 Oba Y, Ojika M, Inouye S. Firefly luciferase is a bifunctional enzyme: ATP-dependent monooxygenase and a long chain fatty acyl-CoA synthetase. *FEBS letters* 2003; **540**: 251–54. [https://doi.org/10.1016/s0014-5793\(03\)00272-2](https://doi.org/10.1016/s0014-5793(03)00272-2).
- 129 Montefiori DC. Evaluating neutralizing antibodies against HIV, SIV, and SHIV in luciferase reporter gene assays. *Curr Protoc Immunol* 2005; **Chapter 12**: Unit 12.11. <https://doi.org/10.1002/0471142735.im1211s64>.
- 130 Sarzotti-Kelsoe M, Bailer RT, Turk E, et al. Optimization and validation of the TZM-bl assay for standardized assessments of neutralizing antibodies against HIV-1. *J Immunol Methods* 2014; **409**: 131–46. <https://doi.org/10.1016/j.jim.2013.11.022>.
- 131 David C. Montefiori, Duke University Medical Center. Standardized Assessments of Neutralizing Antibodies for HIV/AIDS Vaccine Development. <https://www.hiv.lanl.gov/content/nab-reference-strains/html/home.htm> (accessed Mar 08, 2023).
- 132 Vanshylla K, Held K, Eser TM, et al. CD34T+ Humanized Mouse Model to Study Mucosal HIV-1 Transmission and Prevention. *Vaccines (Basel)* 2021; **9**: 198. <https://doi.org/10.3390/vaccines9030198>.
- 133 Palmer S, Wiegand AP, Maldarelli F, et al. New real-time reverse transcriptase-initiated PCR assay with single-copy sensitivity for human immunodeficiency virus type 1 RNA in plasma. *JCM* 2003; **41**: 4531–36. <https://doi.org/10.1128/jcm.41.10.4531-4536.2003>.

- 134 Schommers P, Gruell H, Abernathy ME, et al. Restriction of HIV-1 Escape by a Highly Broad and Potent Neutralizing Antibody. *Cell* 2020; **180**: 471-489.e22. <https://doi.org/10.1016/j.cell.2020.01.010>.
- 135 Kalusche S, Vanshylla K, Kleipass F, et al. Lactobacilli Expressing Broadly Neutralizing Nanobodies against HIV-1 as Potential Vectors for HIV-1 Prophylaxis? *Vaccines (Basel)* 2020; **8**. <https://doi.org/10.3390/vaccines8040758>.
- 136 Brown ME, Zhou Y, McIntosh BE, et al. A Humanized Mouse Model Generated Using Surplus Neonatal Tissue. *Stem cell reports* 2018; **10**: 1175–83. <https://doi.org/10.1016/j.stemcr.2018.02.011>.
- 137 Fukatsu K, Moriya T, Ikezawa F, et al. Interleukin-7 dose-dependently restores parenteral nutrition-induced gut-associated lymphoid tissue cell loss but does not improve intestinal immunoglobulin a levels. *JPEN J Parenter Enteral Nutr* 2006; **30**: 388-93; discussion 393-4. <https://doi.org/10.1177/0148607106030005388>.
- 138 Spahn TW, Kucharzik T. Modulating the intestinal immune system: the role of lymphotoxin and GALT organs. *eGut* 2004; **53**: 456–65. <https://doi.org/10.1136/gut.2003.023671>.
- 139 Bilenker M, Roberts AI, Brolin RE, Ebert EC. Interleukin-7 activates intestinal lymphocytes. *Digestive diseases and sciences* 1995; **40**: 1744–49. <https://doi.org/10.1007/BF02212696>.
- 140 Petrova MI, van den Broek M, Balzarini J, Vanderleyden J, Lebeer S. Vaginal microbiota and its role in HIV transmission and infection. *FEMS-microbiology reviews* 2013; **37**: 762–92. <https://doi.org/10.1111/1574-6976.12029>.
- 141 Rongvaux A, Willinger T, Martinek J, et al. Development and function of human innate immune cells in a humanized mouse model. *Nature biotechnology* 2014; **32**: 364–72. <https://doi.org/10.1038/nbt.2858>.
- 142 Brehm MA, Kenney LL, Wiles MV, et al. Lack of acute xenogeneic graft- versus-host disease, but retention of T-cell function following engraftment of human peripheral blood mononuclear cells in NSG mice deficient in MHC class I and II expression. *Federation of American Societies for Experimental Biology journal* 2019; **33**: 3137–51. <https://doi.org/10.1096/fj.201800636R>.

- 143 López MC, Palmer BE, Lawrence DA. Phenotypic differences between cord blood and adult peripheral blood. *Cytometry B Clin Cytom* 2009; **76**: 37–46. <https://doi.org/10.1002/cyto.b.20441>.
- 144 Lee JG, Jaeger KE, Seki Y, et al. Human CD36hi monocytes induce Foxp3+ CD25+ T cells with regulatory functions from CD4 and CD8 subsets. *Immunology* 2021; **163**: 293–309. <https://doi.org/10.1111/imm.13316>.
- 145 Willinger T, Rongvaux A, Takizawa H, et al. Human IL-3/GM-CSF knock-in mice support human alveolar macrophage development and human immune responses in the lung. *Proc Natl Acad Sci U S A* 2011; **108**: 2390–95. <https://doi.org/10.1073/pnas.1019682108>.
- 146 Lee YJ, Jeong KJ. Challenges to production of antibodies in bacteria and yeast. *Journal of bioscience and bioengineering* 2015; **120**: 483–90. <https://doi.org/10.1016/j.jbiosc.2015.03.009>.
- 147 Larsson P-G, Brandsborg E, Forsum U, et al. Extended antimicrobial treatment of bacterial vaginosis combined with human lactobacilli to find the best treatment and minimize the risk of relapses. *Infectious diseases* 2011; **11**: 223. <https://doi.org/10.1186/1471-2334-11-223>.
- 148 van der Straten A, Stadler J, Montgomery E, et al. Women's experiences with oral and vaginal pre-exposure prophylaxis: the VOICE-C qualitative study in Johannesburg, South Africa. *Public Library of Science one* 2014; **9**: e89118. <https://doi.org/10.1371/journal.pone.0089118>.
- 149 Tanuja Narayansamy Gengiah, Quarraisha Abdool Karim, Ishana Harkoo, et al. CAPRISA 018: a phase I/II clinical trial study protocol to assess the safety, acceptability, tolerability and pharmacokinetics of a sustained-release tenofovir alafenamide subdermal implant for HIV prevention in women. *British medical journal open* 2022; **12**. <https://doi.org/10.1136/bmjopen-2021-052880>.
- 150 Supervie V, García-Lerma JG, Heneine W, Blower S. HIV, transmitted drug resistance, and the paradox of preexposure prophylaxis. *Proc Natl Acad Sci U S A* 2010; **107**: 12381–86. <https://doi.org/10.1073/pnas.1006061107>.
- 151 Gruell H, Klein F. Antibody-mediated prevention and treatment of HIV-1 infection. *Retrovirology* 2018; **15**: 73. <https://doi.org/10.1186/s12977-018-0455-9>.

- 152 Dostalek M, Gardner I, Gurbaxani BM, Rose RH, Chetty M. Pharmacokinetics, pharmacodynamics and physiologically-based pharmacokinetic modelling of monoclonal antibodies. *Clin Pharmacokinet* 2013; **52**: 83–124. <https://doi.org/10.1007/s40262-012-0027-4>.
- 153 Ledgerwood JE, Coates EE, Yamshchikov G, et al. Safety, pharmacokinetics and neutralization of the broadly neutralizing HIV-1 human monoclonal antibody VRC01 in healthy adults. *CEI* 2015; **182**: 289–301. <https://doi.org/10.1111/cei.12692>.
- 154 Roopenian DC, Akilesh S. FcRn: the neonatal Fc receptor comes of age. *Nat Rev Immunol* 2007; **7**: 715–25. <https://doi.org/10.1038/nri2155>.
- 155 Gaudinski MR, Coates EE, Houser KV, et al. Safety and pharmacokinetics of the Fc-modified HIV-1 human monoclonal antibody VRC01LS: A Phase 1 open-label clinical trial in healthy adults. *PLoS Med* 2018; **15**: e1002493. <https://doi.org/10.1371/journal.pmed.1002493>.
- 156 Carter BJ. Adeno-associated virus vectors. *Current opinion in biotechnology* 1992; **3**: 533–39. [https://doi.org/10.1016/0958-1669\(92\)90082-T](https://doi.org/10.1016/0958-1669(92)90082-T).
- 157 Mueller C, Gernoux G, Gruntman AM, et al. 5 Year Expression and Neutrophil Defect Repair after Gene Therapy in Alpha-1 Antitrypsin Deficiency. *Molecular Therapy* 2017; **25**: 1387–94. <https://doi.org/10.1016/j.ymthe.2017.03.029>.
- 158 Martinez-Navio JM, Fuchs SP, Pantry SN, et al. Adeno-Associated Virus Delivery of Anti-HIV Monoclonal Antibodies Can Drive Long-Term Virologic Suppression. *Immunity* 2019; **50**: 567-575.e5. <https://doi.org/10.1016/j.immuni.2019.02.005>.
- 159 Martinez-Navio JM, Fuchs SP, Pedreño-López S, Rakasz EG, Gao G, Desrosiers RC. Host Anti-antibody Responses Following Adeno-associated Virus-mediated Delivery of Antibodies Against HIV and SIV in Rhesus Monkeys. *Molecular Therapy* 2016; **24**: 76–86. <https://doi.org/10.1038/mt.2015.191>.
- 160 Priddy FH, Lewis DJM, Gelderblom HC, et al. Adeno-associated virus vectored immunoprophylaxis to prevent HIV in healthy adults: a phase 1 randomised controlled trial. *Lancet HIV* 2019; **6**: e230-e239. [https://doi.org/10.1016/S2352-3018\(19\)30003-7](https://doi.org/10.1016/S2352-3018(19)30003-7).

161 Parsons MS, Lee WS, Kristensen AB, et al. Fc-dependent functions are redundant to efficacy of anti-HIV antibody PGT121 in macaques. *J Clin Invest* 2019; **129**: 182–91. <https://doi.org/10.1172/JCI122466>.

8. Appendix

8.1. List of tables

Table 3.1 Leukocyte concentrations of the CD34T+ group at w0 and w2	71
Table 3.2 Leukocyte concentrations of the CD34+ control group at w0 and w2 ¹³³	72
Table 3.3 Pharmacokinetics of the bnAb Tri-mix in the CD34T+ mice	84
Table 3.4 V _H H A6 mucosal prevention experiment, table of measured viral loads	90

8.2. List of figures

If not specified otherwise, figures and illustrations are created by myself exclusively for presentation in this work and have not been published elsewhere so far.

Figure 1.1 course of vaginal HIV-1 infection through infected semen depicting targets for prevention.....	19
Figure 1.2 schematic illustration of V _H H in comparison to HCAb and IgG1	24
Figure 1.3 Simplified workflow of the generation of neutralizing nanobodies.....	26
Figure 1.4 Schematic overview of the four most common engraftment methods in humanized mice	33
Figure 2.1 outline of the settings for the viral load determining qPCR.....	65
Figure 3.1 generation of the novel CD34T+ mouse model.....	68
Figure 3.2 Comparison of leukocyte concentrations of the CD34T+ and the CD34+ control group at w0 and w2 ¹¹⁸	70
Figure 3.3 comparison of leukocyte concentrations in the peripheral blood in NRG-UCBC and NRG-PBMC mice ¹¹⁸	74
Figure 3.4 Leukocyte concentrations of CD34T+ mice compared to CD34+-PBMC mice.....	76

Figure 3.5 comparison of leukocyte concentrations in secondary lymphoid tissue of the CD34T+ and the CD34+ control group ¹¹⁸	78
Figure 3.6 IF analysis of human T cells in the ileum, colon and spleen of CD34 and CD34T+ mice at week 2. ¹¹⁸	80
Figure 3.7 correlation of hCD4+ cell concentrations in peripheral blood and regarded secondary lymphoid tissue.....	81
Figure 3.8 CD34T+ mice are highly susceptible to mucosal HIV-1 transmission.....	82
Figure 3.9 protective potential of bnAbs against intrarectal HIV-1 challenge in CD34T+ mice	84
Figure 3.10 TZM-bl assay of V _H H A6 and V _H H 6G2 against HIV-1 NL4-3 _{BAL}	86
Figure 3.11 Determination of baseline infection rate of HIV-1 NL4-3 _{BAL} in CD34T+ mice.....	87
Figure 3.12 V _H H A6 mucosal prevention experiment in CD34T+ mice.....	89

9. Publications

Kalusche S, Vanshylla K, **Kleipass F**, Gruell H, Müller B, Zeng Z, Koch K, Stein S, Marcotte H, Klein F, Dietrich U. *Lactobacilli Expressing Broadly Neutralizing Nanobodies against HIV-1 as Potential Vectors for HIV-1 Prophylaxis?* Vaccines (Basel). 2020 Dec 13;8(4):758. doi: 10.3390/vaccines8040758; PMID: 33322227; PMCID: PMC7768517.

Vanshylla K, Held K, Eser TM, Gruell H, **Kleipass F**, Stumpf R, Jain K, Weiland D, Münch J, Grüttner B, Geldmacher C, Klein F. *CD34T+ Humanized Mouse Model to Study Mucosal HIV-1 Transmission and Prevention.* Vaccines (Basel). 2021 Feb 27;9(3):198. doi: 10.3390/vaccines9030198; PMID: 33673566; PMCID: PMC7997265.

Eberhardt KA, Dewald F, Heger E, Gieselmann L, Vanshylla K, Wirtz M, **Kleipass F**, Johannis W, Schommers P, Gruell H, Brensing KA, Müller RU, Augustin M, Lehmann C, Koch M, Klein F, Di Cristanziano V. *Evaluation of a New Spike (S)-Protein-Based Commercial Immunoassay for the Detection of Anti-SARS-CoV-2 IgG.* Microorganisms. 2021 Mar 31;9(4):733. doi: 10.3390/microorganisms9040733; PMID: 33807490; PMCID: PMC8067155.

Vanshylla K, Di Cristanziano V, **Kleipass F**, Dewald F, Schommers P, Gieselmann L, Gruell H, Schlotz M, Ercanoglu MS, Stumpf R, Mayer P, Zehner M, Heger E, Johannis W, Horn C, Suárez I, Jung N, Salomon S, Eberhardt KA, Gathof B, Fätkenheuer G, Pfeifer N, Eggeling R, Augustin M, Lehmann C, Klein F. *Kinetics and correlates of the neutralizing antibody response to SARS-CoV-2 infection in humans.* Cell Host Microbe. 2021 Jun 9;29(6):917-929.e4. doi: 10.1016/j.chom.2021.04.015. Epub 2021 May 3. PMID: 33984285; PMCID: PMC8090990.

Vanshylla K, Fan C, Wunsch M, Poopalasingam N, Meijers M, Kreer C, **Kleipass F**, Ruchnewitz D, Ercanoglu MS, Gruell H, Münn F, Pohl K, Janicki H, Nolden T, Bartl S, Stein SC, Augustin M, Dewald F, Gieselmann L, Schommers P, Schulz TF, Sander LE, Koch M, Łuksza M, Lässig M, Bjorkman PJ, Klein F. *Discovery of ultrapotent broadly neutralizing antibodies from SARS-CoV-2 elite neutralizers.* Cell Host Microbe. 2022 Jan 12;30(1):69-82.e10. doi: 10.1016/j.chom.2021.12.010. Epub 2021 Dec 18. PMID: 34973165; PMCID: PMC8683262.

Harms M, Smith N, Han M, Groß R, von Maltitz P, Stürzel C, Ruiz-Blanco YB, Almeida-Hernández Y, Rodriguez-Alfonso A, Cathelin D, Caspar B, Tahar B, Sayettat S, Bekaddour N, Vanshylla K, **Kleipass F**, Wiese S, Ständker L, Klein F, Lagane B, Boonen A, Schols D, Benichou S, Sanchez-Garcia E, Herbeuval JP, Münch J. *Spermine and spermidine bind CXCR4 and inhibit CXCR4- but not CCR5-tropic HIV-1 infection.* Sci Adv. 2023 Jul

7;9(27):eadf8251. doi: 10.1126/sciadv.adf8251. Epub 2023 Jul 5. PMID: 37406129; PMCID: PMC10321752.

Tabellarischer Lebenslauf

Franziska Marisa Kleipaß, geboren am 20.01.1997 in Dormagen

Eltern: Gudrun Christa & Christoph Leo Kleipaß

Ausbildung

Seit 07/2024	Assistenzärztin in der Klinik für Hämatologie, Onkologie und Rheumatologie der Universitätsklinik Heidelberg AöR
03/2023-06/2024	Assistenzärztin in der Klinik für Hämatologie, Onkologie, Palliativmedizin und spezielle Schmerzmedizin im Klinikum Leverkusen gGmbH
07-09/2022	Medical Elective an der University of Newcastle (UK)
09/2019-11/2024	Med. Doktorandin im Institut für Virologie, Labor für experimentelle Immunologie der Universitätsklinik Köln
10/2015-12/2022	Studium der Humanmedizin an der Heinrich-Heine-Universität Düsseldorf
2008-2015	Erzbischöfliches Gymnasium Marienberg Neuss, Abschluss: Allgemeine Hochschulreife (Abitur: Gesamtnote 1,0)
2003-2008	Friedrich-von-Saarwerden-Grundschule Zons

Klinische Erfahrung

Praktisches Jahr (11/2021 – 10/2022)

Chirurgie (gesplittet)	Colorectal & General Surgery Freeman Hospital Newcastle Orthopädie & Unfallchirurgie, Thoraxchirurgie FNK Düsseldorf
Innere Medizin	Innere Medizin & Nephrologie & Rheumatologie Knappschafts Krankenhaus Bottrop
Wahltertial	Anästhesie & Intensivmedizin UKD Düsseldorf

Famulaturen

03-04/2020	Infektionsschutzzentrum - Universitätsklinik Köln
08/2019	Hausarztfamulatur - Dr. Kratel Dormagen
03/2019	Paediatric Immunology - Great Ormond Street Hospital for Children London
02 – 03/2018	Neurologie - Universitätsklinikum Düsseldorf
08/2017	Ambulante Palliativmedizin - Dr. Kratel Dormagen

Stipendien

2019-2020	Promotionsstipendium des Deutschen Zentrums für Infektionsforschung
01/2016-12/2022	Stipendiatin der Studienstiftung des deutschen Volkes

